

AD-A098 650

DUKE UNIV DURHAM NC DEPT OF ELECTRICAL ENGINEERING F/G 6/18  
THE ROLE OF ELECTRONICALLY EXCITED STATES AND FREE RADICALS IN --ETC(U)  
DEC 80 H HACKER, B S YAMANASHI F33615-78-C-0621

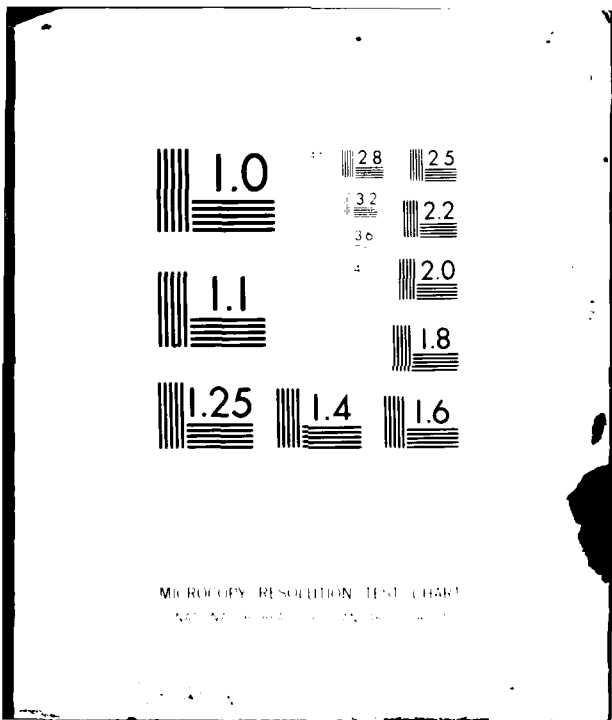
UNCLASSIFIED

SAM-TR-80-28

NL

1 of 1  
424  
299850

END  
DATE  
FILMED  
6-81  
DTIC



MICROCOPY RESOLUTION TEST CHART  
NBS 1963-A

Report SAM-TR-80-28

**LEVEL II**

12  
BS

**THE ROLE OF ELECTRONICALLY EXCITED STATES AND FREE RADICALS IN ULTRAVIOLET-INDUCED LENS OPACIFICATION**

**Herbert Hacker, Ph.D.**  
**Bill S. Yamanashi, Ph.D.**  
Department of Electrical Engineering  
Duke University School of Engineering  
Durham, North Carolina 27706

AD A098650

DTIC  
ELECTR  
MAY 8 1981  
C

December 1980

Final Report for Period 15 March 1978 - 15 March 1979

Approved for public release; distribution unlimited.

Prepared for  
USAF SCHOOL OF AEROSPACE MEDICINE  
Aerospace Medical Division (AFSC)  
Brooks Air Force Base, Texas 78235



DTIC COPY

81 5 08 053

NOTICES

This final report was submitted by Department of Electrical Engineering, Duke University School of Engineering, Durham, North Carolina 27706, under contract F33615-78-C-0621, job order 7757-02-61, with the USAF School of Aerospace Medicine, Aerospace Medical Division, AFSC, Brooks Air Force Base, Texas. Dr. Dwaine M. Thomas (USAFSAM/RZL) was the Laboratory Project Scientist-in-Charge.

When U.S. Government drawings, specifications, or other data are used for any purpose other than a definitely related Government procurement operation, the Government thereby incurs no responsibility nor any obligation whatsoever; and the fact that the Government may have formulated, furnished, or in any way supplied the said drawings, specifications, or other data is not to be regarded by implication or otherwise, as in any manner licensing the holder or any other person or corporation, or conveying any rights or permission to manufacture, use, or sell any patented invention that may in any way be related thereto.

This report has been reviewed by the Office of Public Affairs (PA) and is releasable to the National Technical Information Service (NTIS). At NTIS, it will be available to the general public, including foreign nations.

This technical report has been reviewed and is approved for publication.



DWAINE M. THOMAS, Ph.D.  
Project Scientist



WILLIAM D. GIBBONS, Lieutenant Colonel, USAF  
Supervisor



ROY L. DEHART  
Colonel, USAF, MC  
Commander

UNCLASSIFIED

SECURITY CLASSIFICATION OF THIS PAGE (When Data Entered)

REPORT DOCUMENTATION PAGE		READ INSTRUCTIONS BEFORE COMPLETING FORM
1. REPORT NUMBER SAM-TR-80-28	2. GOVT ACCESSION NO. AD-A098650	3. RECIPIENT'S CATALOG NUMBER
4. TITLE (and Subtitle) THE ROLE OF ELECTRONICALLY EXCITED STATES AND FREE RADICALS IN ULTRAVIOLET-INDUCED LENS OPACIFICATION	5. TYPE OF REPORT & PERIOD COVERED Final Report- 15 March 1978 - 15 March 1979	6. PERFORMING ORG. REPORT NUMBER
7. AUTHOR(s) Herbert Hacker, Ph.D. Bill S. Yamanashi, Ph.D.	8. CONTRACT OR GRANT NUMBER(s) F33615-78-C-0621	
9. PERFORMING ORGANIZATION NAME AND ADDRESS Department of Electrical Engineering Duke University School of Engineering Durham, North Carolina 27706	10. PROGRAM ELEMENT, PROJECT, TASK AREA & WORK UNIT NUMBERS 62202F 7757-02-61	
11. CONTROLLING OFFICE NAME AND ADDRESS USAF School of Aerospace Medicine (RZL) Aerospace Medical Division (AFSC) Brooks Air Force Base, Texas 78235	12. REPORT DATE December 1980	
14. MONITORING AGENCY NAME & ADDRESS (if different from Controlling Office)	13. NUMBER OF PAGES 83	
	15. SECURITY CLASS. (of this report) UNCLASSIFIED	
15a. DECLASSIFICATION/DOWNGRADING SCHEDULE		
16. DISTRIBUTION STATEMENT (of this Report)  Approved for public release; distribution unlimited.		
17. DISTRIBUTION STATEMENT (of the abstract entered in Block 20, if different from Report)		
18. SUPPLEMENTARY NOTES		
19. KEY WORDS (Continue on reverse side if necessary and identify by block number) Cataract                                      Ocular lens                                      UV radiation effects Ultraviolet radiation                      Occupational safety                          Tryptophan Free radicals                                      Electron spin resonance Excited states                                      Spin trapping		
20. ABSTRACT (Continue on reverse side if necessary and identify by block number) Ocular lens safety criteria with respect to UV radiation wavelength and dosage are outlined. These criteria are based on spectroscopic and biochemical studies of UV-exposed and control lenses as well as isolated lens proteins. Excited states of tryptophan in the lens crystallin proteins are implicated as the major species responsible for UV-induced cataractogenesis; possible causal mechanisms including crosslinking of peptides are suggested.		

DD FORM 1473/ JAN 73

UNCLASSIFIED

SECURITY CLASSIFICATION OF THIS PAGE (When Data Entered)

## CONTENTS

	<u>Page</u>
I. INTRODUCTION.....	7
II. EXPERIMENTAL.....	9
A. Wavelength Dependence of UV-Induced Free-Radical Formation in the Human Lens.....	9
B. Minimum Dosage of UV-Induced Free-Radical Formation in the Human Lens.....	10
C. Wavelength Dependence of Photoproduction of the Tryptophan Triplet State.....	10
D. Kinetics of EPR-Monitored Triplet State of N-Formyl Kynurenine Compared with Theoretical Computation (EPR Experiment and Theory).....	10
E. Comparative Kinetics of Free-Radical Formation in the Lens and Cornea.....	12
F. Identification of UV-Induced Free Radicals in Human-Lens Proteins, Amino Acids, and Known Cataractogenic Chemicals (EPR Spin Trapping).....	12
G. Biochemical Analysis on UV-Irradiated Lens Crystallin Proteins...16	
H. Fluorescence Study on UV-Irradiated Crystallin Proteins of the Lens.....	17
I. Photoacoustic Spectra of Human Cataractous Lens Nucleus Vs. Cortex.....	17
III. RESULTS AND DISCUSSION.....	17
A. Intensity of EPR Signal from the Human Lens Vs. Irradiation Wavelength.....	17
B. UV Radiation Dosage Measurement for the Marginally Detectable EPR Signal from the Human Lens.....	19
C. Intensity of EPR Signal from the Tryptophan Triplet State and Its Computer Fitting via a Theoretical Model.....	20
D. EPR-Monitored Kinetics of N-Formyl Kynurenine Triplet State and Its Computer Fitting via a Theoretical Model.....	21

CONTENTS (Continued)

	<u>Page</u>
E. EPR-Monitored Kinetics of the Lens and Cornea; Computer Fitting of the Data via a Two-Component Kinetic Model.....	23
F. Spin Trapping of UV-Induced Free Radicals in Human-Lens Proteins, Amino Acids, and Known Cataractogenic Molecular Species: Analysis of Hyperfine Splittings of Spin Adducts.....	25
G. One- and Two-Dimensional Electrophoresis on the Control and the UV-Irradiated Lens Crystallin Proteins.....	51
H. Fluorescence Spectra of UV-Irradiated Lens Crystallin Proteins.....	55
I. Difference Photoacoustic Spectra Between the Lens Cortex and Nucleus: Consideration of Saturation Effects.....	59
IV. CONCLUSIONS.....	60
A. Ocular Lens Protection Against UV Radiation Wavelength.....	61
B. Ocular Lens Protection Against Radiation Dosage.....	62
C. Role of the Tryptophan-Excited Triplet State in UV-Induced Cataractogenesis.....	63
D. Possible Role of a Photo-Oxidation Product of the Tryptophan Triplet State as an Intermediate in UV-Induced Free-Radical Formation.....	65
E. Two-Component Kinetics of Free-Radical Formation in the Lens and Its Implication with Regard to UV Cataractogenesis.....	66
F. Free-Radical Species Produced Under Monochromatic and Non-monochromatic Irradiation of the Human Lens and Related Materials: Spin Trapping and Implications of Experimental Results.....	67
G. Fingerprinting of UV-Damaged Ocular Lens Proteins with 2-D Electrophoresis.....	76
H. Fluorescence Analysis of UV-Irradiated Lens Crystallin Proteins; $\gamma$ - Crystallin as a UV Susceptibility Factor.....	77
I. Photoacoustic Measurements (PAS).....	77

A	Accession For
	NTIS GRA&I
	DTIC TAB
	Unannounced
	Justification
By	
Distribution/	
Availability Codes	
Avail and/or	
Special	

CONTENTS (Continued)

	<u>Page</u>
J. Summary of Conclusions.....	78
K. Suggestions for Further Investigation.....	78
REFERENCES.....	79

List of Illustrations

<u>Figure</u>	<u>Page</u>
1 Corrected and uncorrected action spectra for free-radical formation in the human lens.....	18
2 (a) Uncorrected phosphorescence excitation spectrum of tryptophan in the human lens.....	19
(b) Action spectrum of UV-induced cataractogenesis in guinea pigs..	19
3 Irradiation-wavelength dependence of EPR signal intensity due to the UV-induced triplet state of tryptophan.....	21
4 Comparison of the experimental irradiation time dependence of tryptophan-excited triplet state, free radicals, and NFK-excited triplet state.....	22
5 EPR-monitored kinetics of the free-radical formation in the human lens.....	23
6 Hyperfine splitting analysis of standard spin adducts.....	26
7A Spin trapping EPR spectrum of UV-induced free radicals in tryptophan aqueous solution with DMPO; monochromatic and broad-band irradiation.....	28
7B Analysis of tryptophan/DMPO spin trapping spectrum.....	29
7C EPR spectrum obtained from aqueous tryptophan and DMPO irradiated at 290 nm for 5 minutes.....	30
7D Analysis of spectrum in Figure 7C.....	31
7E EPR spectrum of radicals trapped by DMPO in an aqueous solution of tryptophan irradiated at 320 nm for 20 minutes.....	32
8 EPR spectrum from spin trapping of UV-induced free radicals in tyrosine aqueous solution by DMPO with monochromatic 300-nm and broad-band irradiation.....	33



List of Illustrations (Continued)

<u>Figure</u>	<u>Page</u>
9 EPR spectrum obtained from spin trapping UV-induced free radicals in the water-soluble fraction of the human-lens protein, compared with that obtained from tyrosine/DMPO aqueous solution.....	35
10 EPR spectrum obtained from spin trapping UV-induced free radicals in the urea-soluble fraction of the human-lens protein, compared with that obtained from tyrosine/DMPO aqueous solution.....	36
11 EPR spectrum obtained from spin trapping UV-induced free radicals in the urea-insoluble fraction of human-lens protein, compared with that obtained from tryptophan/DMPO aqueous solution.....	37
12 EPR spectrum obtained from spin trapping UV-induced free radicals in poly-DL-tryptophan/DMPO solution, compared with that obtained from tryptophan/DMPO solution.....	38
13 Relative intensity via low-field terminal transition.....	39
14 EPR spectrum of free radicals trapped with DMPO in lysozyme, monochromatically irradiated at 300 nm for 10 minutes.....	40
15 EPR spectrum of free radicals trapped with DMPO in phenylalanine irradiated at 300 nm for 10 minutes.....	42
16 EPR spectrum of free radicals trapped with DMPO in histidine irradiated at 300 nm for 10 minutes.....	43
17 EPR spectrum of free radicals trapped with DMPO in N-formyl kynurenine irradiated at 300 nm for 10 minutes.....	44
18 EPR spectrum of free radicals trapped with DMPO in glycine irradiated at 300 nm for 8 minutes.....	45
19 EPR spectrum of free radicals trapped with DMPO in leucine irradiated at 300 nm for 10 minutes.....	46
20 EPR spectrum of free radicals trapped with DMPO in methionine irradiated at 300 nm for 10 minutes.....	47
21 EPR spectrum of free radicals trapped with DMPO in aspartic acid irradiated at 300 nm for 12 minutes.....	48
22 EPR spectrum obtained from aqueous 8-methoxy psolaren, a cataractogenic drug, and DMPO with broad-band irradiation for 5 minutes.....	49

List of Illustrations (Continued)

<u>Figure</u>	<u>Page</u>
23 EPR spectrum of radicals trapped by DMPO in the aqueous solution of 8-methoxy psoralen (8-MOP) irradiated at 320 nm for 40 minutes.....	50
24 EPR spectrum of radicals trapped by DMPO in aqueous ribonuclease.....	51
25 Elution of water-soluble cow-lens proteins and fraction #4 from a Sephadex G-25 fine column.....	52
26 Sephadex G-200 gel chromatographic separation of rabbit-lens crystallin proteins.....	53
27 2-D gel electrophoresis of fraction #1 from rabbit lens, after Sephadex G-200 gel chromatography.....	54
28 2-D gel electrophoresis of fraction #4 from rabbit lens, after Sephadex G-200 gel chromatography.....	55
29 Fluorescence emission spectrum of cow-lens crystallin fraction #1 irradiated with a broad-band UV at 440 mW/cm <sup>2</sup> .....	56
30 Fluorescence emission spectrum of cow-lens crystallin protein fraction #2 irradiated with a broad-band UV at 440 mW/cm <sup>2</sup> .....	57
31 Fluorescence emission spectrum of cow-lens crystallin fraction #3 irradiated with a broad-band UV at 440 mW/cm <sup>2</sup> .....	58
32 Fluorescence emission spectrum of cow-lens crystallin protein fraction #4 irradiated with a broad-band UV at 440 mW/cm <sup>2</sup> .....	59
33 Difference photoacoustic spectrum between the cortex and nucleus of a human cataractous lens.....	60
34 Plot of log of photoacoustic signal amplitude at 230 nm and 280 nm vs. log of modulation frequency.....	61
35 Jablonski-type diagram for molecular electronic processes.....	66

List of Tables

<u>Table</u>	<u>Page</u>
1 Relative intensity of low-field terminal transition in hyperfine splitting of DMPO spin adduct from lysozyme.....	40

List of Tables (Continued)

<u>Table</u>	<u>Page</u>
2 Relative intensity of low-field terminal transition in hyperfine splitting of DMPO spin adduct from poly-DL-tryptophan.....	41
3 Relative intensity of low-field terminal transition in hyperfine splitting of DMPO spin adduct from phenylalanine.....	42
4 Relative intensity of low-field terminal transition in hyperfine splitting of DMPO spin adduct from histidine.....	43
5 Relative intensity of low-field terminal transition in hyperfine splitting of DMPO spin adduct from N-formyl kynurenine.....	44
6 Relative intensity of low-field terminal transition in hyperfine splitting of DMPO spin adduct from glycine.....	45
7 Relative intensity of low-field terminal transition in hyperfine splitting of DMPO spin adduct from leucine.....	46
8 Relative intensity of low-field terminal transition in hyperfine splitting of DMPO spin adduct from methionine.....	47
9 Relative intensity of low-field terminal transition in hyperfine splitting of DMPO spin adduct from aspartic acid.....	48

# THE ROLE OF ELECTRONICALLY EXCITED STATES AND FREE RADICALS IN ULTRAVIOLET-INDUCED LENS OPACIFICATION

## I. INTRODUCTION

The involvement of electronically excited states and free radicals in ultraviolet (UV) induced cataractogenesis was suspected from UV visible absorption, fluorescence, phosphorescence, electron paramagnetic resonance (EPR), and photoacoustic spectra of normal vs. brunescant lenses and young vs. senile lenses (1-5). A progressive increase in the types and concentration of photochemically induced pigments in the aging lens has been demonstrated. Some of these UV-absorbing chromophores appear to be associated with protein cross-linking and the subsequent increase in the concentration of insoluble proteins (6-11). The pigmentation and the crosslinking are now considered to be well-documented parameters for aging as well as brunescant cataractogenesis (12,13). Some of the pigments have been isolated and identified as glucosides of hydroxy kynurenine and other oxidation products of tryptophan (14). The capability of UV radiation (at and above 300 nm) to generate cataracts in experimental animals as well as in the human lens has also been demonstrated (15-17). The possibility of enhanced photobiologic damage via photosensitized reactions due to the accumulation of certain drugs has been investigated (18,19). The effect of intense UV sources, such as UV lasers and high-intensity xenon arc lamps, upon lenses of various animal species indicates that the susceptibility to UV damage appears to differ among species, and the relative amount of  $\gamma$ -crystallin protein with respect to other crystallins such as  $\alpha$ ,  $\beta_H$ , and  $\beta_L$  is suggested as being correlated to such susceptibility (20).

Previous EPR studies yielded (a) signals due to UV-induced free radicals with a g-value or spectroscopic splitting factor of  $\approx 2$ , and (b) signals due to excited triplet states. The former lack hyperfine structure, while the latter are due to the spin-spin dipole interactions between two unpaired electrons and manifest themselves in either  $\Delta M_S = \pm 2$  or  $\Delta M_S = \pm 1$  transitions. Among these, only the so-called half-field transitions,  $H_{min}$ , from the  $\Delta M_S = \pm 2$  of human and animal lenses were observed (4,5,20) and were found to be similar to those of tryptophan (4). Both the control and laser preexposed rhesus monkey lenses exhibited two  $\Delta M_S = \pm 2$   $H_{min}$  transitions, one of which was assigned to the tryptophan triplet state; it was suggested that the other be assigned to the kynurenine family of compounds. The kinetics of the buildup of the free-radical signal and of the decay of the  $H_{min}$  signal of the triplet state of tryptophan were effectively the same. The kinetics of the rise and decay of the excited triplet state of the kynurenine derivative suggested that it may be an intermediate between the  $^3\text{Trp}$  and the free radical (20).

The objectives of this investigation were--

(a) to determine the nature of the involvement of lens chromophores (i.e., light-absorbing molecular species); in particular, the tryptophan-excited states in free-radical formation in ocular lens tissue,

(b) to understand and explain the role of photo-produced free radicals in possible cataractogenic molecular processes, and

(c) to hypothesize a model of UV-induced cataractogenesis based on an assessment of the data we collect.

To accomplish these objectives we have performed experiments on the wavelength and power dependence of UV-induced free-radical production, sought to identify the excited states and free radicals in the lens, studied the kinetics of free-radical formation and decay of excited states, performed biochemical analysis of UV-irradiated lens proteins, and studied the effects of chemicals that influence UV damage of the lens.

The conclusions we have reached are based on the data in this work as well as on previous data and inferences reported in the literature. We placed special attention on the analysis and interpretation of phenomenological data in terms of occupational safety criteria for employees who may be exposed to UV radiation. On the basis of correlating our EPR spin trapping and supplementary data (e.g., biochemical analysis, fluorescence, and photoacoustic spectra) with existing photochemical data, we believe that several possible mechanisms may be operative in UV-induced cataractogenesis. These are discussed later in this report, and the role of free-radical sensitizers (enhancers) and free-radical scavengers in UV cataractogenesis is described. In our conclusions we summarize the knowledge advanced by this investigation as well as data that are not consistent with our hypotheses and hence require further investigation.

The method used for identifying short-lived free radicals in this investigation has been applied to human biological systems only recently (21). Spin trapping is an indirect EPR method of detecting free radicals by letting a free-radical scavenger react with the short-lived radical to be identified and then analyzing the spectral characteristics of the resultant stable radical (or spin adduct). The method was proposed independently in 1968 and in 1969 by five groups of workers (22a-e).

Early work showed that both nitroso and nitron compounds were capable of trapping unstable carbon-centered radicals. By "unstable" we mean radicals that are not highly resonance stabilized or are not strongly protected by sterically hindered substituents. The hyperfine splitting pattern, the value of nitrogen and other nuclear hyperfine splitting constants, and the g-values and linewidths of individual EPR signals are important parameters that contribute to an assignment of structure for the spin adduct. Reports on carbon-centered radicals are extensive and found in three review papers (23,24,25). Nitrogen-centered radicals are also trappable to give detectable spin adducts (26). Oxygen-centered radicals are easily trapped using nitroses (27,28), but form unstable adducts with nitroso compounds. Phosphorus-centered radicals are readily trapped with nitroso or nitron compounds (29). Hydrogen atoms are trapped to produce detectable spin adducts with either nitroso or nitron compounds (30), although only the latter give detectable concentrations of nitroxides with fluorine or chlorine atoms (31,32). Most applications of spin trapping to biological systems involve the use of 2-methyl, 2-nitrosopropane (MNP),  $\alpha$ -phenyl-N-tert-butyl nitron (PBN), and

5,5-dimethyl-pyrroline-N-oxide (DMPO). All of these traps are now available commercially (e.g., Aldrich or Eastman chemicals).

## II. EXPERIMENTAL

### A. Wavelength Dependence of UV-Induced Free-Radical Formation in the Human Lens

Materials--Human lenses ranging in age from 35 to 78 years were obtained from either the eye bank or autopsy. The lenses were kept frozen in distilled water at  $-4^{\circ}\text{C}$  until EPR experiment. A few minutes prior to the experiment, they were thawed to room temperature ( $29^{\circ}\text{C}$ ), separated from the cortex and capsule, cut into 1- x 4-mm strips, and refrozen to  $-196^{\circ}\text{C}$  to facilitate inserting the gelatinous lens nucleus into the fused-silica EPR sample tube. The length of these tubes was approximately 25 cm.

EPR Spectrometer--The spectrometer operating parameters for these experiments were: field-scan range, 3000 to 3200 Gauss; field-scan rate, 85 Gauss/min; amplifier time constant, 1 second; microwave frequency, 9.902 GHz; microwave power, 5 mW; modulation frequency, 100 kHz; and modulation field intensity, 4.0 Gauss RMS.

UV Source--A Hanovia ozone-free xenon arc lamp (model L5179-000) was used as the UV radiation source and was operated at 22 V and 37 A (input power = 814 W). The arc lamp was housed in an Oriel model 6148 housing equipped with a blower, a reflector, and a fused-silica collimating lens.

Monochromator--The wavelength was selected with a Bausch and Lomb model 33-86-01 high-intensity monochromator that covers 200-400 nm, is blazed at 250 nm, and has linear dispersion of 3.2 nm/mm.

IR Filter--The infrared (IR) filtration consisted of a constant-flow, water-cooled filter with a radius of 3.2 cm (1.25 in) and an optical path-length of 16.5 cm (6.5 in).

The IR filter and the monochromator were inserted between the arc lamp and the optical grids of the EPR cavity, with the IR filter next to the arc lamp. The focal length of the collimator was adjusted so that the intensity of a standard EPR signal (i.e., naphthalene  $\Delta M_S = \pm 2$  signal at approximately 1500 Gauss) was maximized.

Procedure--The lens samples were irradiated at several wavelengths between 260 and 330 nm for an average of 25 minutes. After each EPR field scan was completed, the sample was thawed, the liquid nitrogen dewar was refilled, and the sample was repositioned as in the previous scan. The resultant EPR spectral peak-to-peak intensity was then plotted against the irradiation wavelength.

Correction of the Spectral Intensity--The spectral intensity in the above experiment was corrected as follows. A Laser Precision model RK-5100 pyroelectric radiometer and an RKP-545 probe were used for the UV intensity

measurement. Since the probe was too big to be inserted between the pole caps of the EPR magnet, it was placed in a similar arrangement at the same distance from the lamp as in the actual experiment. The radiometer settings were: averaging time, medium; chopping, internal; and background cancel, cold. The ambient light intensity was compensated by use of the background cancel knob on the radiometer; the irradiance was read directly on the digital readout in units of  $W/cm^2$ . The results of the monochromatic irradiance measurements between 260 and 325 nm were used to correct the EPR intensity vs. wavelength plot.

#### B. Minimum Dosage of UV-Induced Free-Radical Formation in the Human Lens

The EPR spectrometer settings were the same as in Section II A, and the technique described in that section was used to prepare a young (16-yr-old) donor lens that did not have visible pigmentation nor opacity. The intensity of the lens free-radical signal was measured for several experimentally accessible irradiance levels obtained by decreasing the lamp voltage. The irradiance level for each reduced lamp output was measured with the pyroelectric radiometer until the EPR signal level dropped to be just distinguishable from the noise level. The irradiance level that produced the minimum detectable EPR signal was recorded as the minimum dosage level.

#### C. Wavelength Dependence of Photoproduction of the Tryptophan Triplet State

A sample of tryptophan (Aldrich Chemical Co.) was dissolved in an aliquot of water, then USP grade ethanol and ethylene glycol were added such that the volume ratio of water, ethylene glycol, and ethanol was 1:2:2. The concentration of Trp was about  $1 \times 10^{-3}M$ . This mixture of solvent was chosen because it forms a rigid and transparent glass at  $-196^\circ C$ , thus optimizing the EPR signal intensity of the  $\Delta M_S = \pm 2$  transition. The EPR instrument parameters were: field range, 1400 to 1480 Gauss; microwave frequency, 9.103 GHz; microwave attenuation, +1 dB; lock-in detector settings: modulation, 1.0 and phase, 185 degrees; gain, 50  $\mu V$ ; recorder settings: X = 10 sec/in, Y = 5 mV/in. The  $\Delta M_S = \pm 2$  signal of tryptophan was monitored at  $H = 1445$  Gauss. We allowed the signal to build up until it reached a plateau, which occurred after about 45 seconds, at which time the relative intensity was measured. At least 40 such measurements were made. After averaging and normalizing, 18 data points were plotted against wavelength.

#### D. Kinetics of EPR-Monitored Triplet State of N-Formyl Kynurenine Compared with Theoretical Computation (EPR Experiment and Theory)

In the lens monitored by us via the EPR  $g = 2.003$  signal, the kinetics of free-radical formation suggests the presence of more than one type of radical. If we assume that there are two main types of free radicals, and that the sources of these radicals are not common, we may fit the experimental peak-to-peak EPR intensity to expressions of the form

$$dI/dH = M_1[1 - \exp(-k_1t)] + M_2[1 - \exp(-k_2t)] \quad [1]$$

where  $M_1$  and  $M_2$  are proportional to the concentrations of the two radicals producing the EPR signal, and  $k_1$  and  $k_2$  are rate constants associated with the processes producing the free radicals. The ratio  $M_2/M_1$  gives the relative concentrations of the radical species even though the value of  $M_2$  (or  $M_1$ ) is arbitrary. Experimental values of the rate constants of the lens are given in Section III D.

N-formyl kynurenine is one of the early photo-oxidation products of tryptophan and may be involved in one of the cataractogenic mechanisms in the following manner:



where  ${}^3\text{Trp}$  is the excited triplet state (lowest energy level),  ${}^3\text{NFK}$  is the triplet state of NFK, and  $R^\cdot$  is one of the free-radical species produced. The parameters  $k_i$  and  $k_{ij}$  are associated rate constants for process equations 2 and 3 respectively. As described on pages 65-66,  ${}^3\text{Trp}$  is produced via absorption and intersystem crossing.

The rate equations have the form

$$d[{}^3\text{Trp}]/dt = -k_i[{}^3\text{Trp}] \quad [4]$$

$$d[{}^3\text{NFK}]/dt = k_i[{}^3\text{Trp}] - k_{ij}[{}^3\text{NFK}] \quad [5]$$

$$d[R^\cdot]/dt = k_{ij}[{}^3\text{NFK}] \quad [6]$$

Integrating Eq. 4, we get

$$[{}^3\text{Trp}] = [{}^3\text{Trp}]_0 \exp(-k_it) \quad [7]$$

and integrating Eq. 5, we get

$$[{}^3\text{NFK}] = \frac{k_i}{k_{ij} - k_i} [{}^3\text{Trp}]_0 [\exp(-k_it) - \exp(-k_{ij}t)] \quad [8]$$

Since  $[{}^3\text{Trp}]_0$  is the initial concentration of  $[{}^3\text{Trp}]$ , then,

$$[{}^3\text{Trp}] + [{}^3\text{NFK}] + [R^\cdot] = [{}^3\text{TRP}]_0 \quad [9]$$

From Eqs. 7, 8, and 9, we have

$$[R^\cdot] = 1 - \frac{k_{ij} \exp(-k_it) + k_i \exp(-k_{ij}t)}{k_{ij} - k_i} \quad [10]$$



We define the lifetime of  $^3\text{Trp}$  as  $\tau_i$  and that of  $^3\text{NFK}$  as  $\tau_{ij}$ , and by definition,

$$k_i = \tau_i^{-1}, k_{ij} = \tau_{ij}^{-1} \quad [11]$$

Substituting Eq. 11 into Eqs. 7, 8, and 9, we obtain

$$[^3\text{Trp}] = [^3\text{Trp}]_0 \exp(-t/\tau_i) \quad [12]$$

$$[^3\text{NFK}] = \frac{\tau_{ij}}{\tau_i - \tau_{ij}} [^3\text{Trp}]_0 [\exp(-t/\tau_i) - \exp(-t/\tau_{ij})] \quad [13]$$

$$[R^*] = [^3\text{Trp}]_0 \left[ 1 - \frac{\tau_i \exp(-t/\tau_i) + \tau_{ij} \exp(-t/\tau_{ij})}{\tau_i - \tau_{ij}} \right] \quad [14]$$

Equation 13 was used to obtain computed values of  $^3\text{NFK}$  with respect to irradiation time. The computer fitting of this theoretical  $^3\text{NFK}$  data to the earlier experiments of Yamanashi and Zuclich yielded theoretical values of  $k_i$  and  $k_{ij}$ .

#### E. Comparative Kinetics of Free-Radical Formation in the Lens and Cornea

The kinetics of free-radical formation was monitored via EPR following the method of Yamanashi and Zuclich (20b) on the lens nucleus and the whole cornea from a 78-year-old human eye. The lens preparation was the same as described in Section II A. The cornea was removed from the extracted eye, cut into 2- x 6-mm strips, and kept frozen at  $-4^\circ\text{C}$  until the kinetic experiments. Data on the whole human cornea may differ from that of its sublayers, so we also investigated the sublayers of a cow cornea since the cow eye is large enough to permit separation of such layers. The cow stroma was separated from the epithelium and endothelium by Dr. G. K. Klintworth of the Duke Pathology Department. Storage and sample preparatory techniques were the same as for the other tissues. Data on the EPR spectra (i.e., intensity vs. magnetic field) for each of these tissues have appeared earlier; e.g., for the lens by Weiter and Finch (3) and for the cornea by Yamanashi et al. (33).

#### F. Identification of UV-Induced Free Radicals in Human-Lens Proteins, Amino Acids, and Known Cataractogenic Chemicals (EPR Spin Trapping)

##### 1. Spin Trapping of UV-Induced Free Radicals in Tryptophan by DMPO

DMPO obtained from Aldrich Chemical Co. was tested by the manufacturer for purity via IR, elemental analysis, and gas chromatography (GC) and was stated to be 97+% pure; however, it was orange colored, implying some conjugated impurity. Further purification was performed by Dr. Rosen of Duke's Pharmacology Department, after which no coloration was observed. Approximately 30  $\mu\text{l}$  of DMPO was mixed with 1 ml of a  $5 \times 10^{-2}\text{M}$   $\text{H}_2\text{O}$  solution of tryptophan (obtained from Calbiochem without purification). The resulting solution was transferred to the EPR aqueous sample cell via a precleaned disposable pipet. The spin trapping method was similar to that of Evans and

Yamanashi (21). The EPR spectrometer operating parameters were: field-scan range, 3330-3420 Gauss; field-scan rate, 40 Gauss/min; amplifier time constant, 0.3 sec; microwave frequency, 9.495 GHz; microwave power, 10 mW; modulation frequency, 100 kHz; modulation intensity, 1.3 Gauss (peak to peak); and lock-in amplifier sensitivity, 20  $\mu$ V. The UV radiation source was a 600-W high-pressure xenon arc lamp. The infrared component of the lamp output was filtered by a continuous-flow water cell with optically flat fused-silica windows (optical pathlength = 16.5 cm). Monochromatic excitation, such as  $\lambda = 300$  nm, was obtained by inserting a Bausch and Lomb model 33-86-01 high-intensity monochromator with 5-nm entrance slit and 3-mm exit slit in the optical path. The linear dispersion of the monochromator was 3.2 nm/mm, so the bandwidth was 9.6 with these slits. The broad-band excitation was accomplished by merely removing the monochromator and leaving the infrared filter in place. Each of the EPR spectra was taken after irradiating the sample for approximately 5 minutes.

## 2. Spin Trapping of UV-Induced Free Radicals from Tyrosine by DMPO

Sample preparation was similar to that for the Trp/DMPO system. The irradiation settings were also the same,  $\lambda = 300$  nm and  $\lambda =$  broad. Tyrosine was obtained from Sigma Chemical Co. and used without further purification. The spectrometer operating parameters were the same as with Trp/DMPO except that the field-scan range was 3330-3430 Gauss and the amplifier time constant was 0.6 second. The sample was irradiated for 10 minutes prior to the EPR scan, and at the end of the scan it had been irradiated for 12.5 minutes.

## 3. Spin Trapping of UV-Induced Free Radicals from Human-Lens Protein; Water-Soluble Fraction

The human lens used in this experiment was from a 7-year-old male donor's eye obtained from the eye bank after the cornea had been removed for transplant surgery. The lens was homogenized with approximately 1 cm<sup>3</sup> of water and then centrifuged at 1500 rpm ( $g = 27,000$ ) for 7 minutes. Then 1 cm<sup>3</sup> of the supernatant was mixed with approximately 30  $\mu$ l of DMPO and transferred to the EPR aqueous cell with a disposable pipet. The EPR spectrometer operating parameters were the same as those used in the tyrosine/DMPO experiment, except phase adjustment on the lock-in amplifier was optimized to 335 degrees. The recorder setting for the X axis was 10 sec/in while the Y axis was 5 mV/in with the vernier dial at 40%.

## 4. Spin Trapping of UV-Induced Free Radicals from Human Lens Protein; Urea-Soluble Fraction

The precipitate of the centrifuged sample described in the preceding section (F 3) was dissolved in 8M urea (2 cm<sup>3</sup>), and the resultant mixture was recentrifuged at 1500 rpm ( $g = 27,000$ ) for 7 minutes. Approximately 30  $\mu$ l of DMPO was added to this mixture, shaken thoroughly, and transferred to the EPR aqueous cell via disposable pipet. The EPR instrument parameters were the same as those in Section F 3. The sample was irradiated for approximately 5 minutes at  $\lambda = 300$  nm before the field scan. The control run without the excitation light (ambient light) was negligibly free of artifactual signals.

5. Spin Trapping of UV-Induced Free Radicals from Human-Lens Protein; Urea-Insoluble Fraction

The precipitate of the recentrifuged sample obtained from the preceding section (F 4) was suspended in deionized water. Approximately 30  $\mu$ l of DMPO was added to the suspension, mixed thoroughly, and transferred to the EPR aqueous cell via a clean disposable pipet. The irradiation setting was broad band, as described in Section F 1. The EPR spectrometer operating parameters were the same as those described in Section F 3.

6. Spin Trapping of UV-Induced Free Radicals from Poly-DL-Tryptophan

To 2  $\text{cm}^3$  of the saturated aqueous solution of poly-DL-tryptophan of 1500 mol. wt., 15  $\mu$ l of DMPO was added. An aliquot of this mixture was transferred to the EPR aqueous sample cell with a disposable pipet. The irradiation wavelength was 300 nm, and the EPR spectrometer operating parameters were the same as those in section F 3. The EPR spectrum was taken after approximately 5 minutes of irradiation.

7. Spin Trapping of UV-Induced Free Radicals from Lysozyme and Poly-DL-Tryptophan; Irradiation Wavelength and Time Dependence of the Adduct Formation

Lysozyme was obtained from Dr. K. Yu of the Duke Department of Pediatrics (Div. of Pediatric Metabolism) and was used without further purification. Poly-DL-tryptophan was obtained from Sigma Chemical Co. (kept frozen at  $-4^\circ\text{C}$  until EPR experiment) and used without further purification. A saturated water solution of lysozyme mixed with 15  $\mu$ l DMPO was transferred to the EPR aqueous sample cell via a disposable pipet. The EPR spectrometer operating parameters were: field-scan range, 3330-3430 Gauss; field-scan rate, 8 Gauss/min; amplifier time constant, 0.6 sec; microwave frequency, 9.500 GHz; microwave power, 10 mW; modulation frequency, 100 kHz; modulation intensity, 1.3 Gauss (peak to peak); and lock-in amplifier sensitivity, 100  $\mu$ V. The UV radiation source was a 600-W high-pressure xenon arc lamp. The infrared component of the lamp was filtered by a continuous-flow water cell with optically flat fused-silica windows (optical pathlength = 16.5 cm). Monochromatic excitation, such as  $\lambda = 300$  nm, was obtained by inserting a Bausch and Lomb model 33-86-01 high-intensity monochromator with 5.00-mm entrance slit and 3.00-mm exit slit into the optical path. The bandwidth of the excitation light was 9.6 nm with these slits. The broad-band excitation (ca. 200-800 nm) was accomplished by removing the monochromator from the optical path but leaving the infrared filter in place. EPR spectra were taken as follows: Immediately after the sample was prepared, a spectrum was taken with the excitation lamp off; i.e., in the ambient room light. After this experiment, a shutter was placed in the optical path and the monochromator was inserted with the dial setting of  $\lambda = 300$  nm. The shutter was then opened and a few EPR spectra were taken after initial 2-minute exposures at 5-minute intervals. The nonmonochromatic excitation EPR spectra were taken similarly but without the monochromator. In the experiments performed during this period, we noticed that the rates of spin adduct formation were not uniform among the different samples. Although detailed and precise kinetic measurements were not done for each spin adduct, we recorded EPR spectra of a given sample/DMPO system at intervals of a few minutes starting from the onset of the UV irradiation.

The relative intensity among spin adduct spectra was obtained by comparing the signal intensities produced by the lowest field terminal transitions (LFTT). Identification of the free-radical species was based on the analysis of hyperfine splittings of the spin adduct spectra as described in Section III F. Also described in Section III F is the method of analyzing the relative intensities of the EPR signals from spin adducts by utilizing the LFTT.

8. Spin Trapping of UV-Induced Free Radicals from Some Aromatic Species in Ocular Proteins: Phenylalanine, Histidine, and N-Formyl Kynurenine; Irradiation Wavelength and Time Dependence of Adduct Formation

Phenylalanine and histidine (obtained from Dr. K. Yu of the Duke Department of Pediatrics) and N-formyl kynurenine (from Aldrich Chemical) were kept frozen at  $-4^{\circ}\text{C}$  until the EPR experiment. The EPR samples were prepared in the same way as those for lysozyme/DMPD (Section II F 7); also, the EPR spectrometer operating parameters were the same except that the field-scan rate was 40 Gauss/min and the lock-in amplifier sensitivity was 50  $\mu\text{V}$ . The UV irradiation source and the monochromator operating parameters were the same.

9. Spin Trapping of UV-Induced Free Radicals from Some Aliphatic Amino Acids: Glycine, Leucine, Methionine, and Aspartic Acid; Irradiation Wavelength and Time Dependence

The sources of glycine, leucine, methionine, and aspartic acid, as well as the EPR spectrometer operating parameters and UV irradiation parameters, were the same as those described in Section F 7.

10. Spin Trapping of UV-Induced Free Radicals from 8-Methoxy Psoralen (8-MOP), a Known Cataractogenic Drug

To a saturated solution of 8-MOP (the solubility of 8-MOP in water at  $25^{\circ}\text{C}$  is approximately  $1 \times 10^{-5}\text{M}$ ), 15  $\mu\text{l}$  of DMPD was added and mixed thoroughly. The resultant solution was immediately transferred to a fused-silica EPR aqueous sample cell with a disposable pipet.

EPR instrument operating parameters were the same as in Section F 7, except the recorder Y-axis setting was 50 mV/cm with the vernier at 80%.

The UV irradiation wavelength settings were: wide band (without the monochromator),  $\lambda = 320 \text{ nm}$ , and  $\lambda = 360 \text{ nm}$ . The former is the absorption maxima for some of the photo-oxidation products of tryptophan, while the latter is the phosphorescence excitation maximum for 8-MOP.

11. Spin Trapping of UV-Induced Free Radicals in Ribonuclease, a Protein Without Tryptophan

To a saturated aqueous solution of ribonuclease, 15  $\mu\text{l}$  of DMPD was added and mixed thoroughly. The resultant solution was immediately transferred to an EPR aqueous solution sample cell.

EPR parameters were the same as in Section II F 7; the UV irradiation settings were:  $\lambda = \text{wide band}$ ,  $\lambda = 290 \text{ nm}$ ,  $\lambda = 320 \text{ nm}$ , and  $\lambda = 360 \text{ nm}$ .

## G. Biochemical Analysis on UV-Irradiated Lens Crystallin Proteins

### 1. Preliminary Experiments with 2-Dimensional Gel Electrophoresis for Human-Lens Proteins

The determination of the best conditions for a 2-dimensional analysis of the lens proteins was investigated. Whole-cow-lens extract and four fractions of water-soluble lens proteins obtained from Sephadex G-200 gel chromatography were used as samples. Water-soluble and urea-soluble fractions from human lenses were also used.

Isoelectric focusing, which constitutes the separation of the sample in the first dimension, was performed in cylindrical gels (150-mm x 2-mm ID). Various voltages and time intervals were tested; the most successful run was obtained overnight at a constant voltage of 400 V. Under these conditions, and at a final concentration of 2% Ampholine (LKB Instruments, Inc.) in the gel, a linear pH gradient between the values of 4 and 8 was obtained. The pH gradient was determined by cutting the gel into 5-mm-long slices and extracting the Ampholine for 30 minutes in 0.5 ml distilled water. Little or no precipitation of the proteins was observed at the point of application, and all proteins in the sample focused within the pH range.

For the second dimension, different gel concentrations were tested. The separation was carried out at a constant value of 30 mA, and the length of the run was determined by the marker reaching the bottom of the slab. The final acrylamide concentration in the gel was 15% after the run.

### 2. Development of 2-Dimensional Electrophoretic Analysis of Lens Proteins and Their Fractions

To obtain optimal resolution of the subunits of the lens proteins, some modifications were introduced in the method reported by O'Farrel (34). The final acrylamide concentration in the isoelectric focusing gel (first dimension) was increased from 4% to 5% T (staining solution). This increase resulted in better polymerization and higher mechanical resistance of the gels and thus improved the reproducibility of the results. Furthermore, extraction time for measuring the pH gradient in the isoelectric focusing gels was increased to 2 hours at room temperature, resulting in a more accurate determination of the gradient.

For the second dimension, 15% T, 2.6% C stock solution of pancreatic DNase) acrylamide gel was chosen, but the pH of the gel buffer was lowered to 8.6 (from the original value of 8.8). This resulted in a slower migration of the protein subunits in the second dimension, giving better separation and therefore higher resolution of the various components. This method was used to analyze the lens crystallin proteins after the irradiation experiment.

### 3. Irradiation Experiment

The four protein fractions obtained after Sephadex G-200 chromatography (25) were exposed to UV light for different time periods. Each sample was diluted with distilled water to a final concentration of 20 mg/ml. The exposure was carried out in quartz semimicro cuvettes which are transparent to UV

light. Controls for each fraction, containing the same amount of protein as the exposed samples, were put in glass vials wrapped in aluminum foil and were placed behind the cuvetts with respect to the light source to ensure the same conditions (i.e., rise in temperature) except for UV exposure.

The light source was a Hanovia 1000-W xenon high-pressure arc lamp operated at 22 V and 38 A. The intensity of the light beam was measured with a pyroelectric radiometer (Laser Precision Corp. model RK-5100 and an RKP 545 probe). The intensity of the light beam impinging on the samples was 440 mW/cm<sup>2</sup>. A wide lamp beam was used to accommodate all four samples in the same plane in front of the lamp. The samples were irradiated for 2 and 4 hours and stored frozen prior to their use in the fluorescence and electrophoresis studies.

#### H. Fluorescence Study on UV-Irradiated Crystallin Proteins of the Lens

The emission spectra of the four samples were studied at excitation wavelengths of 295 and 360 nm. These values correspond to the excitation wavelengths of tryptophan and N-formyl kynurenine, respectively, and produce emission peaks at 360 and approximately 440 nm. The fluorescence spectra were obtained with an Aminco SPF-500 spectrofluorometer connected to an SPF-599 X-Y recorder. The final protein concentration was 0.2 mg/ml in 9M urea for all samples.

#### I. Photoacoustic Spectra of Human Cataractous Lens Nucleus Vs. Cortex

Immediately after its surgical removal, a 40-year-old nucleosclerotic lens was obtained from the Duke Eye Center and kept frozen until the PAS experiment. A Princeton Applied Research model 6001 PAS spectrometer was used. The light source was internally modulated; i.e., not with a mechanical chopper but with an intensity modulator (built into the power source) at 50 Hz. The spectral resolution was 8 nm. Other details of the PAS experiment are similar to those described by Lerman et al (5).

### III. RESULTS AND DISCUSSION

#### A. Intensity of EPR Signal from the Human Lens Vs. Irradiation Wavelength

The uncorrected and corrected plots of the EPR peak-to-peak intensities vs. wavelength are shown in Figure 1. The source (1000-W Xe arc lamp) correction shifts the maximum of the spectrum from about 300 nm to about 290 nm; it also adds intensity to the lower wavelength side of the maximum. The uncorrected spectrum is effectively the same as the phosphorescence excitation of tryptophan in the human lens given by Kurzel et al. (2), which is also uncorrected (Fig. 2a). Since these authors used the same irradiation source, the effect of the source correction should be similar. Neither of the uncorrected spectra in Figures 1a and 2a were influenced by the corneal absorption since the experiments were done with extracted lenses.

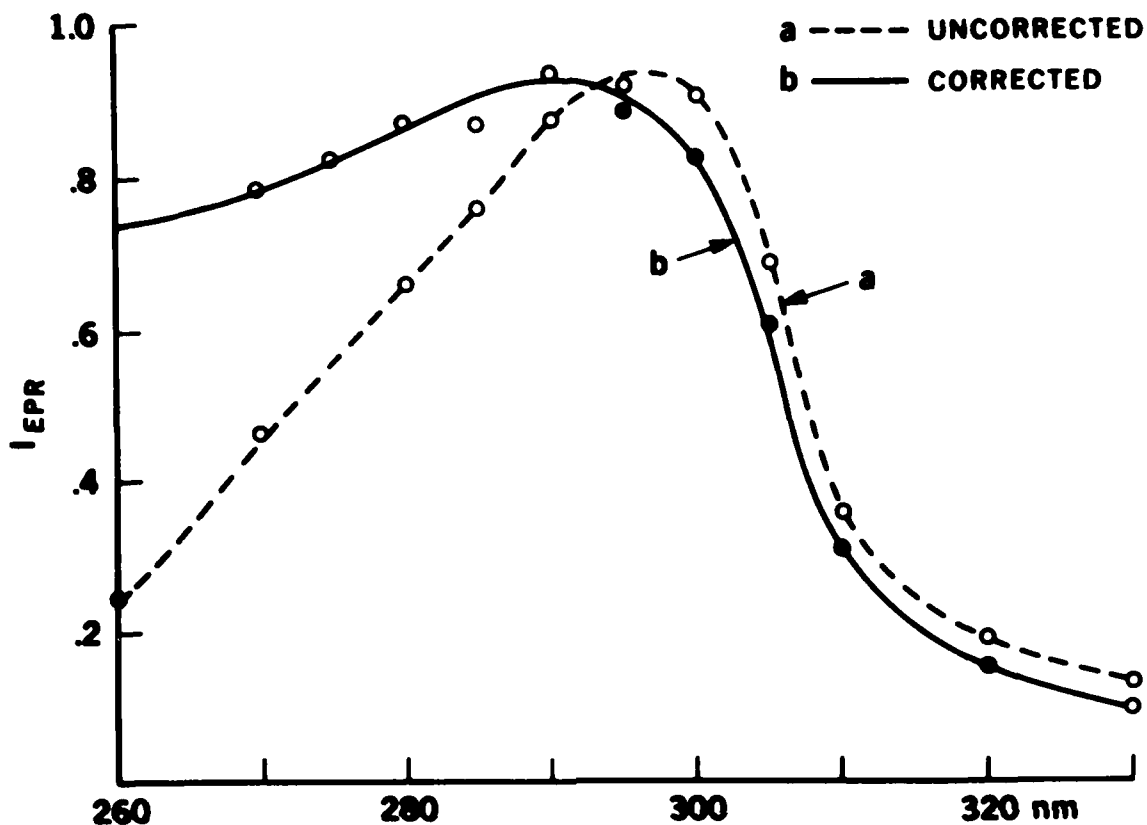


Figure 1. Corrected and uncorrected action spectra for free-radical formation in the human lens.

Bachem's action spectrum of UV-induced cataract (15), Figure 2b, on the other hand, was obtained from live-guinea-pig corneas and with a Hg arc lamp. The abrupt drop to the left of the maximum, which occurs near 300 nm, is most likely due to the corneal absorption, and the maximum at 300 nm may not be the true maximum because of (a) the corneal absorption concealing the true maximum and (b) the source correction effect. The portion of Bachem's spectrum unaffected by the corneal absorption (i.e., the right side of the maximum) closely resembles Figure 1.

These comparative studies suggest (a) UV-induced cataractogenesis in mammals, (b) the UV-induced triplet-state population via the intersystem crossing from the first excited singlet state, and (c) the UV-induced free radical formation occurring within the same region of UV-visible wavelengths. In vivo, the corneal absorption is always present, so any conjecture must take it into account. Further implications in view of previous data will be discussed in Section IV A.

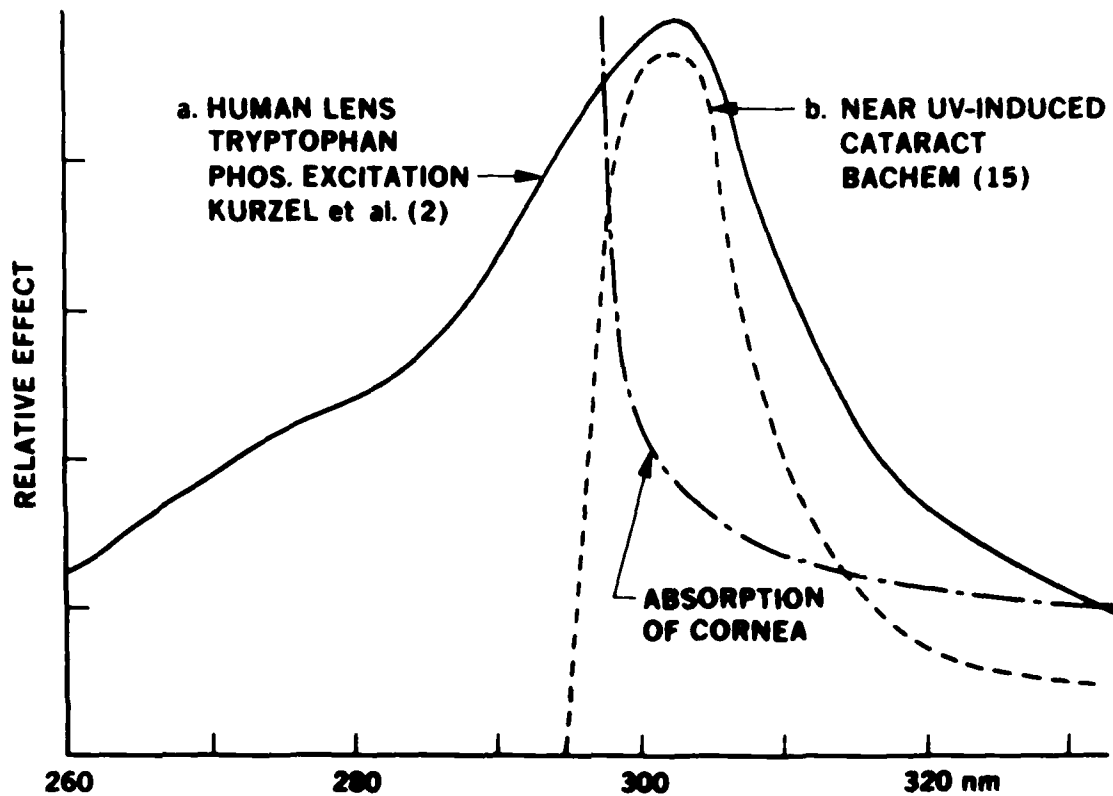


Figure 2. (a) Uncorrected phosphorescence excitation spectrum of tryptophan in the human lens (adopted from Kurzel et al.); (b) action spectrum of UV-induced cataractogenesis in guinea pigs (adopted from Bachem).

#### B. UV Radiation Dosage Measurement for the Marginally Detectable EPR Signal from the Human Lens

Experiments following the method described in Section II B indicated that a minimal dosage of  $0.05 \text{ mW/cm}^2$  produced a detectable EPR signal. This implies that in a human eye without a cornea,  $0.05 \text{ mW/cm}^2$  at  $290 \text{ nm}$  will produce free radicals in excess of  $10^{10}$  spins. (This is based on the assumption that the maximum achievable sensitivity of a high-quality spectrometer is about  $5 \times 10^9$  spins.) The EPR experiment was performed at liquid nitrogen temperature so that the free radicals would accumulate exponentially until saturation of the signal occurred. We assume that in vivo these free radicals would undergo chemical reactions of various types with functional groups in the ocular crystallin proteins. These chemical reactions are likely to include crosslinking between peptides. In the  $-196^\circ\text{C}$  EPR experiment, approximately 30 minutes must elapse before the signal is saturated. The dosage  $0.05 \text{ mW/cm}^2$  is for an extracted, transparent, young (16-yr-old) normal lens without the cornea; hence, in older or cataractous eyes with cornea, the minimum



irradiance for free-radical formation is expected to be considerably higher. We suggest the figure 0.05 mW/cm<sup>2</sup> only as a ballpark indicator. Its implications with regard to occupational safety is discussed in Section IV B.

### C. Intensity of EPR Signal from the Tryptophan Triplet State and Its Computer Fitting via a Theoretical Model

If the conjecture that a significant portion of the free radicals produced in the lens may be mediated via the triplet state of tryptophan, then the intensity vs. wavelength plot of the free-radical formation in the lens should agree with that of the tryptophan triplet-state formation. The EPR monitored peak-to-peak intensity vs. irradiation wavelength plot obtained using the method described in Section II C is shown in Figure 3. The triplet-state signal from free tryptophan exhibited  $\Delta M_S = \pm 2$  transitions at  $H = 1440$  Gauss with  $\gamma = 0.097$  GHz. The uncorrected plot of intensity vs. irradiation wavelength of this signal has a maximum at about 295 nm. The corrected maximum is at 285 nm; this value is correct for free tryptophan with neutral pH. If the peptide-bound tryptophan or the lens-protein-bound tryptophan (pH  $\approx 7.4$ )  $\Delta M_S = \pm 2$  EPR signal is monitored and subsequently plotted against irradiation wavelength, we expect a bathochromic shift of the maximum such that the maximum will be at about 290-295 nm. This remains to be confirmed at a later date, using the improved S/N capability of our spectrometer; hence, any inference derived only from our experiments to date, on the definite involvement of the tryptophan triplet state, is not yet conclusive. Additional discussion of the implications of the tryptophan triplet state appears in Section IV C. Note that the  $\Delta M_S = \pm 2$  transition is only one of the seven main transitions due to a single triplet-state species (the other six being  $\Delta M_S = \pm 1$  transitions). In randomly oriented samples (e.g., powders or glasses),  $\Delta M_S = \pm 2$  has the greatest transition moment because of the stationary resonance conditions at X-band microwave frequency (35). The field value of all seven major transitions can be computed if the zero-field splitting parameters D and E or the principal values of dipole-dipole interaction tensor X, Y, and Z are known along with the microwave frequency. For free tryptophan (as opposed to peptide-bound Trp),  $X = 0.0085$ ,  $Y = 0.0644$ ,  $Z = -0.0729$  cm<sup>-1</sup>, and  $\nu = 9.11 \times 10^9$  sec<sup>-1</sup>. The field value of the  $\Delta M_S = \pm 2$  triplet-state signal  $H_{\min}$  is predictable from

$$H_{\min} = (2g\beta)^{-1}[\delta^4 + 4(XY + XZ + YZ)]^{1/2} \quad [15]$$

$$= 1447 \text{ Gauss}$$

where  $\delta = \nu/c = 9.11 \times 10^9 \text{ sec}^{-1} / 2.9979 \times 10^{10} \text{ cm sec}^{-1}$

$$= 3.0387 \times 10^{-1} \text{ cm}^{-1}$$

The field value of  $H_{\min}$  differs slightly among published reports because resonance frequencies vary from 9.00 to 9.50 GHz.

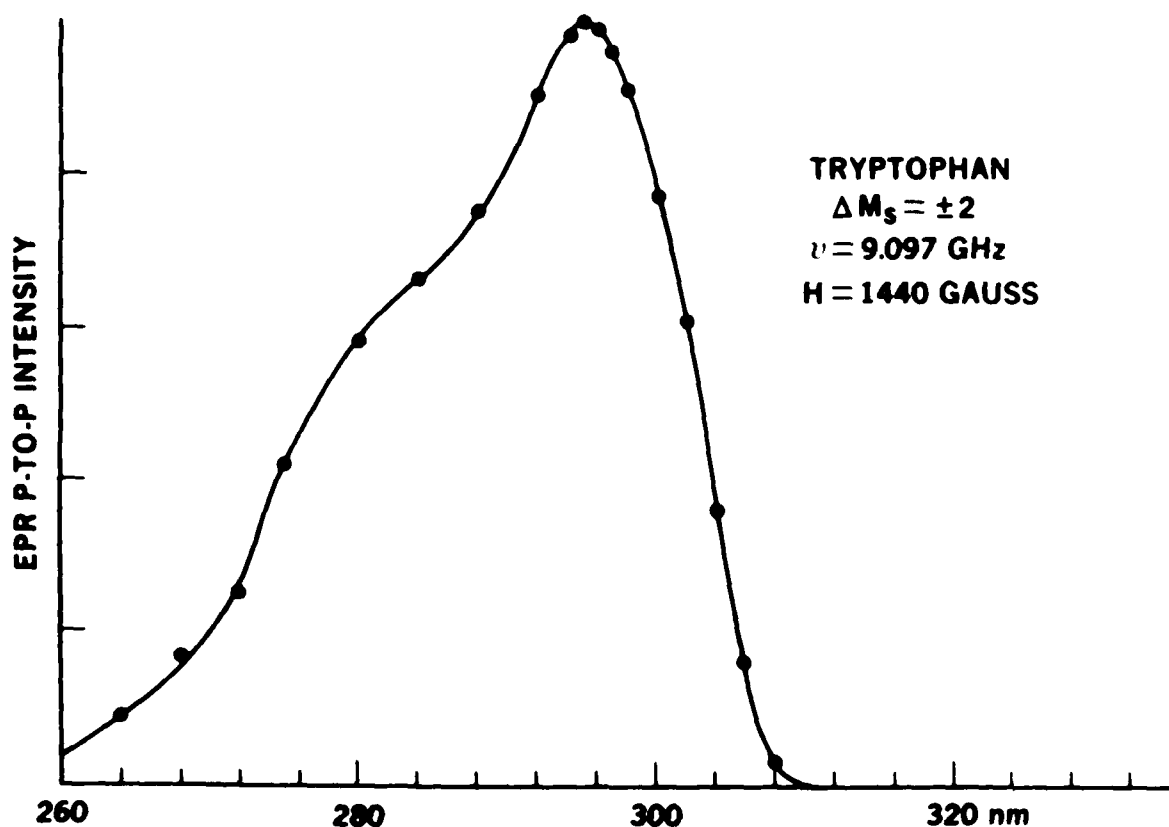
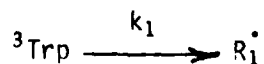


Figure 3. Irradiation-wavelength dependence of EPR signal intensity due to the UV-induced triplet state of tryptophan.

D. EPR-Monitored Kinetics of N-Formyl Kynurenine Triplet State and Its Computer Fitting via a Theoretical Model

The decay of the  $\Delta M_s = \pm 2$  triplet-state signal of N-formyl kynurenine was previously monitored by Yamanashi and Zuclich (20). A theoretical model in which the triplet state of kynurenine,  $^3\text{NFK}$ , plays a role as the intermediate species between the triplet tryptophan,  $^3\text{Trp}$ , and the UV-induced free-radical,  $R^\cdot$ , is described in Section II D. The experimental data and computer-fitted results are shown in Figure 4. The kinetic parameters, applicable to Eq. 8, were found to be  $k_j = 0.051$  and  $k_{ji} = 0.143 \text{ sec}^{-1}$ . The result of this fitting and the previous work on the decay of  $^3\text{Trp}$  and the buildup of  $R^\cdot$  in the lens (21) suggest the possibility that after the production of  $^1\text{Trp}$  and the production of  $^3\text{Trp}$  via the intersystem crossing, the following chemical reactions proceed:



[15]



where  $R_1^\cdot$  is the radical whose buildup rate is the same as the decay rate of  ${}^3\text{Trp}$ , and  $R_2^\cdot$  is another free-radical species, different from  $R_1^\cdot$ , which is produced via  ${}^3\text{NFK}$  as the reaction intermediate. In the following section, we examine the two component kinetics of the buildup of free radicals in the lens, cornea, and aqueous--all of which contain Trp. More evidence and implications on the involvement of NFK in the cataractogenic processes are discussed in Section IV D.

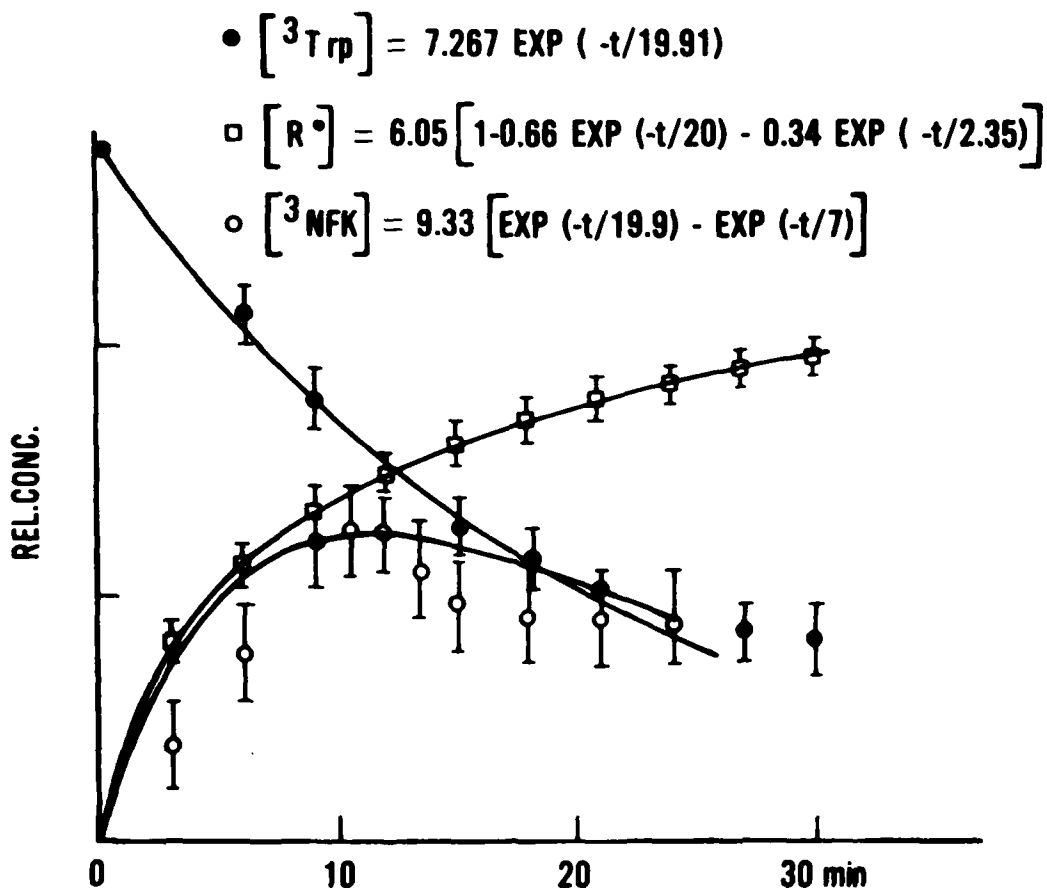


Figure 4. Comparison of the experimental irradiation time dependence of tryptophan-excited triplet state, free radicals, and NFK-excited triplet state. Solid lines are least-squares fittings according to theoretical expressions in Eqs. 12-14.

E. EPR-Monitored Kinetics of the Lens and Cornea; Computer Fitting of the Data via a Two-Component Kinetic Model

The EPR-monitored kinetics of free-radical formation in the human lens, following the method described in Section II E, is represented by the solid line in Figure 5. The computer fitting was performed according to the expression

$$dI/dH = M_1[1-\exp(-k_1t)] + M_2[1-\exp(-k_2t)] \quad [19]$$

Equation 19 assumes two main types of free radicals, where  $M_1$  and  $M_2$  are proportional to the concentration of the two radicals producing the free radicals. The ratio  $M_2/M_1$  gives the relation concentrations of the radical species even though the value of  $M_2$  (or  $M_1$ ) is arbitrary.

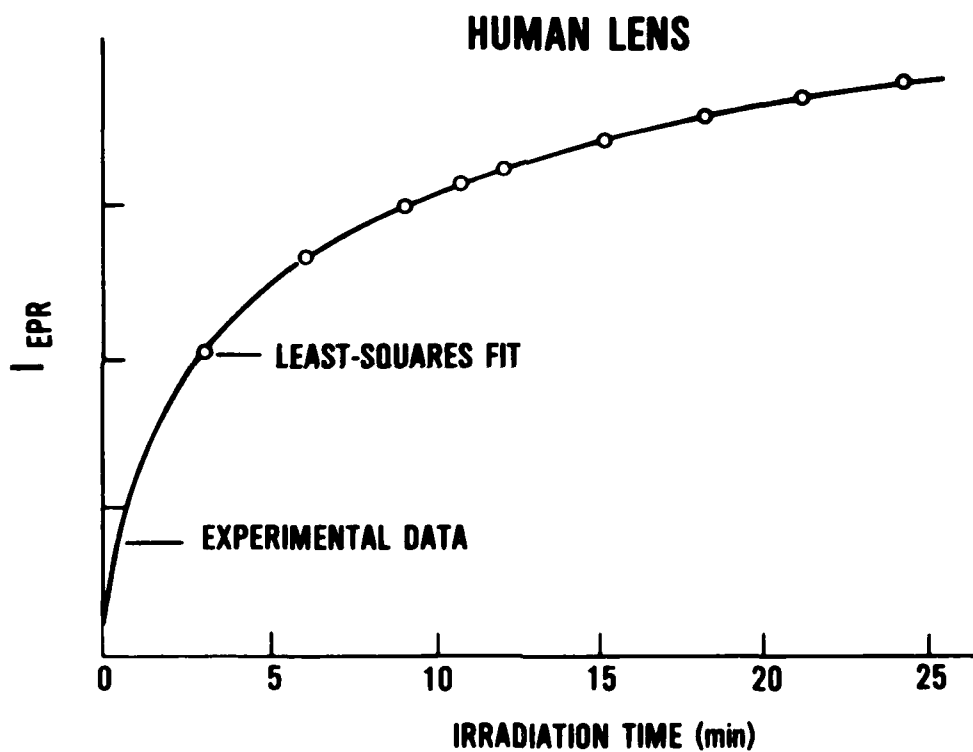


Figure 5. EPR-monitored kinetics of the free-radical formation in the human lens.  $I_{EPR}$  is the EPR signal intensity; the least-squares fit is based on the two-component exponential model. Kinetic parameters were obtained from this model.

The kinetic parameters obtained from the computer fitting of the human lens and cornea experiment are:

<u>Kinetic parameter</u>	<u>Human lens</u>	<u>Cornea</u>
$k_1$	$0.21 \pm .005 \text{ min}^{-1}$	$0.15 \pm .005 \text{ min}^{-1}$
$k_2$	$0.015 \pm .005 \text{ min}^{-1}$	$0.015 \pm .005 \text{ min}^{-1}$
$M_1/M_2$	$3.04 \pm .005$	$4.00 \pm .005$

Those obtained from the fitting of a similar experiment on the sublayers of a cow cornea are:

<u>Kinetic parameter</u>	<u>Cow epithelium</u>	<u>Stroma</u>	<u>Endothelium</u>
$k_1$	$0.71 \pm .005 \text{ min}^{-1}$	$0.71 \pm .005 \text{ min}^{-1}$	$0.58 \pm .005 \text{ min}^{-1}$
$k_2$	$0.06 \pm .005 \text{ min}^{-1}$	$0.06 \pm .005 \text{ min}^{-1}$	$0.69 \pm .005 \text{ min}^{-1}$
$M_1/M_2$	$2.10 \pm .005$	$3.30 \pm .005$	$2.00 \pm .005$

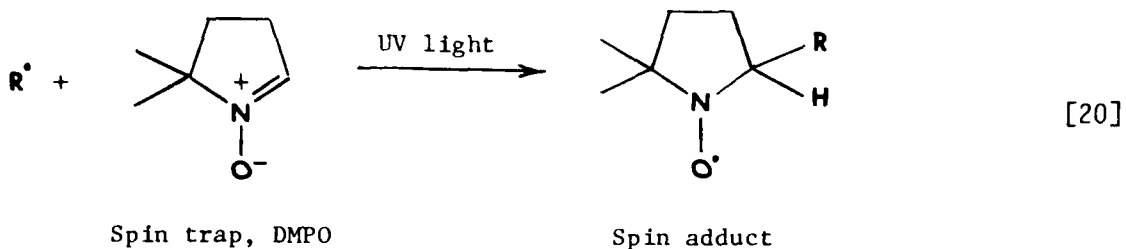
The lens and cornea data suggest that one of the main free-radical species produced (that associated with  $k = 0.015$ ) is common to both the lens and the cornea. The origin of this radical is likely to be proteins since the EPR intensity vs. wavelength data on the lens (this work) and on the cornea (as measured by Yamanashi et al., 33) yielded a maximum at 290 nm, and Trp in protein is the only species that possesses a corresponding  $s_1$  state.

The human- and cow-cornea data (i.e., a comparison of the whole human cornea to the cow stroma, a major portion of the cow cornea) exhibit somewhat different kinetic parameters. By contrast, an inspection of the human vs. rabbit data from a previous investigation by Yamanashi and Zuclich (20) shows similar kinetics. From these observations we can assume that the kinetics of free-radical formation may be correlated to the suggestion that the susceptibility of the lens to UV damage varies among animals (primates being more susceptible than cows). The influence of cataractogenic agents and protective enzymes on the kinetics of free-radical formation is discussed in Section IV E.

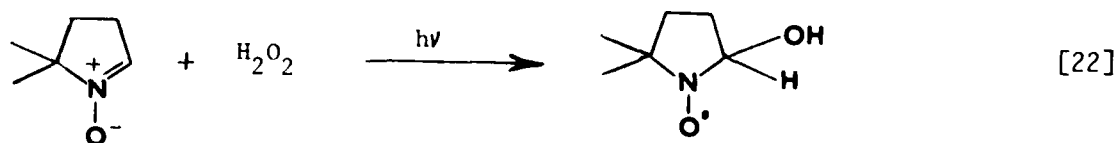
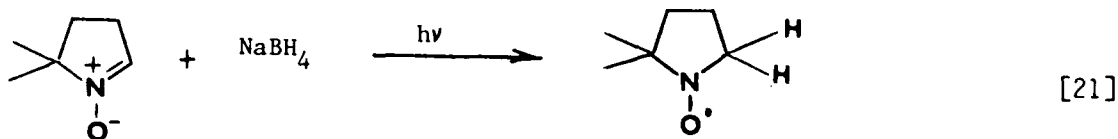
Our kinetic data and subsequent analysis via the two-component model do not rule out the possibility that lens proteins produce more than two types of free radicals. Because the g-value of most organic radicals is very close to the free electron value,  $g = 2.0023$ , we cannot distinguish free radicals on the basis of their g-values. In addition, the more polyatomic the radicals are, the less distinct their hyperfine splitting patterns become. In most macromolecular species, only a single broadened line due to the Zeeman interaction is observed since the hyperfine structure is obscured because of line overlap. Additional discussion of the kinetics of UV-induced free-radical formation is found in Section IV E.

F. Spin Trapping of UV-Induced Free Radicals in Human-Lens Proteins,  
Amino Acids, and Known Cataractogenic Molecular Species:  
Analysis of Hyperfine Splittings of Spin Adducts

Before presenting the result of DMPPO spin trapping of various lens-related materials, we briefly describe the chemical reaction involved in spin trapping and the method of analyzing the EPR spectra of the spin adduct.



In Eq. 20, the spin trap is DMPPO. Excitation of DMPPO with UV light causes the N,C double bond to be homolytically cleaved, and the short-lived radical  $R^\bullet$  is added to the 2 position of the ring, leaving the unpaired electron in the proximity of the oxygen. The interaction between this electron and any nuclei with nonzero spin angular momentum (contact hyperfine interaction), together with the interaction between the unpaired electron and the external field (Zeeman interaction), gives a typical spin-adduct spectrum with characteristic hyperfine splittings.



In Eq. 21, hydrogen atoms  $\text{H}^\bullet$  are produced and trapped by DMPPO; in Eq. 22, hydroxy radicals are produced and trapped. Figure 6 summarizes the analysis of hyperfine splittings obtained from these standard spin adducts. In the hydrogen atom adduct the unpaired electron interacts with two approximately equivalent (locationwise) protons to give a binomial-line intensity ratio of 1:2:1 with hyperfine splitting of  $a_{\text{H}} = 22/5$  Gauss. Each of these three is split into three others via the interaction of the unpaired electron with the nitrogen nucleus, with hyperfine splitting of  $a_{\text{N}} = 16.5$  Gauss. Hence the two parameters  $a_{\text{H}}$  and  $a_{\text{N}}$  account for the 9-line spectrum of the hydrogen atom adduct with DMPPO. In the phenyl radical adduct, the unpaired electron's interaction with five protons in the phenyl ring ( $\text{Ph} = \begin{array}{c} \text{HH} \\ | \\ \text{C}_6\text{H}_5 \\ | \\ \text{HH} \end{array} \text{H}$ ) is negligible;

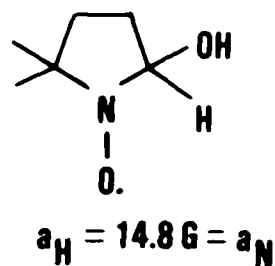
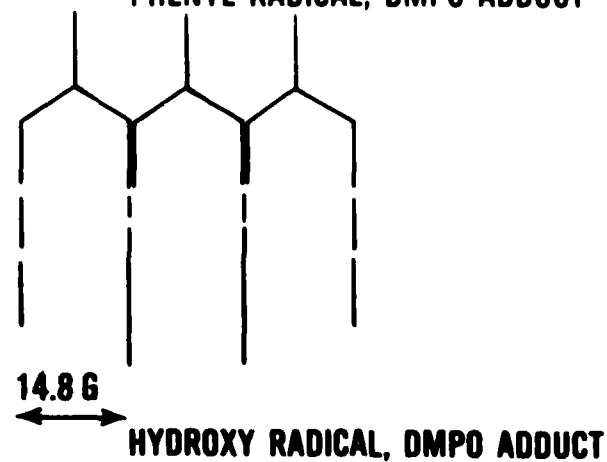
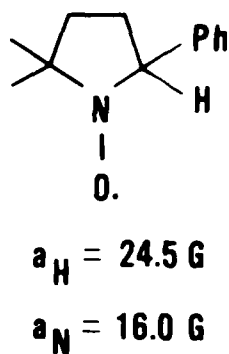
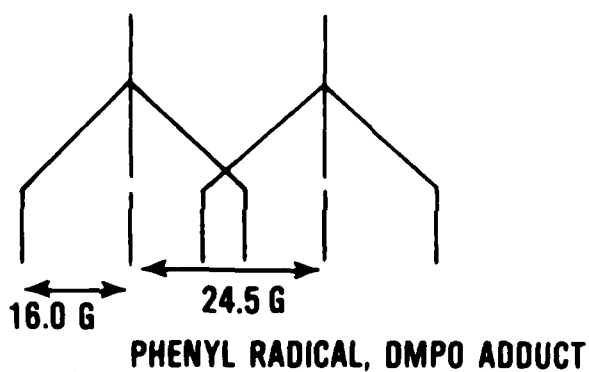
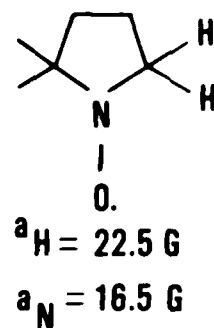
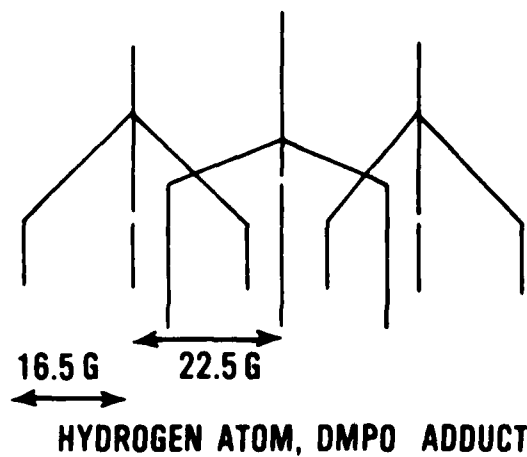


Figure 6. Hyperfine splitting analysis of standard spin adducts.

hence, the interaction with one proton nucleus gives rise to a binomial-line intensity ratio of 1:1 with hyperfine splitting of  $a_H = 24.5$  Gauss, each of which is split into three lines via the interaction with the nitrogen nucleus to give another hyperfine splitting of  $a_N = 16.0$  Gauss. All carbon-centered radicals exhibit similar 6-line spectra. Small differences in the values of  $a_H$  and  $a_N$  of various types of carbon radicals were reported by Janzen (36). However, the type of carbon-centered radicals cannot be positively identified on the bases of  $a_H$  and  $a_N$  alone because more than one type of carbon-centered radical may possess the same  $a_H$  or  $a_N$  values. In the case of the hydroxy radical, the magnitude of the two interactions (the unpaired electron with the nitrogen nucleus and that with the proton nucleus nearby) are indistinguishable, but one may rationalize the intensity ratio of this spectra (1:2:2:1) by assigning both  $a_H$  and  $a_N$  the same value of 14.9 Gauss. These standard adducts' hyperfine splittings will be used in the same analyses to follow.

#### 1. UV-Induced Free Radicals from Tryptophan

In Figure 7A, the EPR spectrum obtained from spin trapping by DMPD in tryptophan aqueous solution with  $\lambda = 300$ -nm irradiation is compared with that obtained under broad-band irradiation which covers approximately 200-800 nm. Analysis of the broad-band spectrum yielded two types of radicals from this 15-line spectrum, based on Figure 7B. Nine lines result from hydrogen atom adduct with an intensity ratio of 1:1:2:1:2:1:2:1:1 and with two hyperfine splitting parameters,  $a_H = 20.0$  Gauss and  $a_N = 15.0$  Gauss. Six lines arise from a carbon-centered radical with an intensity ratio of 1:1:1:1:1:1 and with two hyperfine splitting parameters,  $a_H = 19.8$  Gauss and  $a_N = 13.8$  Gauss (Fig. 7B). The control run with the light source off (ambient light) did not yield a significant spectrum. We may tentatively conclude that (a) under nonmonochromatic, broad-band UV-visible radiation, at least two types of radicals are produced in tryptophan: hydrogen atoms and carbon-centered radicals; and (b) under monochromatic radiation with  $\lambda = 300$  nm, where the  $g = 2.003$  radical is maximally produced, the ratio of the concentration of the hydrogen atom to that of the carbon-centered radical is less than the same ratio obtained under broad-band excitation. DMPD spin trapping of tryptophan at  $\lambda = 300$  nm (the uncorrected maximum for free-radical production in the lens) produced carbon-centered and hydrogen radicals within 5 minutes. When  $\lambda = 290$  nm (the corrected maximum for free-radical production in the lens) was used, the results shown in Figure 7C indicate the presence of hydrogen and hydroxy radical adducts (as observed at  $\lambda = 300$  nm) but no carbon-centered radical adduct. Hyperfine splitting parameter values and their analyses are indicated in Figure 7D.

Figure 7E shows the EPR spectrum of the DMPD adducts formed in tryptophan after 20 minutes of irradiation at  $\lambda = 320$  nm (the absorption maximum of the tryptophan photo-oxidation product, N-formyl kynurenine). The main quartet splitting indicates an oxygen-centered radical such as hydroxide,  $-\dot{O}H$ , or hydroperoxide,  $-\dot{O}OH$ ; however, whether or not the  $-\dot{O}OH$  radical species is unequivocally produced requires further confirmation. In contrast to the  $\lambda = 290$ -nm experiment, the experiment conducted at  $\lambda = 300$  nm produced a negligible amount of  $-\dot{H}$  or  $-\dot{C}$  radicals.



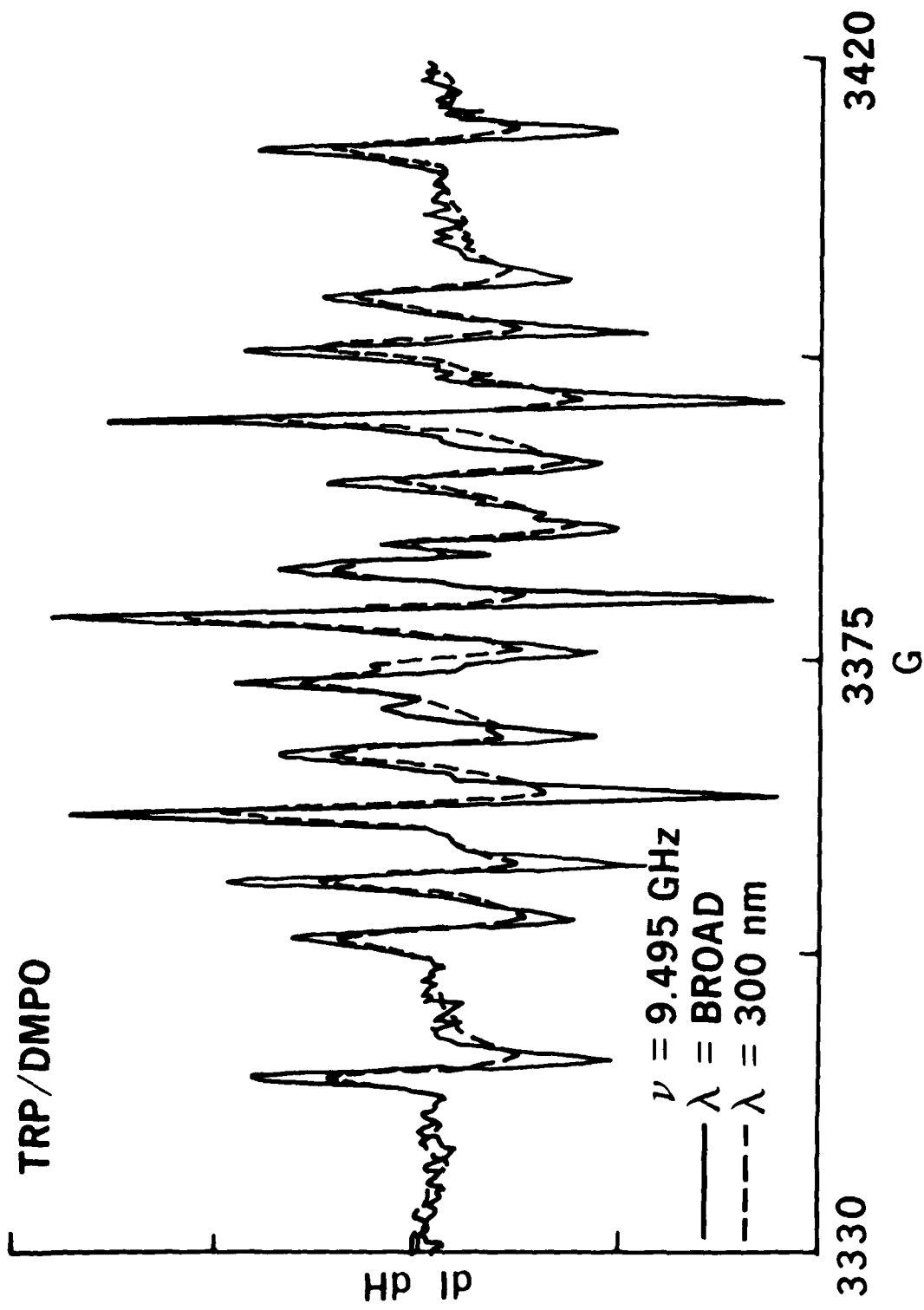


Figure 7A. Spin trapping EPR spectrum of UV-induced free radicals in tryptophan aqueous solution with DMPO; monochromatic and broad-band irradiation.

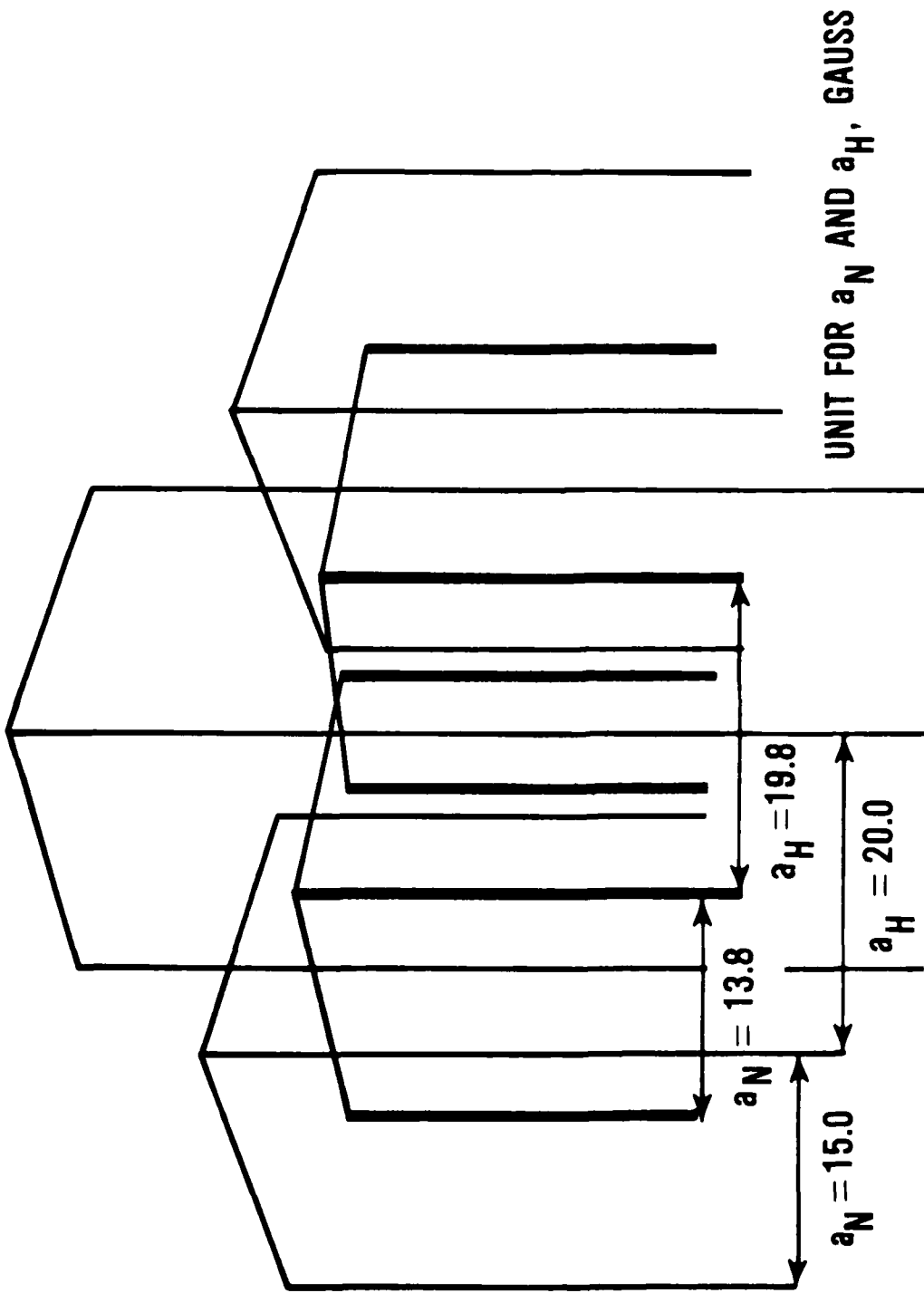


Figure 7B. Analysis of tryptophan/DMPD spin trapping spectrum (Fig. 7A) showing 9-line hyperfine splitting from the hydrogen-atom adduct and 5-line hyperfine splitting from the carbon-centered-radical adduct.

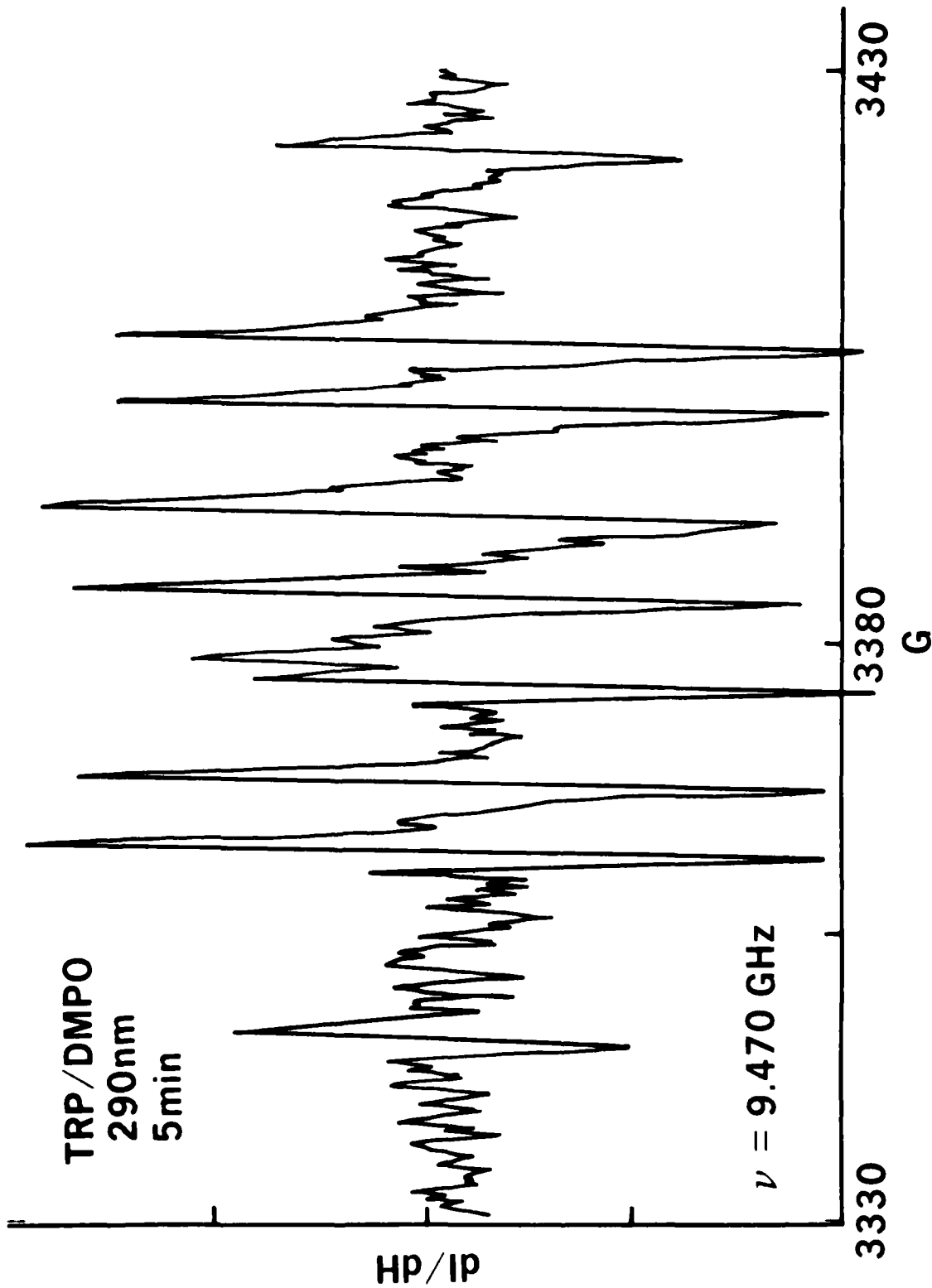


Figure 7C. EPR spectrum obtained from aqueous tryptophan and DMPO irradiated at 290 nm for 5 minutes.

## TRP/DMPO SPECTRAL ANALYSIS

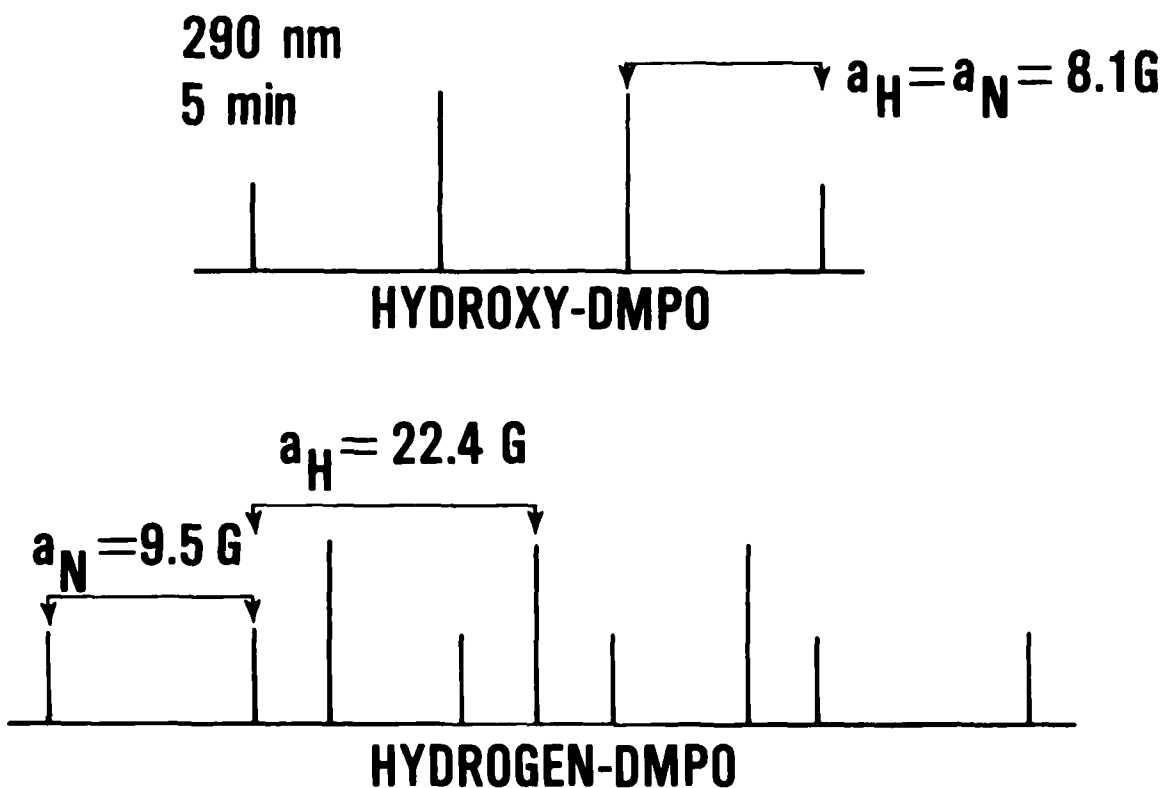


Figure 7D. Analysis of spectrum in Figure 7C, indicating the presence of hydroxy and hydrogen radicals trapped by DMPO; hyperfine splitting parameters are also shown.

### 2. UV-Induced Free Radicals from Tyrosine

Figure 8 shows the EPR spectra obtained from spin trapping in tyrosine aqueous solution with monochromatic radiation at  $\lambda = 300$  nm and with broad-band irradiation. The spectrum obtained under broad-band irradiation consists of 15 lines, whereas that obtained with monochromatic radiation at  $\lambda = 300$  nm has only nine lines. The apparent complexity of these spectra may be resolved by assuming that the 15-line broad-band spectrum consists of three different radical adducts: namely, the hydrogen atom adduct with a 9-line spectrum having hyperfine splitting parameters,  $a_H = 20.0$  Gauss,  $a_N = 15.0$  Gauss, and an intensity ratio of 1:1:2:1:2:1:2:1:1; the carbon-centered radical adduct with a 6-line spectrum with hyperfine splitting parameters,  $a_H = 19.8$  Gauss,  $a_N = 13.8$  Gauss, and an intensity ratio of 1:1:1:1:1:1; and the hydroxy radical adduct with a 4-line spectrum with hyperfine splitting parameters,  $a_H = a_N = 13.2$  Gauss, and an intensity ratio of 1:2:2:1, which superposes over 4 of the 9 hydrogen adduct lines. Since our EPR spectrum is

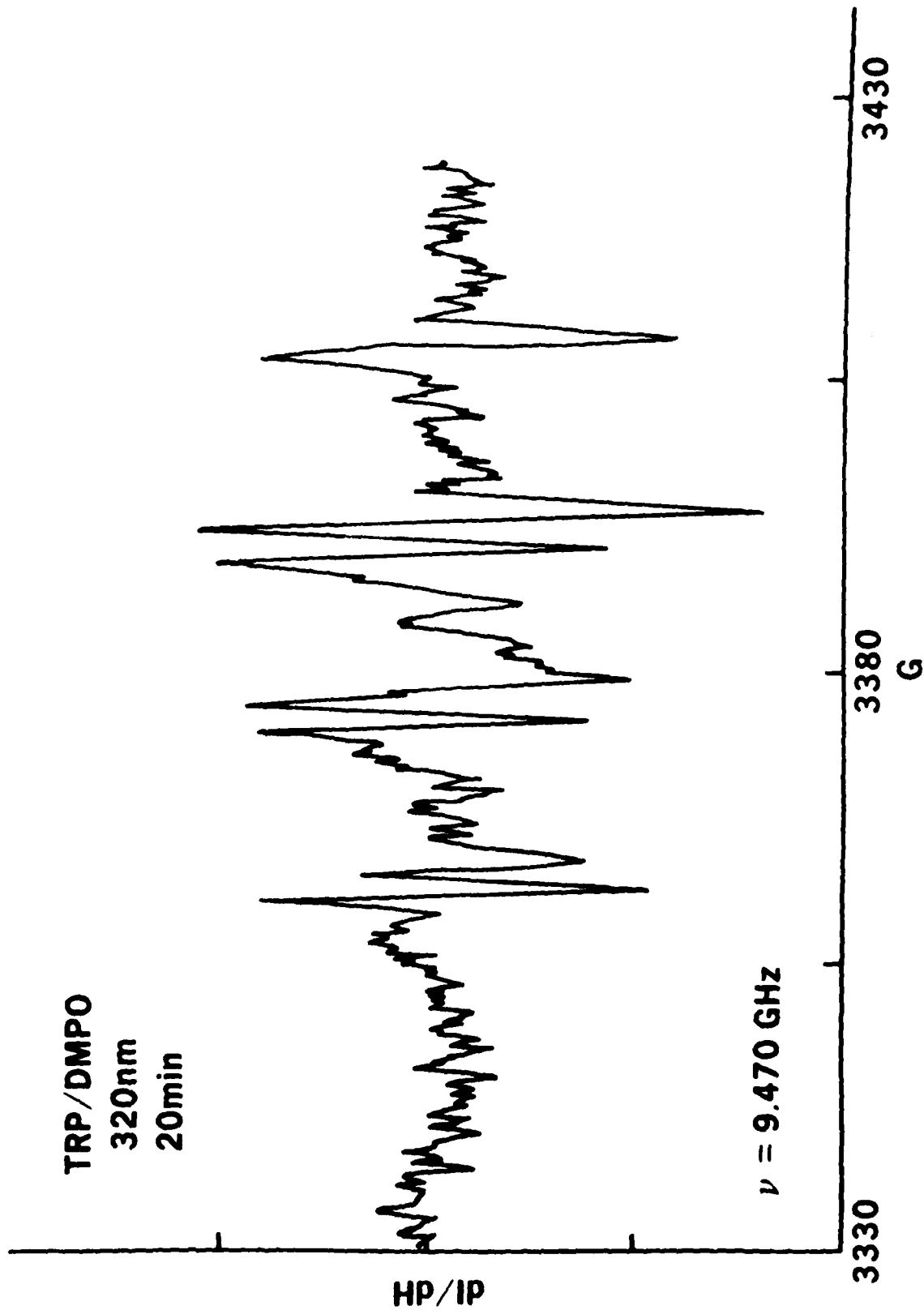


Figure 7E. EPR spectrum of radicals trapped by DMPO in an aqueous solution of tryptophan irradiated at 320 nm for 20 minutes. Note the absence of hydrogen radical adduct hyperfine splittings.

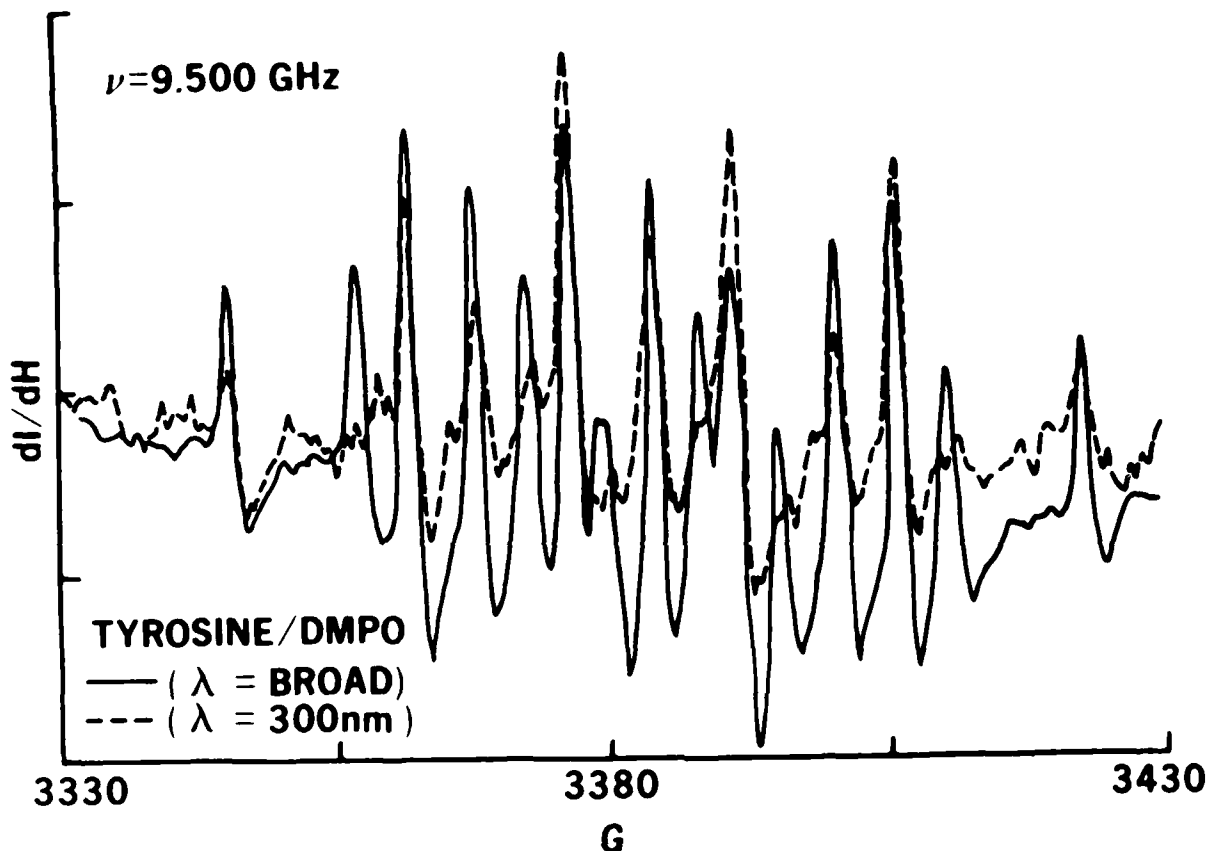
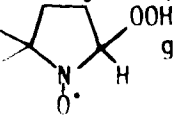


Figure 8. EPR spectrum from spin trapping of UV-induced free radicals in tyrosine aqueous solution by DMPO with monochromatic 300-nm and broad-band irradiation.

the first derivative of the absorption spectrum, a minor shift of a few Gauss occurs when this superposition takes place within the scan range. From this analysis of the tyrosine/DMPO system in aqueous solution, we can tentatively conclude the following:

- (a) In the UV-visible irradiation of tyrosine at least three types of free radicals are produced: hydrogen atoms, hydroxy radicals, and carbon-centered radicals. The identity of the carbon-centered radical remains to be determined.
- (b) The difference between the monochromatic spectrum ( $\lambda = 300 \text{ nm}$ ) and the broad-band excitation spectrum, based on this analysis, is that in the former the concentration of the carbon-centered radical is negligible.

(c) Peroxy radicals may be produced in this tyrosine/DMPO system; however, the spin adduct  gives an identical spectrum to that of the hydroxy radical adduct and hence is not distinguishable with the DMPO trap.

### 3. UV-Induced Free Radicals from the Water-Soluble Human-Lens Protein Fraction

In Figure 9 the EPR spectrum obtained from spin trapping in the human lens water-soluble protein by DMPO (under broad irradiation) is contrasted with the spin adduct spectrum obtained from that of the tyrosine/DMPO system under monochromatic irradiation,  $\lambda = 300$  nm. Although degraded by the low concentration of the sample and, hence, poor signal-to-noise ratio, the EPR spectrum is in good agreement with that of tyrosine/DMPO at  $\lambda = 300$  nm. The spectra suggest the presence of hydroxy radicals and hydrogen atoms, with the former in relative abundance. We do not wish, at this time, to exclude the presence of other radicals that we may not be able to see in these spectra due to their extremely low concentration. Crystallin lens proteins such as  $\alpha$ ,  $\beta_H$ ,  $\beta_L$ , and  $\gamma$  are presumably present in this sample; hence, the spin adducts may be produced from some of these crystallin proteins or from smaller peptides.

### 4. UV-Induced Free Radicals from the Urea-Soluble Human-Lens Protein Fraction

Figure 10 represents the comparison between the spin adduct EPR spectrum obtained from the human lens protein urea-soluble fraction/DMPO mixture and that of tyrosine/DMPO mixture under monochromatic irradiation at  $\lambda = 300$  nm. Noticeable here is the presence of hyperfine splittings due to carbon-centered radicals in the urea-soluble human lens protein. In tyrosine these were observed under broad-band excitation (cf. Fig. 6), but not under monochromatic excitation at  $\lambda = 300$  nm. We may, therefore, suggest that even though the spin adduct spectrum of the urea-soluble lens protein resembles that of the tyrosine/DMPO spectrum, the source of some of the radicals, such as the carbon-centered radical, may or may not be tyrosine in the peptide chain, but perhaps some other molecular species in the chain.

At least three different types of radicals--hydrogen atoms, hydroxy radicals, and carbon-centered radicals--are produced and trapped by DMPO in the monochromatically irradiated urea-soluble human-lens protein fraction. Again, radical species that DMPO is not capable of trapping should not be excluded from the list of possible radicals.

### 5. UV-Induced Free Radicals from Urea-Insoluble Human-Lens Protein Fraction

Figure 11 illustrates the EPR spin adduct spectrum obtained from the urea-insoluble fraction of the human-lens protein under broad-band irradiation. A comparison with the spectrum of the tryptophan/DMPO mixture suggests that in the water suspension of this urea-insoluble lens protein fraction, at least two free-radical species--hydrogen atoms and carbon-centered radicals--are produced, based on the tryptophan spectrum analysis. The similarity and the coincidence of the hyperfine splittings do not warrant an identity of the

radical sources; however, we now know some of the identities of the UV-produced radicals.

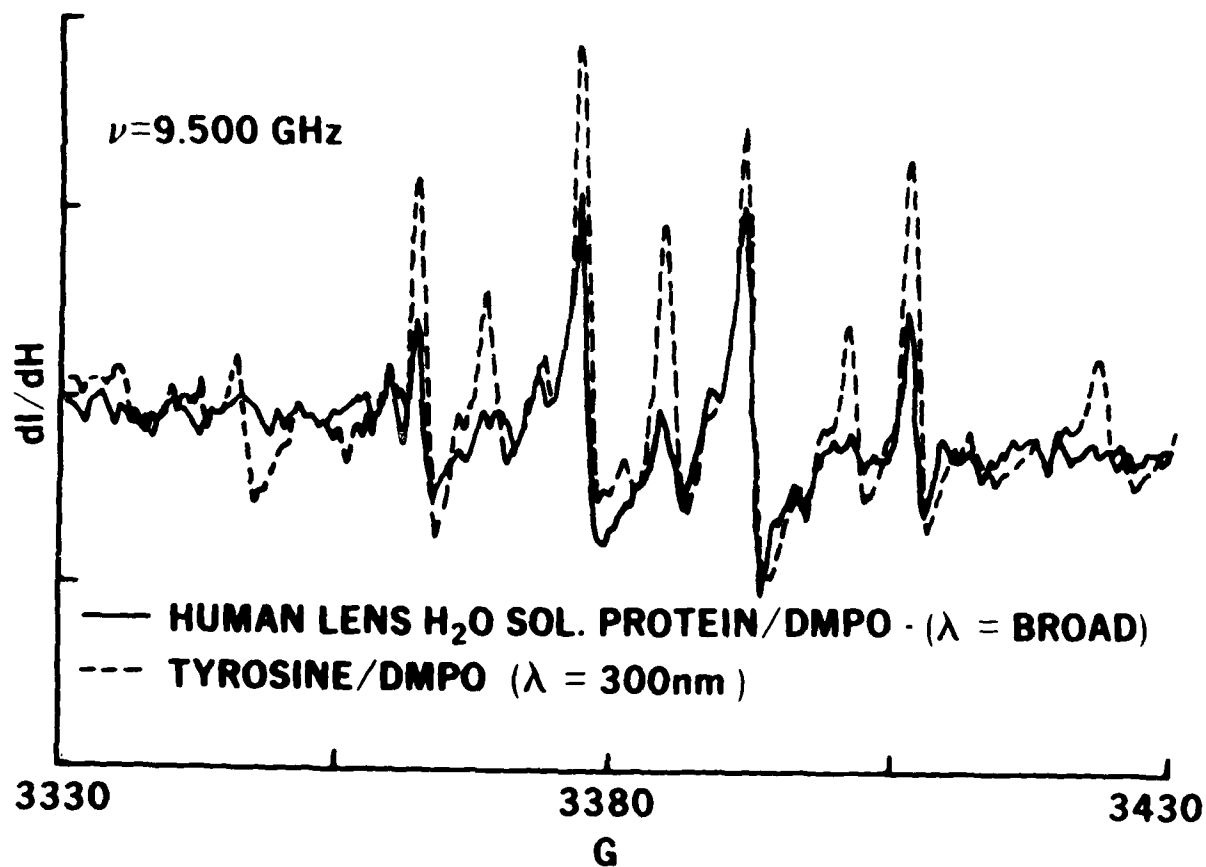


Figure 9. EPR spectrum obtained from spin trapping UV-induced free radicals in the water-soluble fraction of the human lens protein, compared with that obtained from tyrosine/DMPO aqueous solution.



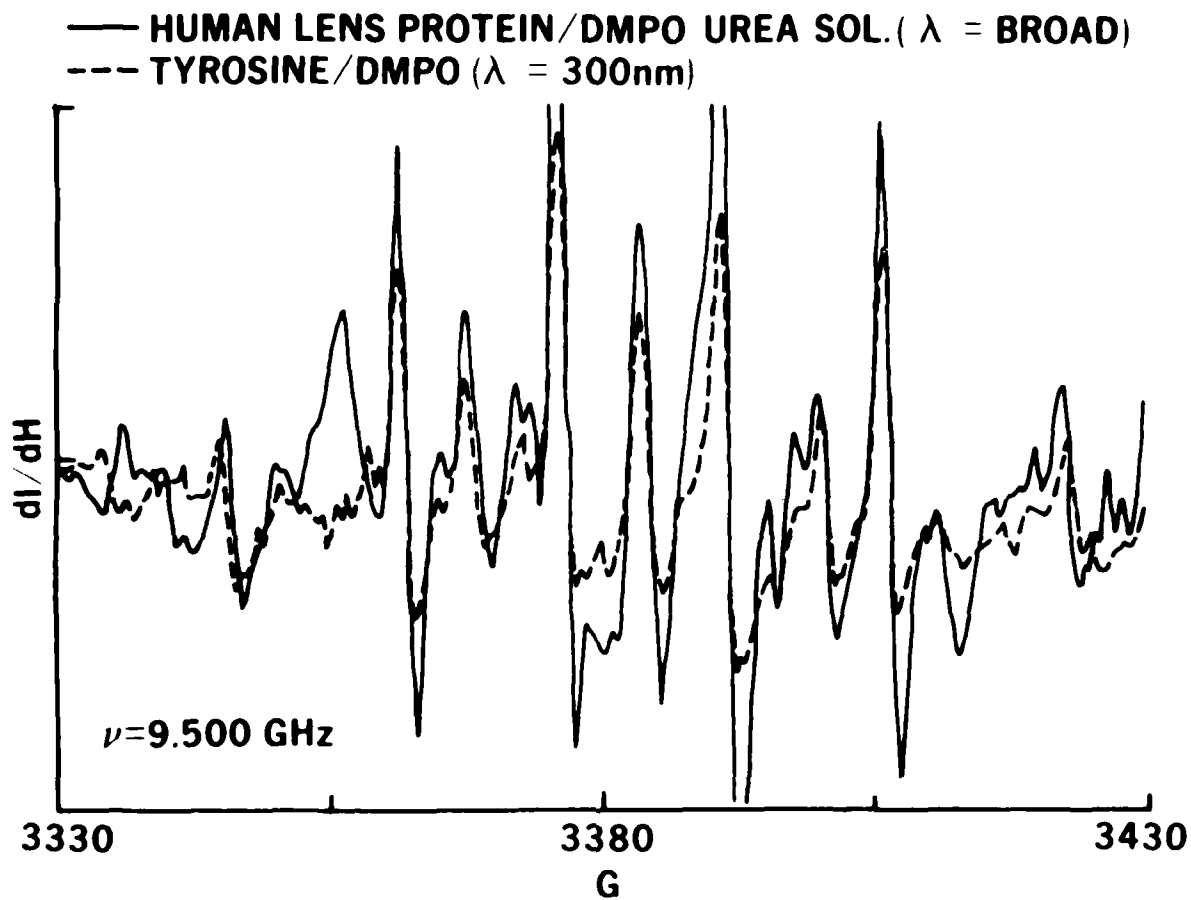


Figure 10. EPR spectrum obtained from spin trapping UV-induced free radicals in the urea-soluble fraction of the human-lens protein, compared with that obtained from tyrosine/DMPO aqueous solution.

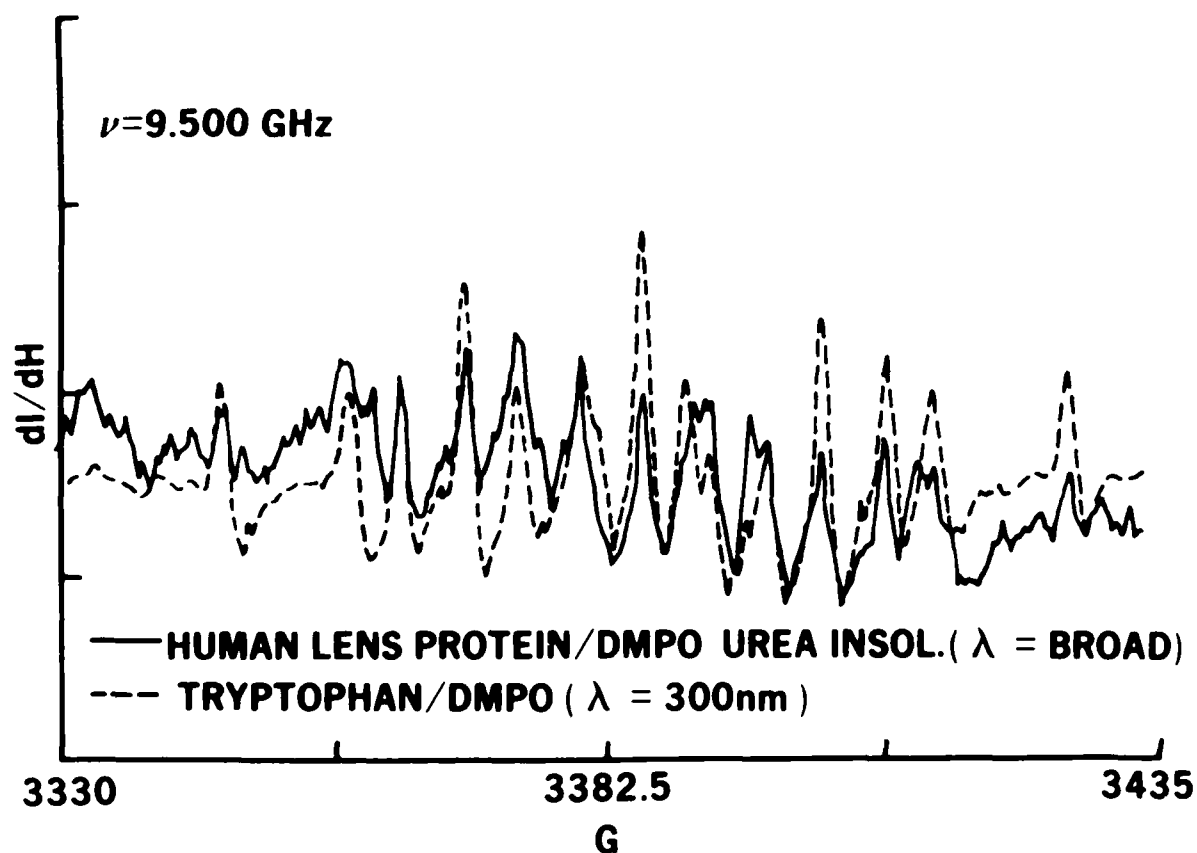


Figure 11. EPR spectrum obtained from spin trapping UV-induced free radicals in the urea-insoluble fraction of human-lens protein, compared with that obtained from tryptophan/DMPO aqueous solution.

#### 6. UV-Induced Free Radicals from Poly-DL-Tryptophan

In Figure 12 an EPR spectrum of a monochromatically irradiated ( $\lambda = 300 \text{ nm}$ ) sample of a poly-DL-tryptophan/DMPO mixture is compared with one from a tryptophan/DMPO solution. Both spectra have 15 lines, and the field range of these spectra are the same. However, there is variation in the line positions of some of the lines toward the center of the EPR spectrum. A careful comparison between Figure 12 and Figure 8 (tryosine/DMPO) suggests that in the poly-DL-tryptophan, hydroxy radicals are produced in addition to carbon-centered radicals and hydrogen atoms.

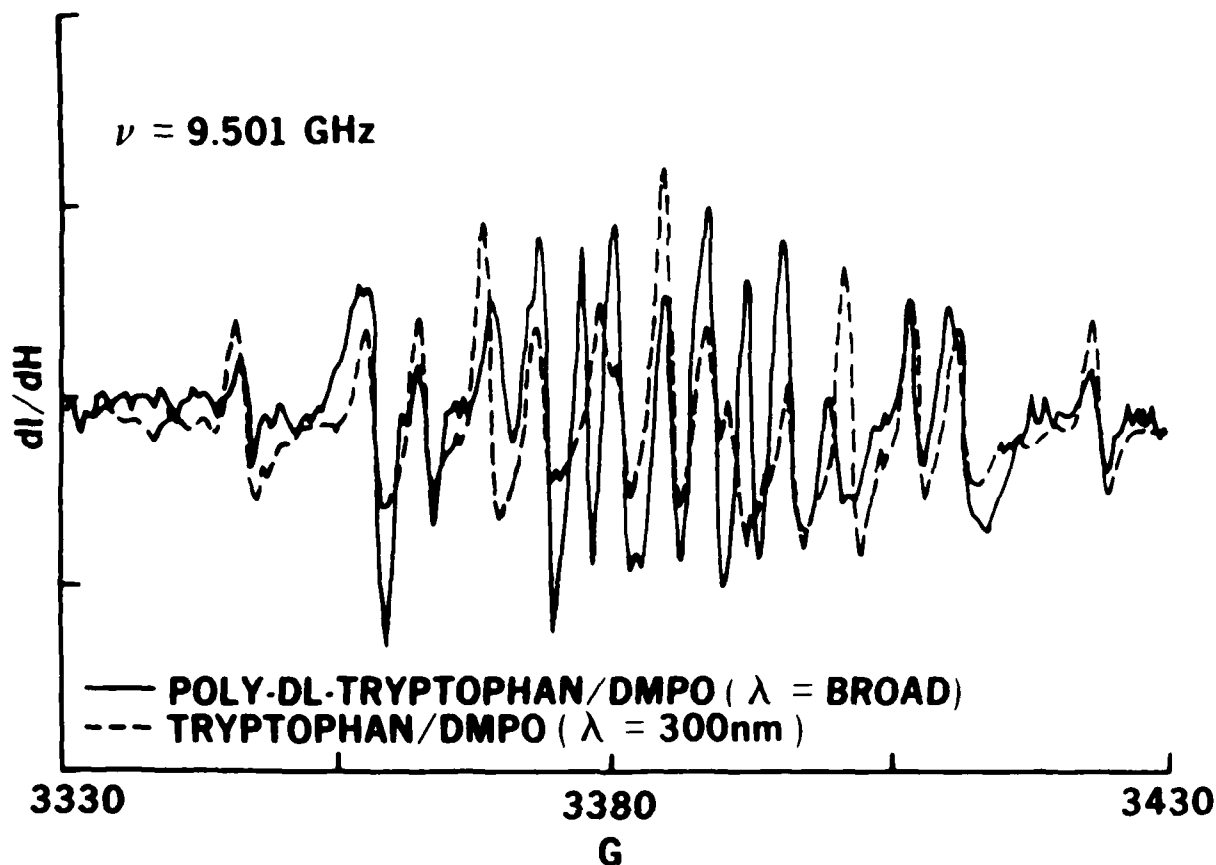


Figure 12. EPR spectrum obtained from spin trapping UV-induced free radicals in the poly-DL-tryptophan/DMPO solution, compared with that obtained from tryptophan/DMPO solution.

7. UV-Induced Free Radicals from Lysozyme and Poly-DL-Tryptophan; Time and Wavelength Dependence of Spin Adduct Formation with DMPO

We selected lysozyme as an example of a noncrystallin protein. It has a molecular weight of  $14,400 \pm 100$  and is found in tears, nasal mucus, milk, saliva, and blood serum and is known to possess antibiotic properties. In terms of molecular weight, it is comparable to  $\gamma$ -crystallin protein of the lens. However, the rationale for our selection of lysozyme was simply to compare how the free-radical species and the parameters related to their production under UV irradiation compare with those in the lenticular crystallin proteins. (Our lens fraction homogenates are a mixture of crystallin proteins.) The water- and urea-soluble fraction contains  $\alpha$  (MW  $\sim 800,000$ ),  $\beta_H$  (MW  $\sim 400,000$ ),  $\beta_L$  (MW  $\sim 200,000$ ), and  $\gamma$  (MW  $\sim 20,000$ ) crystallin proteins and smaller peptides, whereas the urea-insoluble fraction contains albuminoids (a combined term for proteins with MWs in excess of  $10^6$ ) in addition to all four of the crystallin proteins.

We selected polytryptophan peptide (MW ~ 13,000) to compare its free radical production under UV irradiation with that of free tryptophan and of ocular crystallin protein mixtures that contain tryptophan. If the "energy sink" hypothesis\* is operative, it should exhibit very similar free-radical production parameters (e.g., free-radical species, relative concentrations, irradiation-time dependence, and wavelength dependence of emission). Figure 13 illustrates the method of using the lowest field terminal transitions (LFTT) to compare the relative intensities of two different and overlapping signals that possess hyperfine splittings.

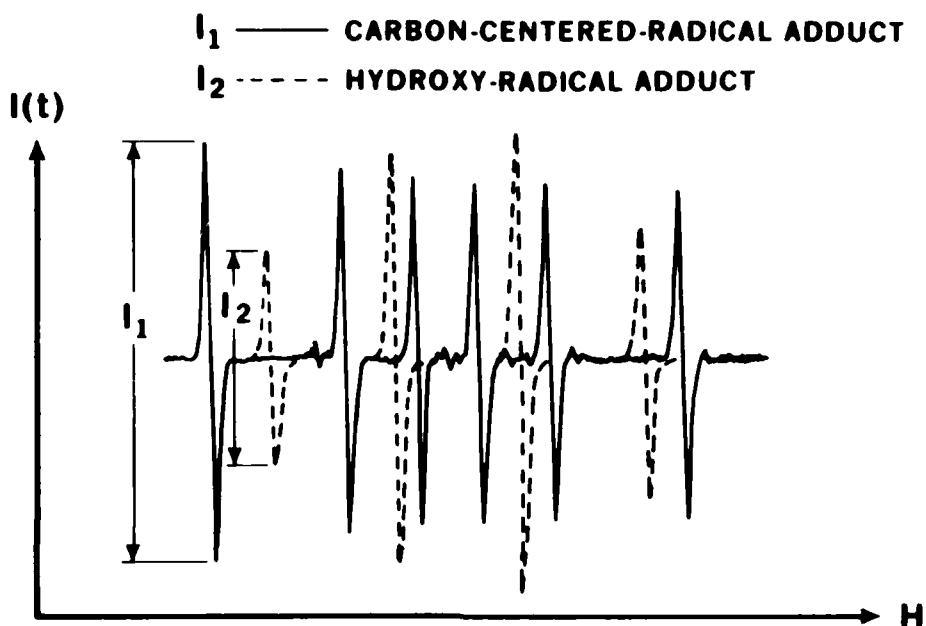


Figure 13. Relative intensity via low-field terminal transition (LFTT). The relative intensities are determined of two irradiation-time-dependent EPR spin trapping spectra. The carbon-centered-radical DMPO adduct diminishes with irradiation time, and the hydroxy-radical DMPO adduct increases.

Lysozyme/DMPO--Figure 14 shows the EPR spectrum of free radicals trapped with DMPO in UV-irradiated lysozyme. Negligible amounts of hydroxy radicals and carbon-centered radicals were detected in the absence of excitation light (ambient light). However, after the excitation light was turned on, only EPR transitions due to hydrogen atoms and carbon-centered radicals persisted. Except for the relative intensity for each radical, this spectrum is identical to that of tryptophan. As shown in Table 1, no radical species difference was observed between  $\lambda = 300$  nm and  $\lambda = 200-800$  nm. However, there was a

\*Energy sink hypothesis: Electronic excitation energy in a protein (peptide) is funneled to the lowest electronic state within the peptide; hence, in a regular peptide, to the lowest triplet state of tryptophan. Free radicals are assumed to be produced from this species.

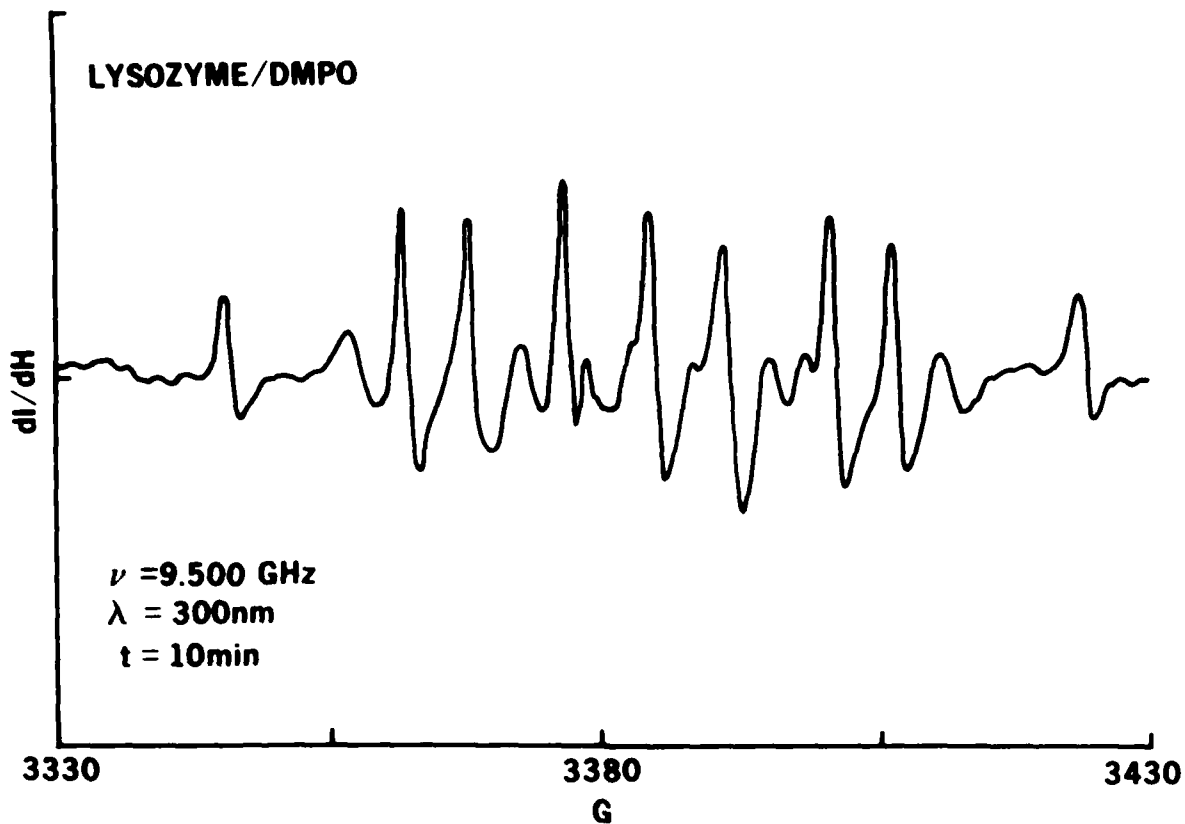


Figure 14. EPR spectrum of free radicals trapped with DMPO in lysozyme, monochromatically irradiated at 300 nm for 10 minutes.

TABLE 1. RELATIVE INTENSITY OF LOW-FIELD TERMINAL TRANSITION (LFTT) IN HYPERFINE SPLITTING OF DMPO SPIN ADDUCT FROM LYSOZYME

Excitation wavelength (nm)	Irradiation time (min)	Type of spin adduct		
		Relative intensity of LFTT		
		Hydrogen atom	Hydroxy	Carbon-centered
Light off 300	-	-	0.3	0.6
	2	1.8	-	1.0
	10	1.7	-	1.1
	17	2.6	-	0.9
200-800	2	0.6	-	0.6

pronounced negative effect of the broad-band irradiation on both the hydrogen-atom and the carbon-centered radical adduct concentrations. Under monochromatic irradiation ( $\lambda = 300$  nm), only the hydrogen-atom adduct concentration increased (by 40% in 15 minutes) with respect to the irradiation time, whereas the concentration of the carbon-centered radical effectively remained constant.

Poly-DL-Tryptophan/DMPO--As indicated in Table 2, the detectable free-radical species in the poly-DL-tryptophan/DMPO system are the same as those in the lysozyme/DMPO system. However, both the wavelength and the irradiation time dependence of the intensity of each radical adduct signal (monitored via LFTT) are quite different from those of lysozyme. With monochromatic irradiation ( $\lambda = 300$  nm), the hydrogen-atom adduct concentration decreased after 7 minutes and the carbon-centered radical adduct concentration first increased and then decreased after 12 minutes. Under nonmonochromatic broad-band irradiation, only the carbon-centered radical adduct concentration appeared to increase with respect to irradiation time; the concentration of hydrogen-atom adduct was constant. The ratio of H to  $\cdot\dot{C}$  for poly-DL-tryptophan after 2 minutes of  $\lambda = 300$ -nm irradiation was 0.14, whereas that for lysozyme was 1.8.

TABLE 2. RELATIVE INTENSITY OF LOW-FIELD TERMINAL TRANSITION (LFTT) IN HYPERFINE SPLITTING OF DMPO SPIN ADDUCT FROM POLY-DL-TRYPTOPHAN

Excitation wavelength (nm)	Irradiation time (min)	Type of spin adduct		
		Relative intensity of LFTT		
		Hydrogen atom	Hydroxy	Carbon-centered
Light off 300	-	0.5	-	2.5
	2	0.7	-	5.0
	7	0.5	-	3.8
	12	0.2	-	2.8
	17	0.3	-	1.7
	200-800	2	0.5	-
	7	0.5	-	3.8

8. UV-Induced Free Radicals from Some Aromatic Species in Ocular Lens Proteins: Phenylalanine, Histidine, and N-Formyl Kynurenine; Irradiation Time and Wavelength Dependence of Spin Adduct Formation with DMPO

Phenylalanine/DMPO--Figure 15 represents the spin-trapped EPR spectrum of phenylalanine with DMPO as the trap. The spectrum was taken after 8 minutes of irradiation with  $\lambda = 300$ -nm excitation light. The free-radical species detected with the excitation light off were hydroxy and carbon-centered radicals, whereas both broad-band ( $\lambda = 200$ -800 nm) and monochromatic ( $\lambda = 300$  nm) irradiation produced the hydroxy and carbon-centered radicals and hydrogen atoms. The time and wavelength dependence of the relative spectral intensities of these radicals monitored via LFTT are indicated in Table 3. With monochromatic ( $\lambda = 300$  nm) irradiation, all three types of radical adduct concentrations increased with respect to irradiation time and reached their saturation limit within 20 minutes. Nonmonochromatic irradiation experiments subsequent to the monochromatic experiments showed an initial diminishing effect of  $\lambda = 200$ -800-nm excitation light on all three types of radical adducts within 15 minutes; however, the intensities for hydrogen atoms and hydroxy radical adducts appeared to increase somewhat after 30 minutes of broad-band irradiation.

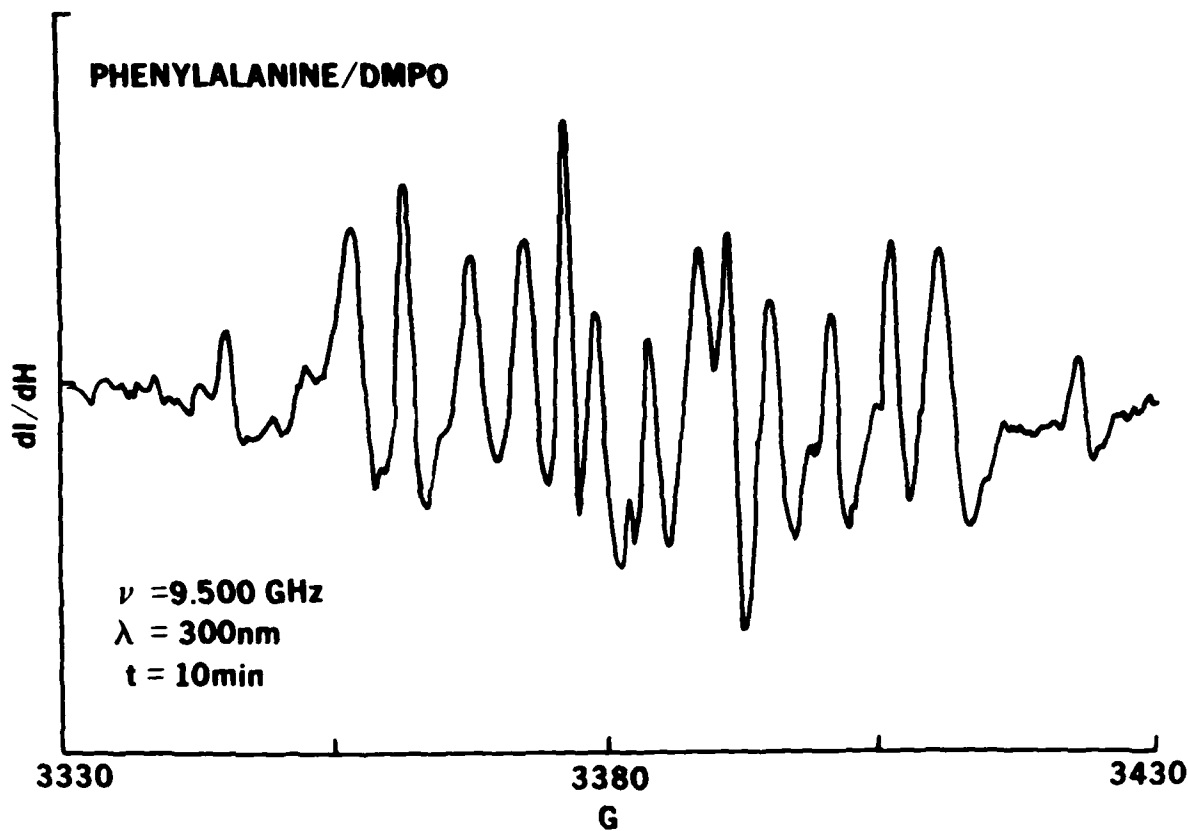


Figure 15. EPR spectrum of free radicals trapped with DMPO in phenylalanine irradiated at 300 nm for 10 minutes.

TABLE 3. RELATIVE INTENSITY OF LOW-FIELD TERMINAL TRANSITION (LFTT) IN HYPERFINE SPLITTING OF DMPO SPIN ADDUCT FROM PHENYLALANINE

Excitation wavelength (nm)	Irradiation time (min)	Type of spin adduct		
		Relative intensity of LFTT		
		Hydrogen atom	Hydroxy	Carbon-centered
Light off 300	-	-	2.2	4.2
	3	1.4	2.5	3.7
	8	1.5	2.9	3.5
	20	1.5	2.8	3.8
200-800	5	1.8	4.2	6.5
	15	1.0	0.3	4.0
	30	1.7	0.7	4.0

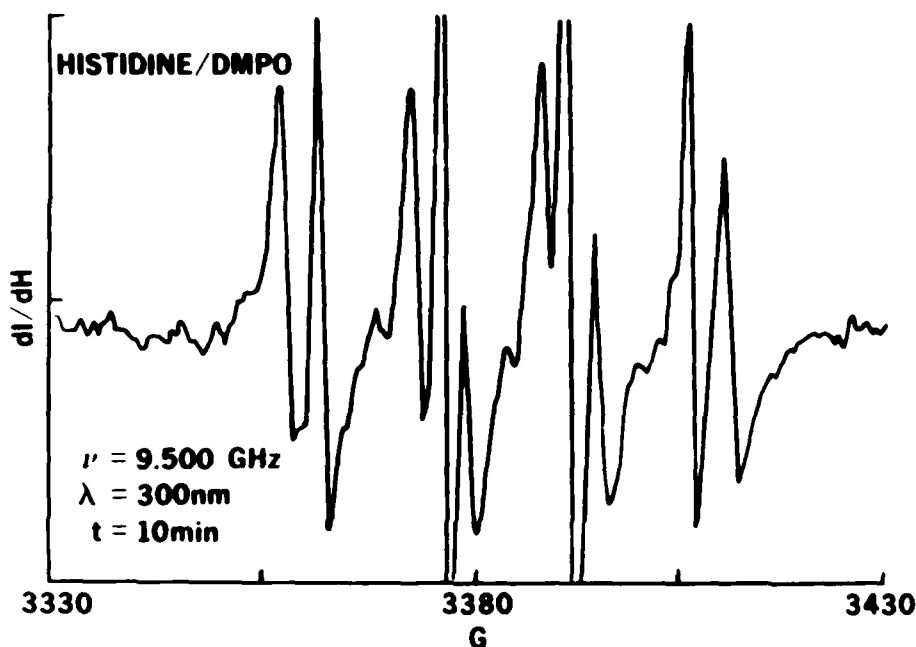


Figure 16. EPR spectrum of free radicals trapped with DMPO in histidine irradiated at 300 nm for 10 minutes.

Histidine/DMPO--Figure 16 is the spin trapping EPR spectrum of histidine with DMPO as the trap. The spectrum was taken after 10 minutes of  $\lambda = 300\text{-nm}$  excitation. As shown in Table 4, types of free radicals detected--hydroxy and carbon-centered radicals--did not differ under the following conditions: UV lamp off,  $\lambda = 300\text{ nm}$ , and  $\lambda = 200\text{-}800\text{ nm}$ . With  $\lambda = 300\text{-nm}$  excitation, the concentration of both radicals (in the form of spin-trapped adducts) increased with respect to the irradiation time. With nonmonochromatic irradiation ( $\lambda = 200\text{-}800\text{ nm}$ ), a decrease in intensity for the hydroxy radical adduct and a significant increase in intensity for the carbon-centered radical were observed during the interval from 3 to 10 minutes of irradiation.

TABLE 4. RELATIVE INTENSITY OF LOW-FIELD TERMINAL TRANSITION (LFTT) IN HYPERFINE SPLITTING OF DMPO SPIN ADDUCT FROM HISTIDINE

Excitation wavelength (nm)	Irradiation time (min)	Type of spin adduct		
		Hydrogen atom	Hydroxy	Carbon-centered
Light off 300	-	-	7.4	3.1
	3	-	8.7	5.3
	10	-	9.4	6.3
200-800	3	-	5.0	5.0
	10	-	2.2	23.1



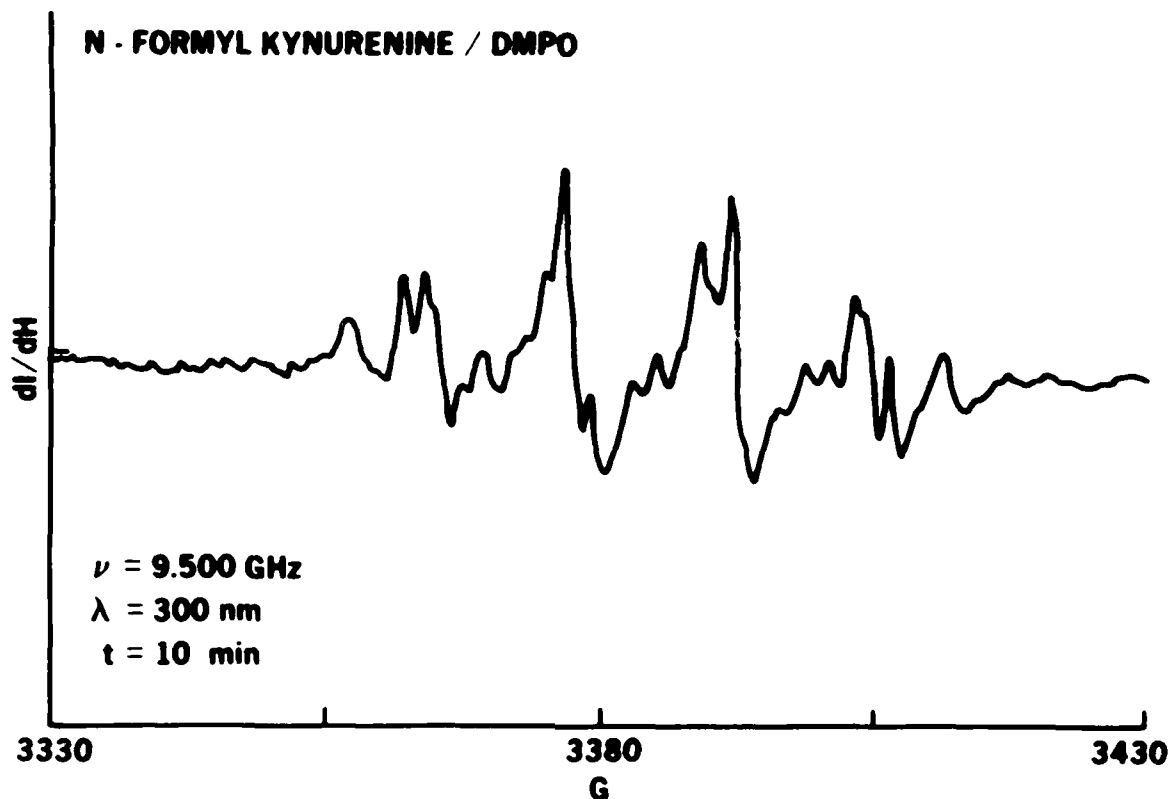


Figure 17. EPR spectrum of free radicals trapped with DMPO in N-formyl kynurenine irradiated at 300 nm for 10 minutes.

N-Formyl Kynurenine/DMPO--Figure 17 illustrates the spin trapping EPR spectrum of N-formyl kynurenine (a photo-oxidation product of tryptophan) after 10 minutes of  $\lambda = 300$ -nm irradiation. With the excitation light off and also with nonmonochromatic irradiation ( $\lambda = 200$ - $800$  nm), the detected free-radical species were hydroxy and carbon-centered radicals. With monochromatic irradiation ( $\lambda = 300$  nm) these radicals and hydrogen atoms were detected. The time and wavelength dependence of the relative spectral intensities of these radicals, monitored via LFTT, are summarized in Table 5.

TABLE 5. RELATIVE INTENSITY OF LOW-FIELD TERMINAL TRANSITION (LFTT) IN HYPERFINE SPLITTING OF DMPO SPIN ADDUCT FROM N-FORMYL KYNURENINE

Excitation wavelength (nm)	Irradiation time (min)	Type of spin adduct		
		Relative intensity of LFTT		
		Hydrogen atom	Hydroxy	Carbon-centered
Light off	-	-	0.8	1.5
300	2	0.4	2.8	0.9
	10	0.4	2.1	0.7
200-800	2	-	0.7	0.9

9. UV-Induced Free Radicals from Some Aliphatic Amino Acids: Glycine, Leucine, Methionine, and Aspartic Acid, All Trapped with DMPO; Irradiation Wavelength and Time Dependence of Spin Adduct Formation

Spin trapping spectra for glycine, leucine, methionine, and aspartic acid are shown in Figures 18 through 21 respectively. The time dependences of the relative spectral intensities among the detected radicals, monitored via LFTT, under different wavelength conditions, are summarized in Tables 6 through 9

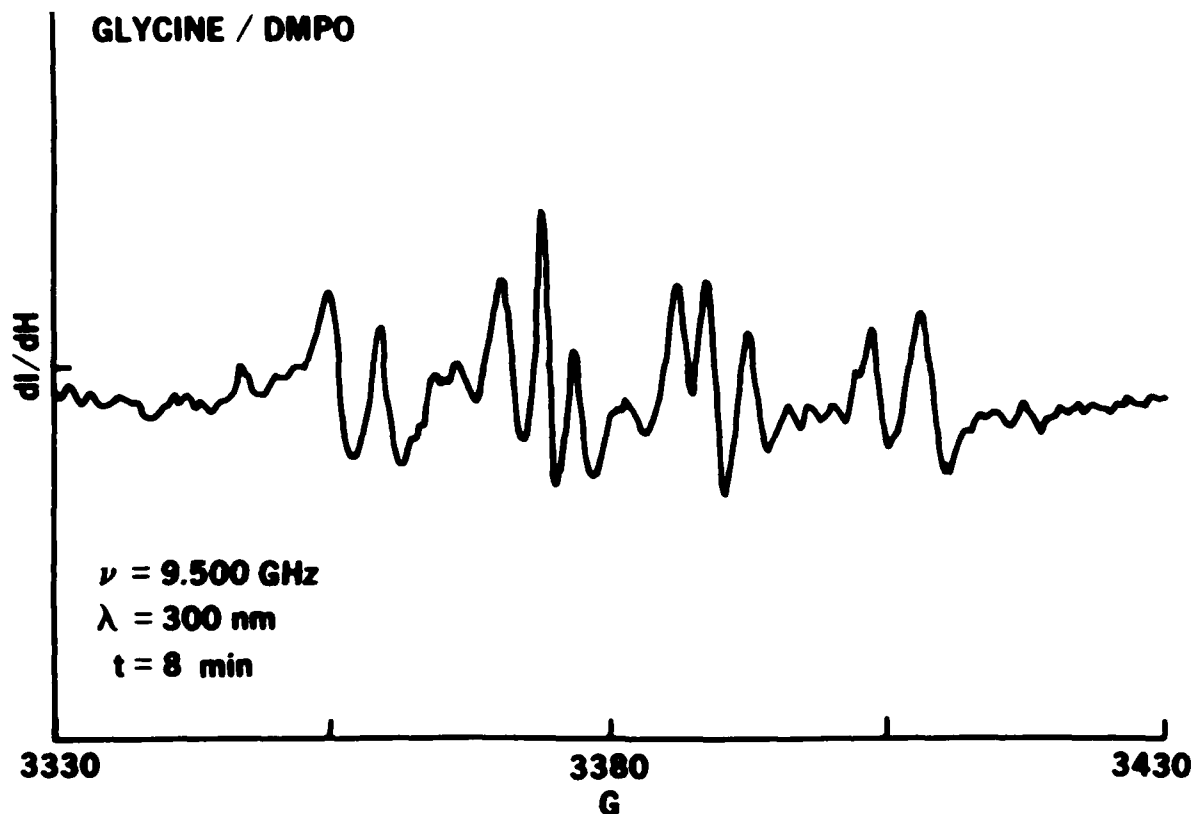


Figure 18. EPR spectrum of free radicals trapped with DMPO in glycine irradiated at 300 nm for 8 minutes.

TABLE 6. RELATIVE INTENSITY OF LOW-FIELD TERMINAL TRANSITION (LFTT) IN HYPERFINE SPLITTING OF DMPO SPIN ADDUCT FROM GLYCINE

Excitation wavelength (nm)	Irradiation time (min)	Type of spin adduct		
		Relative intensity of LFTT		
		Hydrogen atom	Hydroxy	Carbon-centered
Light off 300	-	-	2.4	1.4
	2	-	1.7	2.0
	8	-	1.8	2.2
200-800	8	-	2.2	3.2

respectively. The following common features were exhibited among these four aliphatic amino acids: (a) hydroxy and carbon-centered radicals were detected, (b) radical species remain the same under all wavelength conditions (excitation off,  $\lambda = 300$ , and  $\lambda = 200-800$  nm), and (c) intensity of the spin adduct signals increased with respect to irradiation time from 2 to 12 minutes. The only difference among their spectra appeared to be the relative intensities of the hydroxy and the carbon-centered adducts.

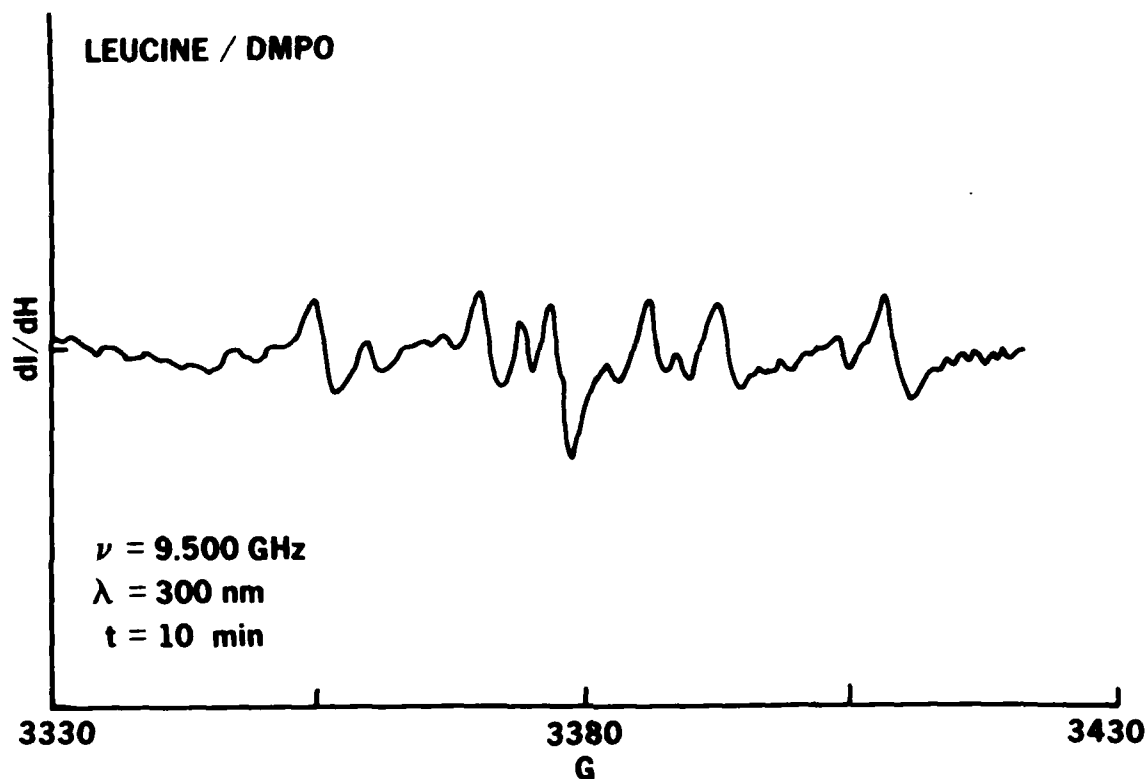


Figure 19. EPR spectrum of free radicals trapped with DMPO in leucine irradiated at 300 nm for 10 minutes.

TABLE 7. RELATIVE INTENSITY OF LOW-FIELD TERMINAL TRANSITION (LFTT) IN HYPERFINE SPLITTING OF DMPO SPIN ADDUCT FROM LEUCINE

Excitation wavelength (nm)	Irradiation time (min)	Type of spin adduct		
		Relative intensity of LFTT		
		Hydrogen atom	Hydroxy	Carbon-centered
Light off	-	-	0.2	0.6
300	2	-	0.4	1.2
	10	-	0.4	1.4
200-800	2	-	0.8	1.3
	10	-	1.2	1.4

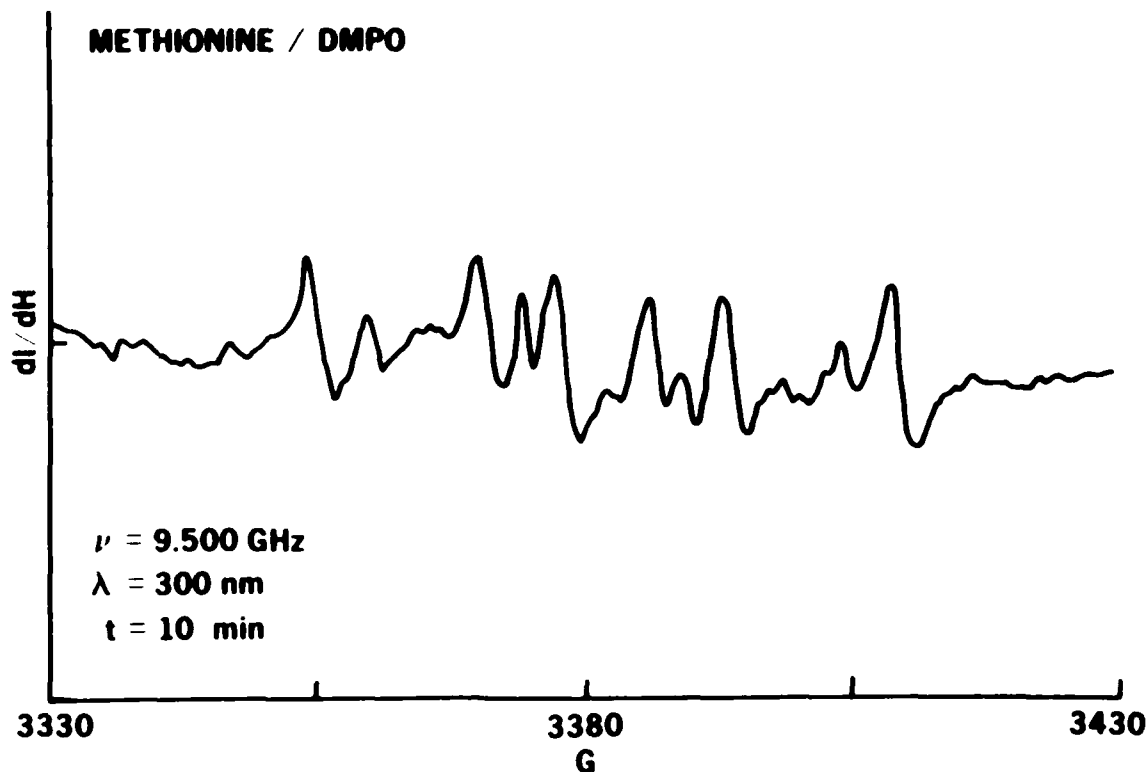


Figure 20. EPR spectrum of free radicals trapped with DMPO in methionine irradiated at 300 nm for 10 minutes.

TABLE 8. RELATIVE INTENSITY OF LOW-FIELD TERMINAL TRANSITION (LFTT) IN HYPERFINE SPLITTING OF DMPO SPIN ADDUCT FROM METHIONINE

Excitation wavelength (nm)	Irradiation time (min)	Type of spin adduct		
		Relative intensity of LFTT		
		Hydrogen atom	Hydroxy	Carbon-centered
Light off 300	-	-	0.4	1.0
	2	-	0.7	1.2
	10	-	0.8	1.9
200-800	3	-	1.4	5.0
	10	-	1.8	6.2

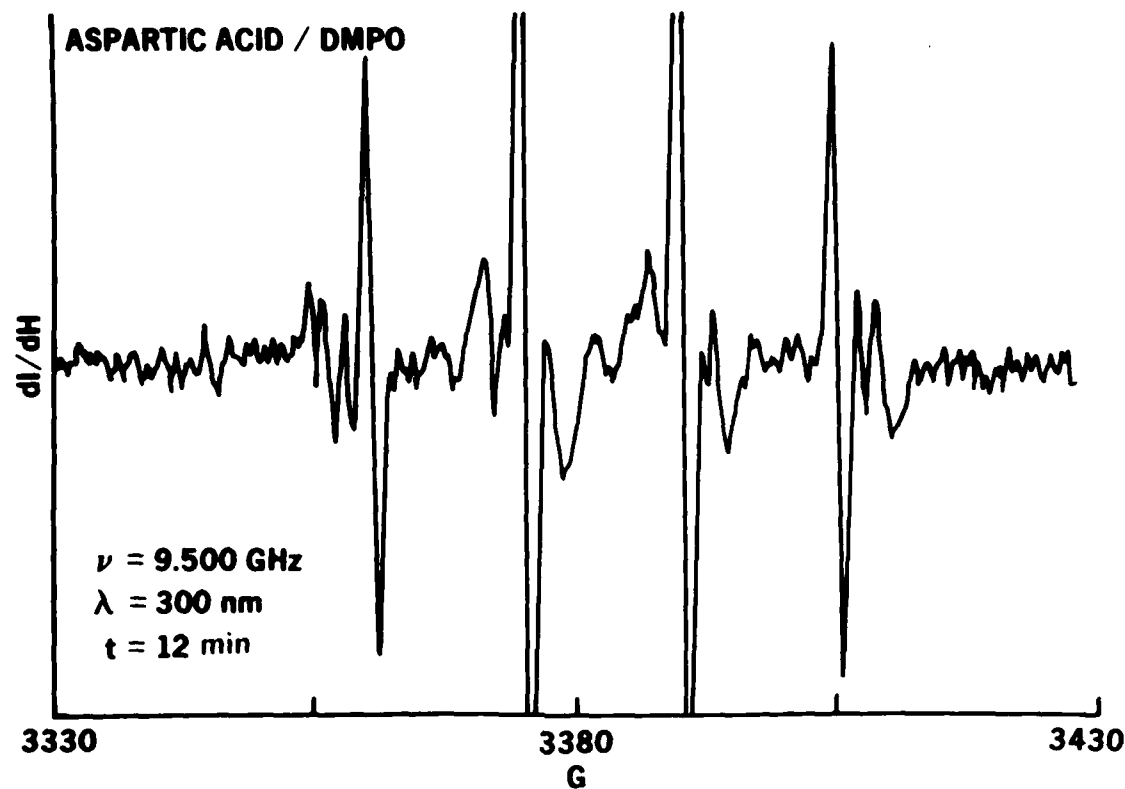


Figure 21. EPR spectrum of free radicals trapped with DMPO in aspartic acid irradiated at 300 nm for 12 minutes.

TABLE 9. RELATIVE INTENSITY OF LOW-FIELD TERMINAL TRANSITION (LFTT) IN HYPERFINE SPLITTING OF DMPO SPIN ADDUCT FROM ASPARTIC ACID

Excitation wavelength (nm)	Irradiation time (min)	Type of spin adduct		
		Relative intensity of LFTT		
		Hydrogen atom	Hydroxy	Carbon-centered
Light off 300	-	-	3.3	1.0
	2	-	5.2	1.8
	4	-	6.1	1.7
	12	-	8.5	2.3
200-800	2	-	4.1	2.1
	10	-	8.3	10.1
	13	-	22.0	32.0

10. UV-Induced Free Radicals from a Known Cataractogenic Drug, 8-Methoxy Psoralen, Trapped with DMPO

The control for this experiment--8-MOP, H<sub>2</sub>O, and DMPO--without UV irradiation, exhibited no radical signals. These samples were subsequently examined after 5, 10, and 20 minutes of UV exposure.

DMPO Spin Trapping of 8-MOP under Broad-Band Irradiation--Figure 22 shows the EPR spectrum of free radicals trapped by DMPO under broad-band (250-800 nm) irradiation for 5 minutes in 8-MOP aqueous solution. It represents a mixture of hydrogen atom, hydroxy, and carbon-centered radical adducts to DMPO. (The number of hyperfine splitting lines, intensity ratio, and hyperfine splitting parameters  $a_H$  and  $a_N$  were given in Figs. 7A-7D.) The spectrum does not show all hyperfine splitting lines for the three types of radicals (a total of 19), which indicates that some of the lines overlap.

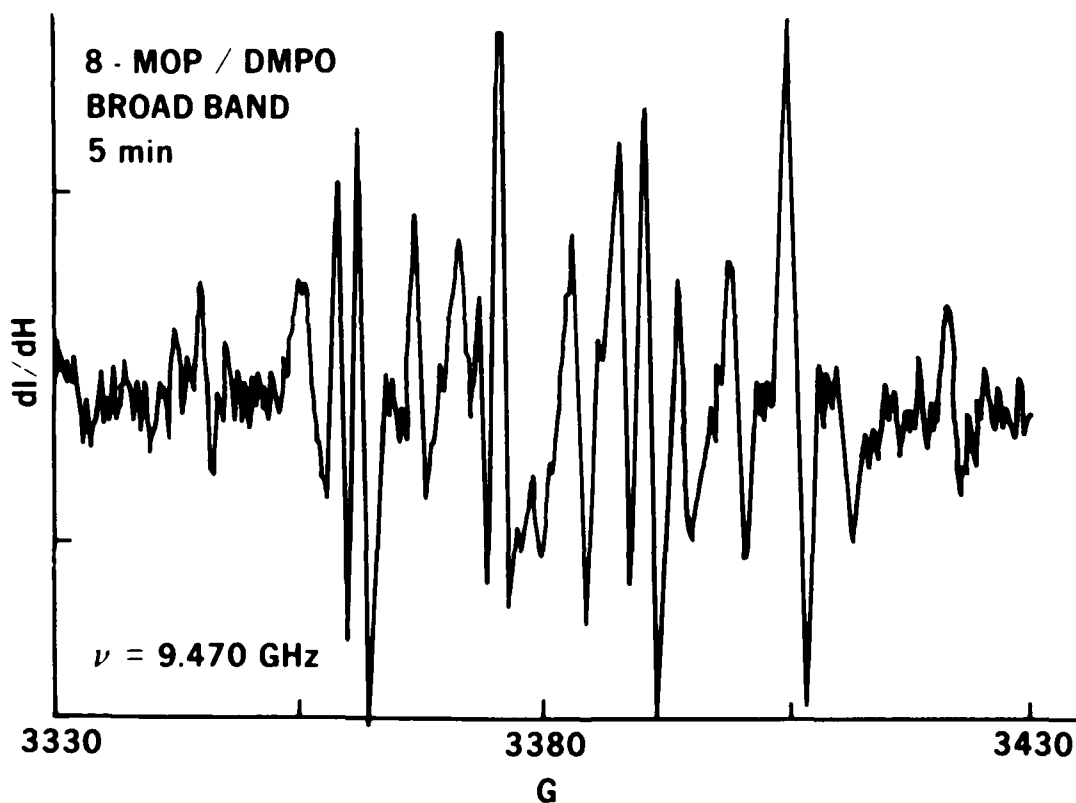


Figure 22. EPR spectrum obtained from aqueous 8-methoxy psoralen, a cataractogenic drug, and DMPO with broad-band irradiation for 5 minutes.

DMPO Spin Trapping of 8-MOP at  $\lambda = 320$  nm--The EPR spectrum obtained from aqueous 8-MOP/DMPO irradiated at  $\lambda = 320$  nm for 40 minutes is shown in Figure 23. The free radicals trapped were the same as those observed under broadband irradiation; however, the relative concentration of carbon-centered radicals to that of hydroxy (or oxygen-centered) radicals is significantly greater in the  $\lambda = 320$ -nm experiment, suggesting an irradiation time dependence of the concentration for these radicals. When the irradiation light source was extinguished, the radical signals remained essentially the same for more than 30 minutes at room temperature. No change in hyperfine splitting was observed during this time interval.

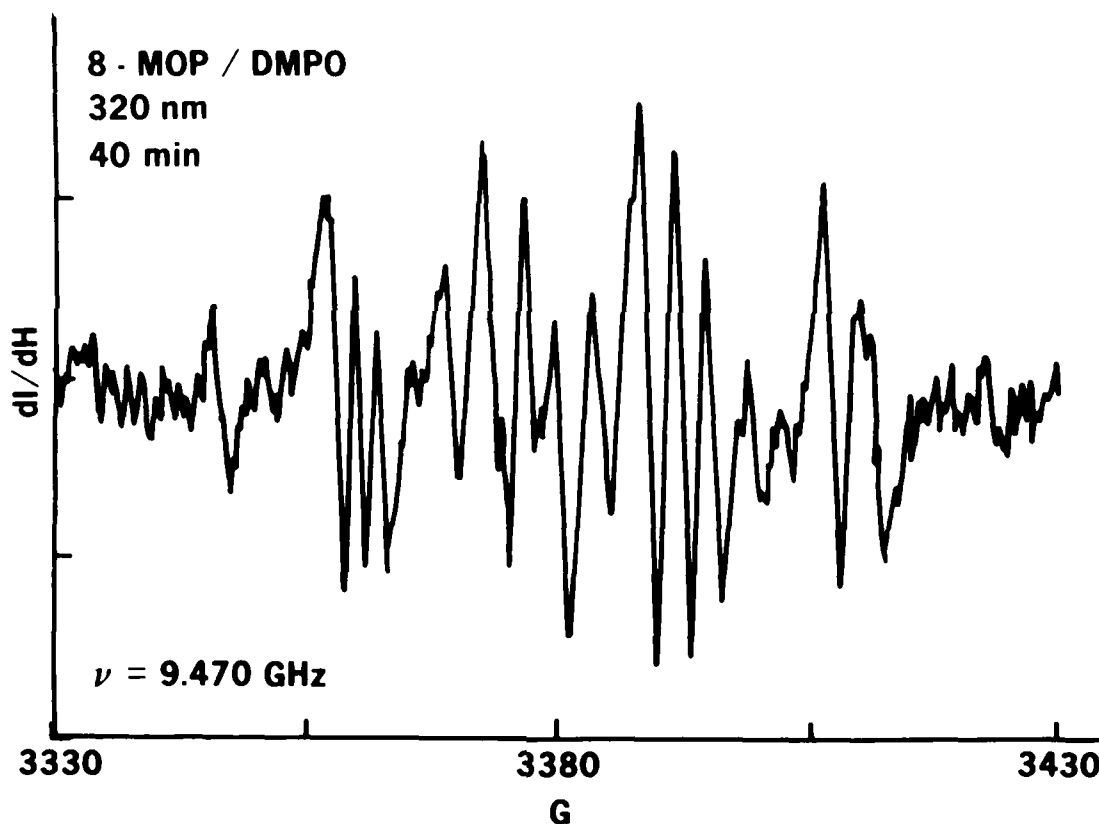


Figure 23. EPR spectrum of radicals trapped by DMPO in the aqueous solution of 8-methoxy psoralen (8-MOP) irradiated at 320 nm for 40 minutes.

## 11. UV-Induced Free Radicals from Ribonuclease, a Protein Without Tryptophan

Figure 24 shows the combined EPR spectrum of the DMPO spin trapping of ribonuclease at  $\lambda =$  broad band,  $\lambda = 290$  nm, and  $\lambda = 320$  nm. No radical adducts were observed in the broad-band experiment; however, the  $\lambda = 290$ -nm and  $\lambda = 320$ -nm experiments exhibited a trace of oxygen-centered radicals. These spectra are quite different from those of tryptophan and human-lens protein at  $\lambda = 290$  nm.

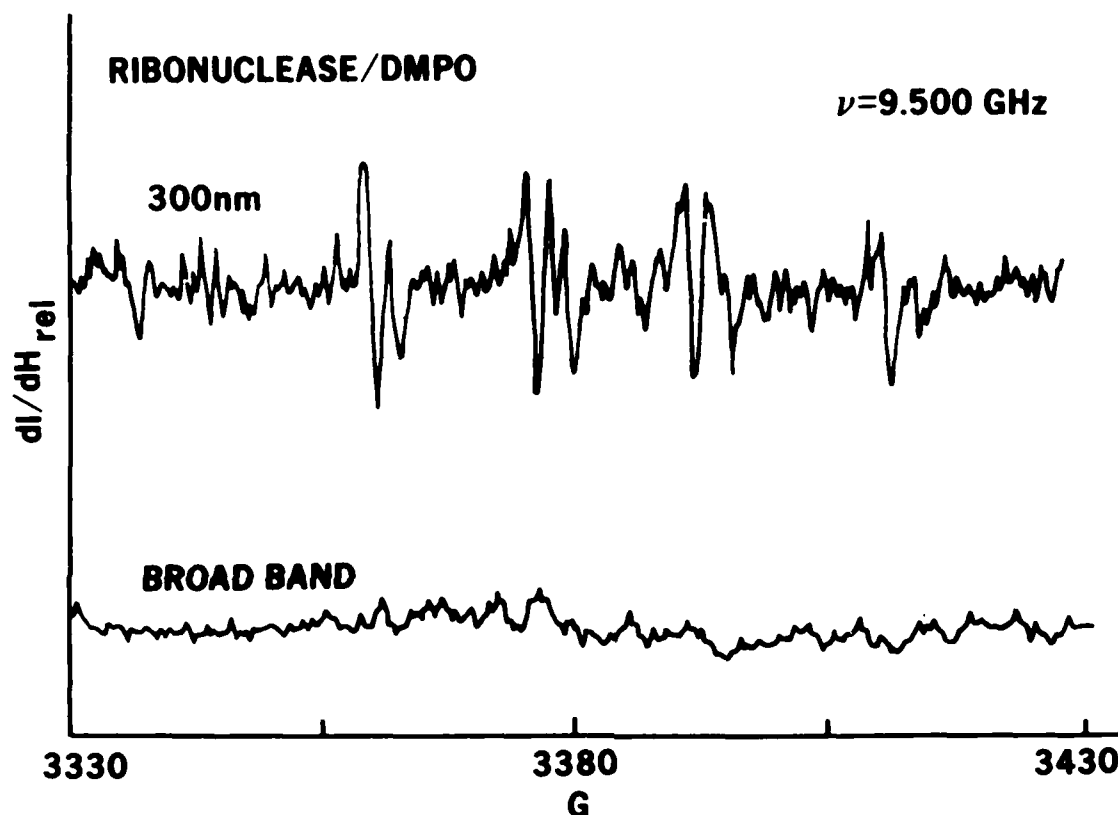


Figure 24. EPR spectrum of radicals trapped by DMPO in aqueous ribonuclease, a protein that contains no tryptophan but does contain tyrosine, phenylalanine, and histidine.

### G. One- and Two-Dimensional Electrophoresis on the Control and the UV-Irradiated Lens Crystallin Proteins

#### 1. Preliminary Experiments

A gel slab of whole-cow-lens homogenate was made under isoelectric focusing and SDS electrophoresis. The final acrylamide concentration in the gel was 15%. To obtain the optimal resolution of the protein bands, gels at higher concentrations were also tested. These preliminary experiments indicated that in order to resolve all components in the sample, the amount of protein used should be higher than the 150  $\mu$ g suggested by O'Farrel (34).



## 2. Improved 2-Dimensional Electrophoretic Methods for Lens Crystallin Proteins

Results from 2-D gel electrophoresis indicate that the 2-dimensional analysis resolves a greater number of components than does SDS gel electrophoresis, which is the method used by other workers for similar purposes (Kebbelaar and Bloemendal, 37).

We noted that the protein determination, according to the methods of Warburg and Christian (38a) and Lowry et al. (39), gave results overestimating the protein content of both the whole-lens extract and the fractions recovered after Sephadex G-200 chromatography. Both methods are affected by the presence in the sample of free amino acids, which are known to be present in considerable amounts in lens preparations. Dialysis with three changes of distilled water did not remove all the low-molecular-weight material absorbing at 230 nm; therefore, all preparations were filtered through a Sephadex G-25 column (0.9 x 30 cm). As shown in Figure 25, the whole-lens extract and fraction #4 still contained a certain amount of UV-absorbing, low-molecular-weight

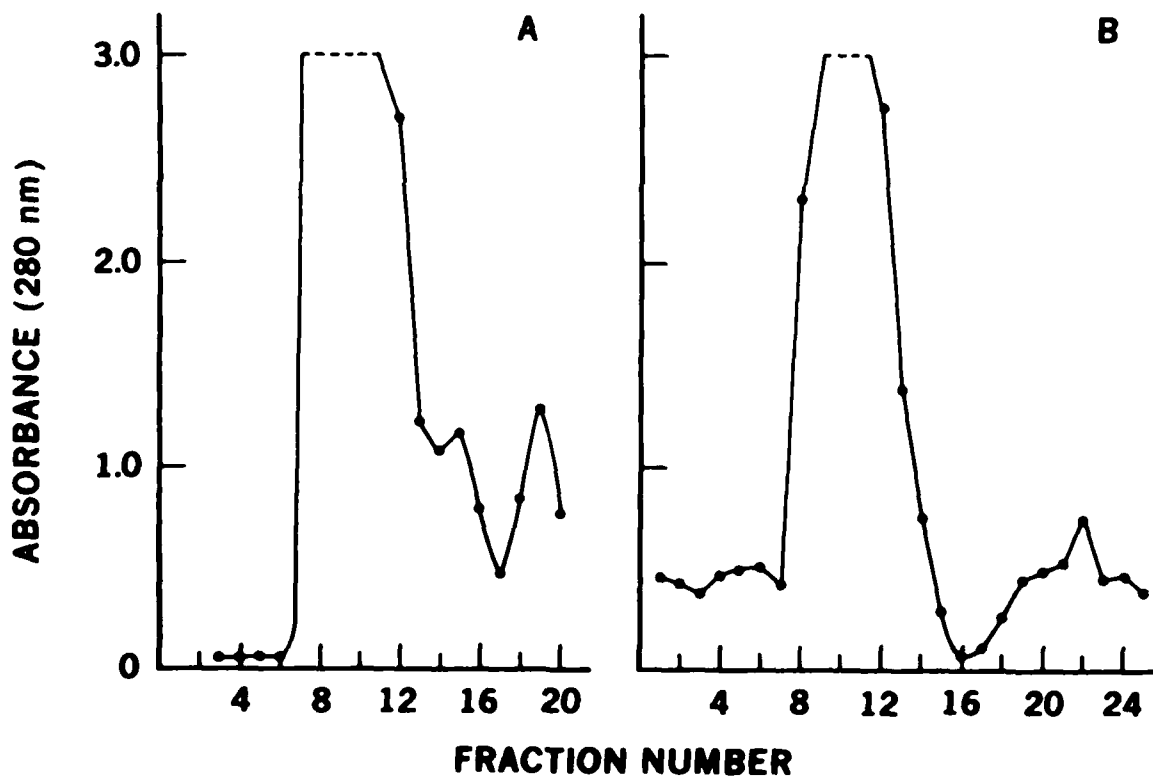


Figure 25. Elution of water-soluble cow-lens proteins (A) and fraction #4 (B) from a Sephadex G-25 fine column (0.9 x 30 cm, 19 ml), equilibrated with 50 mM tris-HCl, pH 7.3, containing 0.1 M KCl, 10 mM  $\beta$ -mercaptoethanol, and 1 mM EDTA, 1.2 ml per tube were collected.

material. An additional purification step had to be adopted to obtain samples free from amino acids (e.g., tryptophan and tyrosine). This step was especially important in view of the subsequent irradiation experiments, in which it was necessary to determine if the modifications in the proteins were caused by free or bound tryptophan.

### 3. Electrophoresis Studies (1- and 2-D) after UV Irradiation

Both exposed and control samples were analyzed by SDS electrophoresis carried out in cylindrical gels, using the method of Weber and Osborn (38b). The formation of a very slow moving band due to high-molecular-weight material, as well as the relative disappearance of some bands, was observed when the UV-treated fractions were compared to untreated ones.

Figure 26 shows the chromatographic separation of rabbit lens crystallin proteins, Figures 27 and 28 show some of the 2-D gels of the treated fractions and their controls. The main modification that can be observed in the gel is the appearance of some spots with slower migration rates toward the anode. This indicates the formation of higher molecular weight aggregates. Three spots do not show a significant modification of their isoelectric points, suggesting that aggregation occurred among subunits of similar composition. The

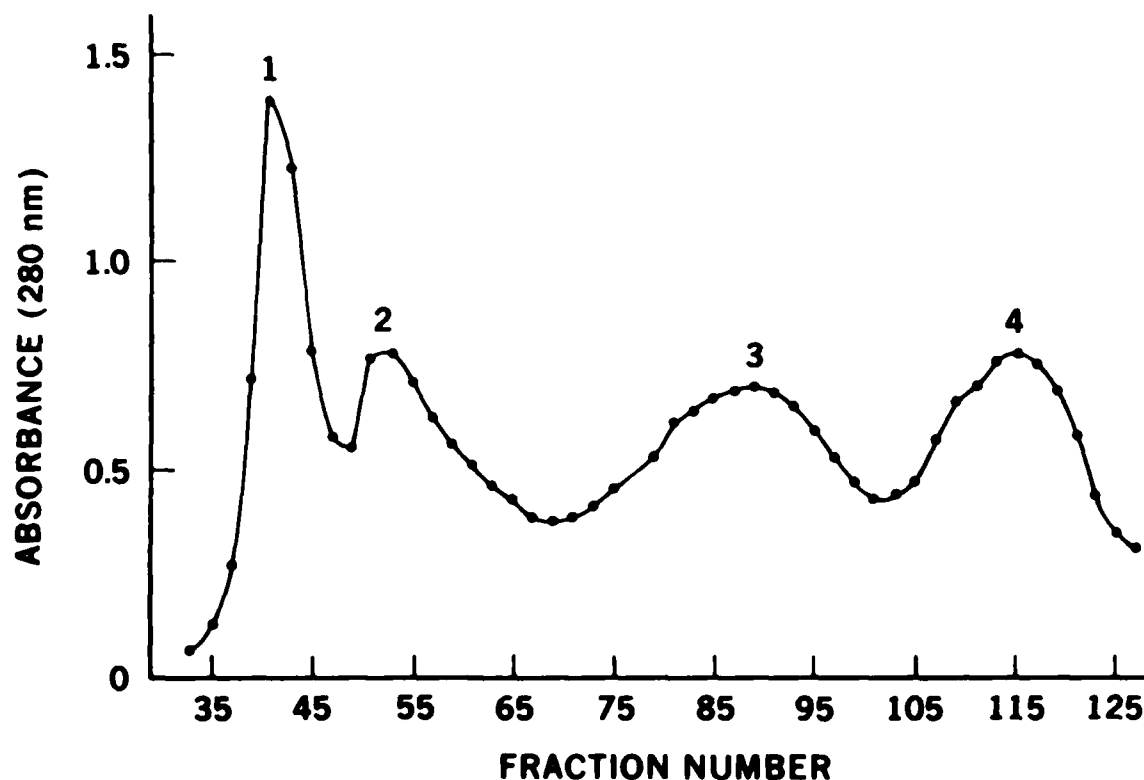


Figure 26. Sephadex G-200 gel chromatographic separation of rabbit lens crystallin proteins. Fraction number 1-4 refer to  $\alpha$ ,  $\beta_H$ ,  $\beta_Z$ , and  $\gamma$  protein fractions, respectively.

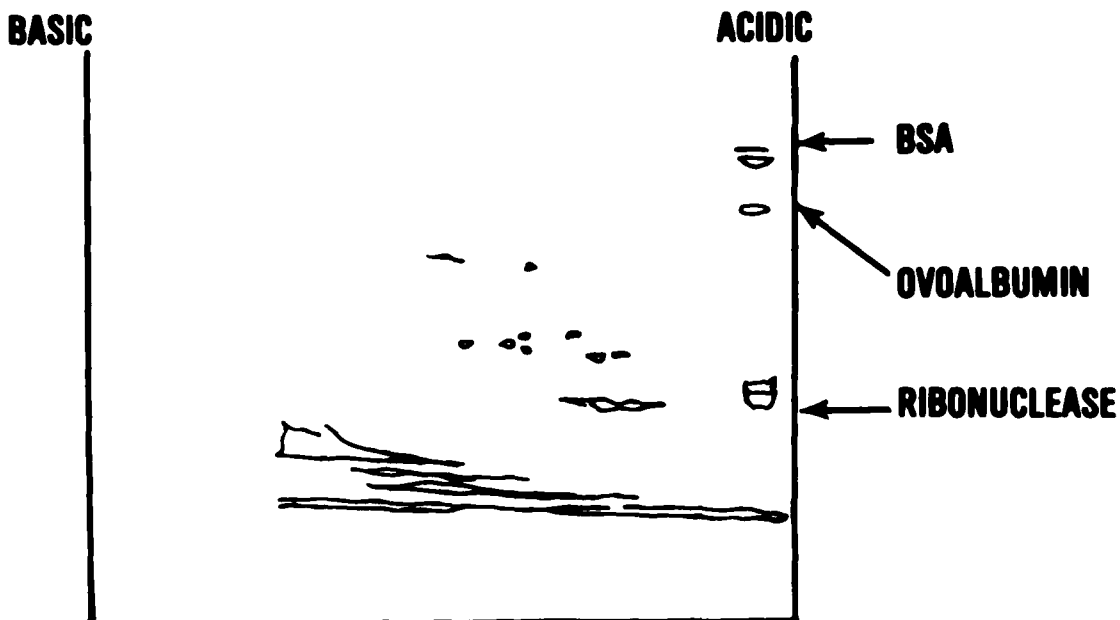


Figure 27. 2-D gel electrophoresis of fraction #1 ( $\alpha$ -crystallin) from rabbit lens, after Sephadex G-200 gel chromatography. References: BSA (67,500), ovalbumin (45,000), and ribonuclease (13,700).

same spots also appear clearly in the controls, which were kept in the same conditions except for UV-light exposure. This can be explained by assuming that a certain amount of heat is generated during the exposure, in spite of the infrared-filter unit placed between the light source and the samples being irradiated. It seems, therefore, that the effects of heat are strikingly similar to the effects of irradiation, excluding the formation of fluorogen which is not present in any of the controls.

For the behavior of crystallins originating from different species to be compared, rabbit lens crystallins were separated according to Ziegler and Sidbury's procedure (40). As they pointed out, the rabbit lens shows a higher percentage of  $\gamma$ -crystallin than cow lens, for example, which could be responsible for the higher susceptibility to UV light observed in extracted lenses by Yamanashi and Zuclich (20). The fractions obtained after chromatography were concentrated by ammonium sulfate precipitation, exhaustively dialyzed against cold distilled water, and frozen until further use. Aliquots of each fraction were used for 2-D gel electrophoresis. Figures 27 and 28 show the result of such analysis for fractions #1 and #4 respectively. As compared to the corresponding fractions of bovine lens crystallins,  $\alpha$ -crystallin in rabbit presents only two main components, with noticeably different isoelectric points; and  $\gamma$ -crystallin in rabbit also has only two main components, both of which have more basic isoelectric points than  $\gamma$ -crystallin from bovine lens.

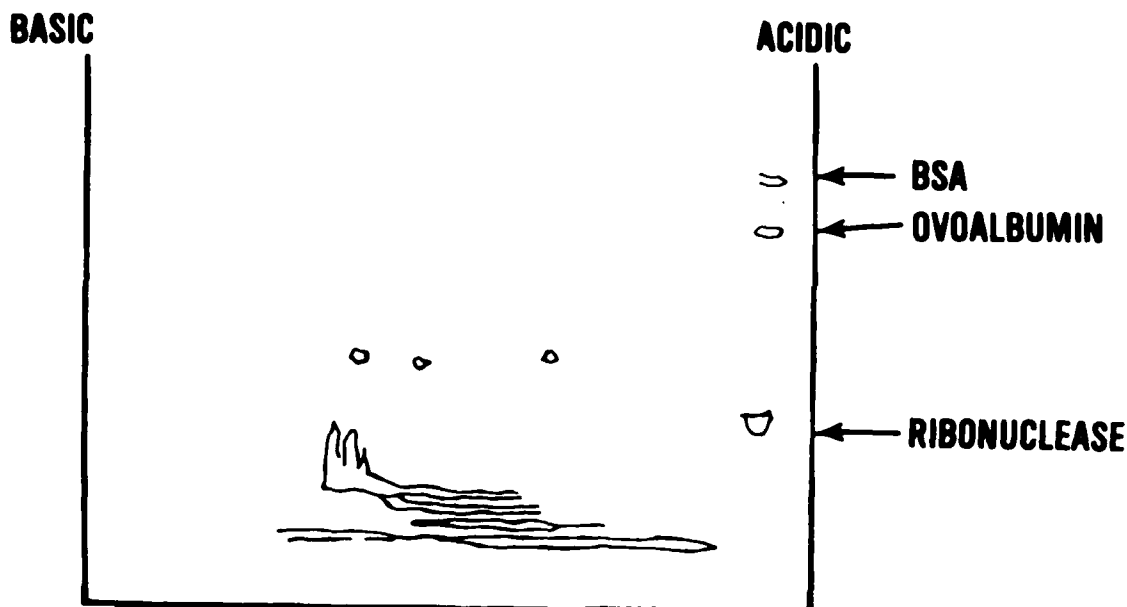


Figure 28. 2-D gel electrophoresis of fraction #4 ( $\gamma$ -crystallin) from rabbit lens, after Sephadex G-200 gel chromatography. References: BSA (67,500), ovoalbumin (45,000), and ribonuclease (13,700).

#### H. Fluorescence Spectra of UV-Irradiated Lens Crystallin Proteins

The emission spectra of the four sample fractions were studied at excitation wavelengths of 295 and 360 nm. These values corresponded to the excitation wavelengths of tryptophan and N-formyl kynurenine, respectively, and produced emission peaks at 360 and approximately 440 nm. The fluorescence spectra were obtained with an Aminco SPF-500 spectrofluorometer connected to an SPF-599 X-Y recorder. The final protein concentration was 0.2 mg/ml in 9 M urea for all samples.

As shown in Figures 29-32, the intensity of tryptophan fluorescence (360-nm emission) progressively decreased as exposure time increased, except for fraction #4 ( $\gamma$ -crystallin) which appears to be almost unaffected by the treatment (consistent with the data of Yamanashi and Zuclich (20) on UV susceptibility). At the same time NFK emission (around 440 nm) progressively increased with time.

The broad and asymmetrical emission peaks suggest that more than one molecular species is produced by UV irradiation that emits fluorescence in this region. N-formyl kynurenine, with emission peak at 440 nm, has already been detected in irradiated lens proteins, together with kynurenine and with unidentified fluorescent components (41,42) probably derived from the photo-oxidation of tryptophan. The four fractions ( $\alpha$ ,  $\beta_H$ ,  $\beta_L$ , and  $\gamma$  crystallin)

show somewhat different behaviors. Fraction 4, containing  $\gamma$ -crystallin, is the least affected. The remaining fractions show decreased tryptophan fluorescence and increased NFK emission around 440 nm with different exposure times, although fraction #3 ( $\beta_L$  crystallin) showed a more symmetric and intense peak around 440 nm after 2 hours than after 4 hours of exposure. This suggests that products of tryptophan photo-oxidation produced initially can be modified still further with longer exposure.

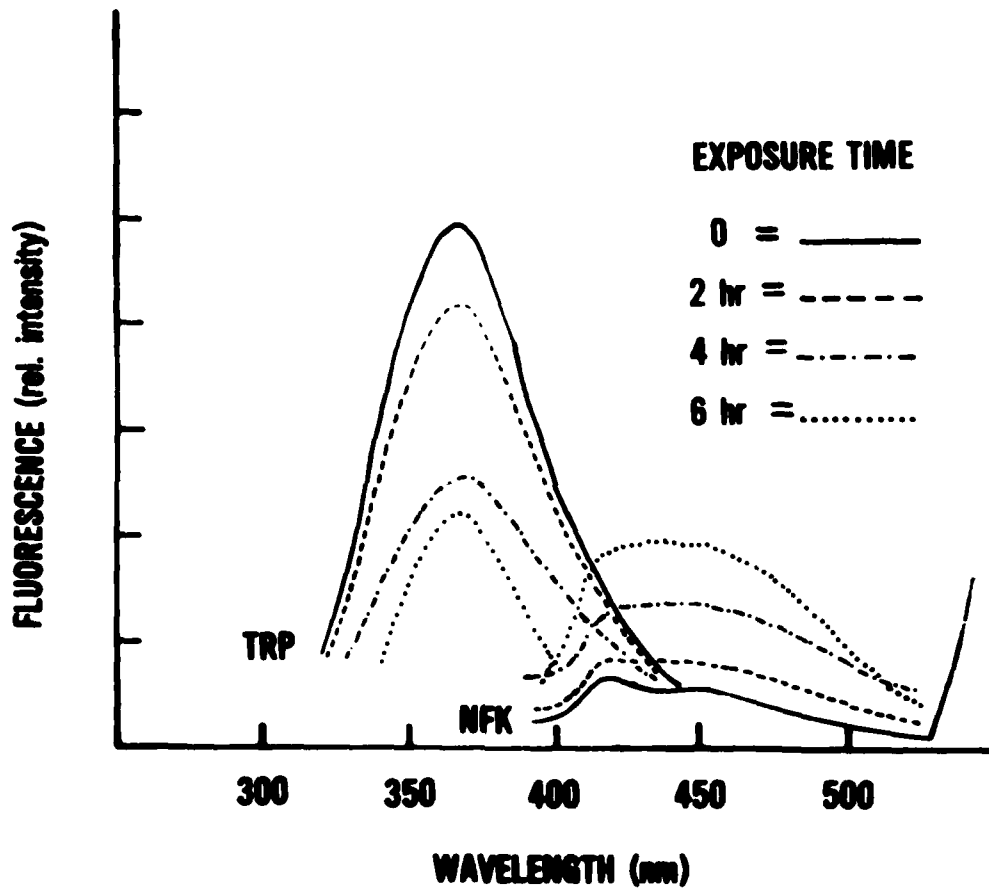


Figure 29. Fluorescence emission spectrum of cow-lens crystallin fraction #1 ( $\alpha$ -crystallin) irradiated with a broad-band UV at 440 mW/cm<sup>2</sup> for 0 to 6 hours.

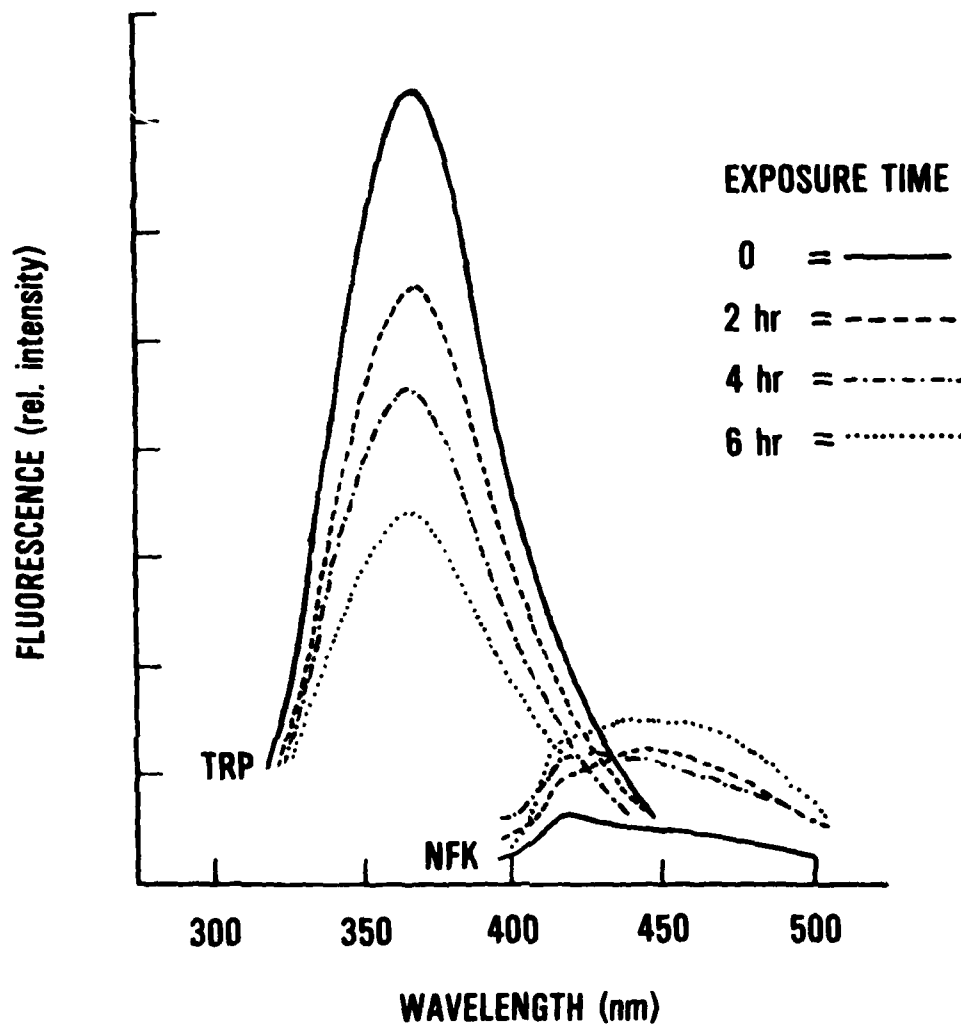


Figure 30. Fluorescence emission spectrum of cow-lens crystallin protein fraction #2 (8H-crystallin) irradiated with a broad-band UV at 440 mW/cm<sup>2</sup> for 0 to 6 hours.

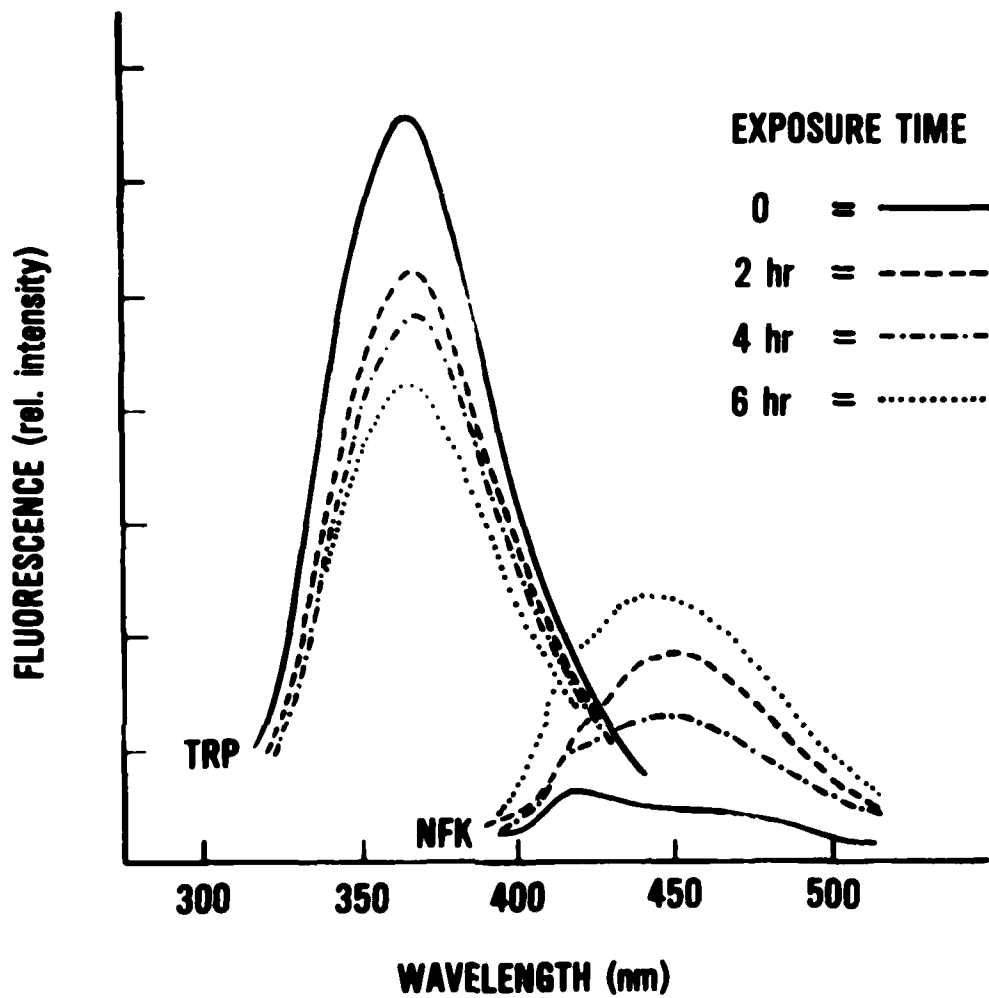


Figure 31. Fluorescence emission spectrum of cow-lens crystallin fraction #3 ( $\beta_L$ -crystallin) irradiated with a broad-band UV at  $440 \text{ mW/cm}^2$  for 0 to 6 hours.

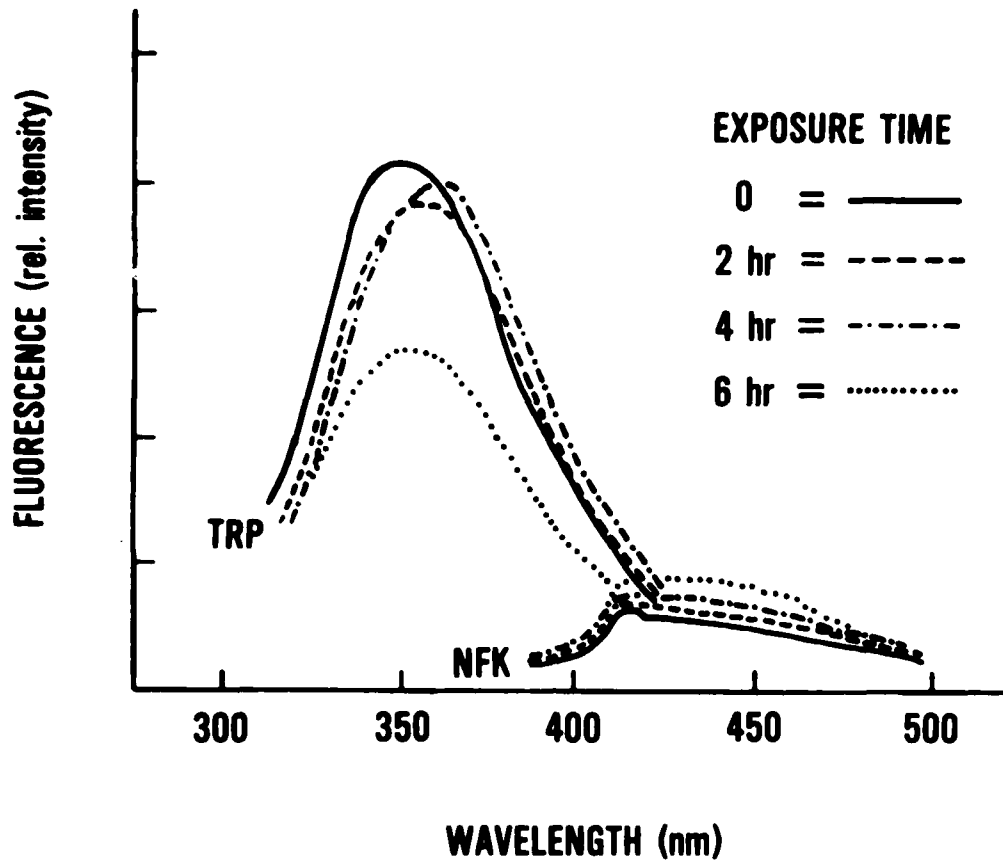


Figure 32. Fluorescence emission spectrum of cow-lens crystallin protein fraction #4 ( $\gamma$ -crystallin) irradiated with a broad-band UV at  $440 \text{ mW/cm}^2$  for 0 to 6 hours.

#### I. Difference Photoacoustic Spectra Between the Lens Cortex and Nucleus: Consideration of Saturation Effects

Figure 33 indicates the difference spectrum between the cortex and nucleus, normalized by a reference (carbon black). Figure 34 shows a log-log plot of signal amplitude versus frequency. According to this plot, the difference in intensity at  $230 \text{ nm}$  cannot be interpreted quantitatively since  $m > -1.0$  indicates saturation (43). Hence, in Figure 33 the difference spectrum at  $\lambda_{\text{max}} = 350 \text{ nm}$  and  $\lambda_{\text{max}} = 280 \text{ nm}$  may be quantitatively studied with more reliability on the former. We have also examined PAS spectra of the human lens, up to  $2000 \text{ nm}$ . Water absorption becomes pronounced in the IR region of the PAS spectra, but this may be conveniently used to monitor the water content of the particular components of the lens.



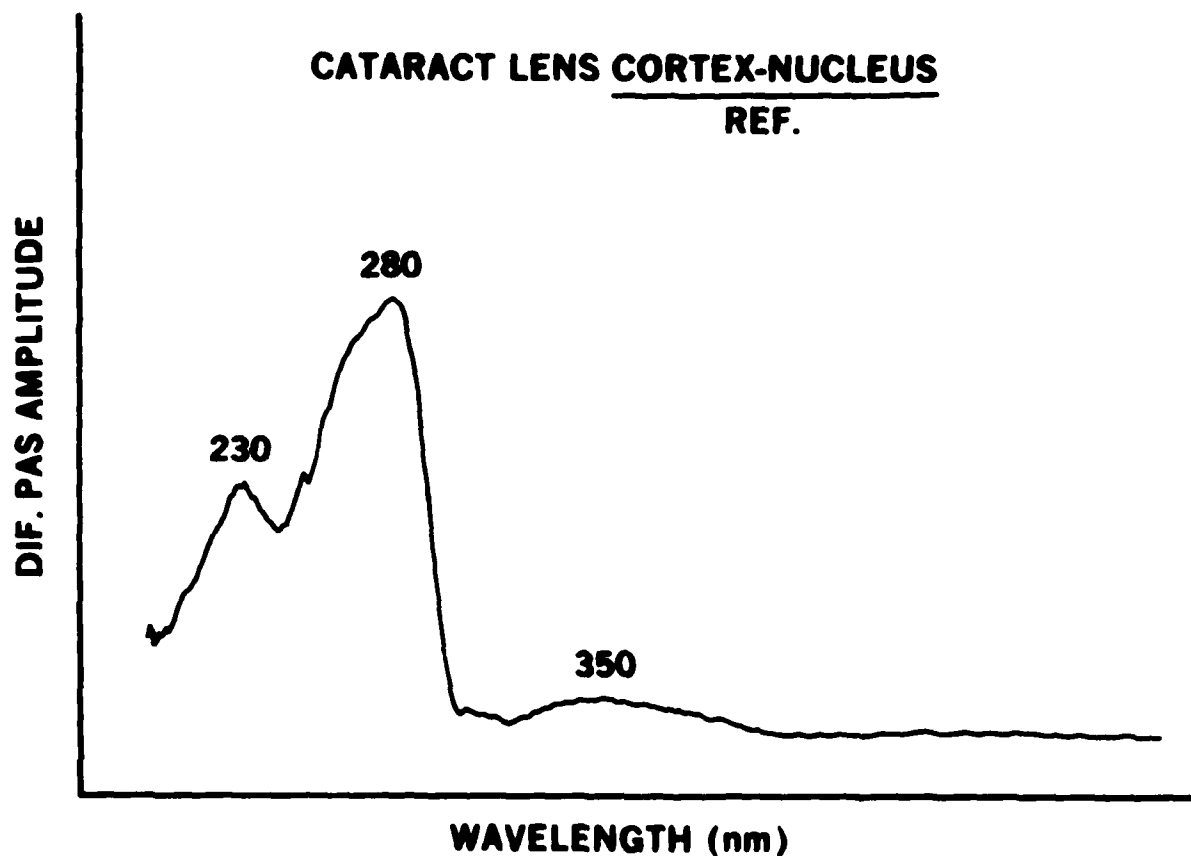


Figure 33. Difference photoacoustic spectrum between the cortex and nucleus of a human cataractous lens.

Along with our fluorescence study, the broadness of the 340-360-nm PAS signal suggests the existence of more than one chromophore. This is consistent with the observation of UV absorbers/fluorogens at 360/440 and 435/520 nm by Lerman et al. (5). The 360/440-nm response is coincidental with kynurenine in its zwitterionic form, but this is not claimed here since several biological fluorogens absorb and fluoresce within this same wavelength region.

#### IV. CONCLUSIONS

In Section III, our experimental results and their direct implications were presented. In this section, inferences are made based on the results of accumulated previous work, including ours, and the aspects of occupational

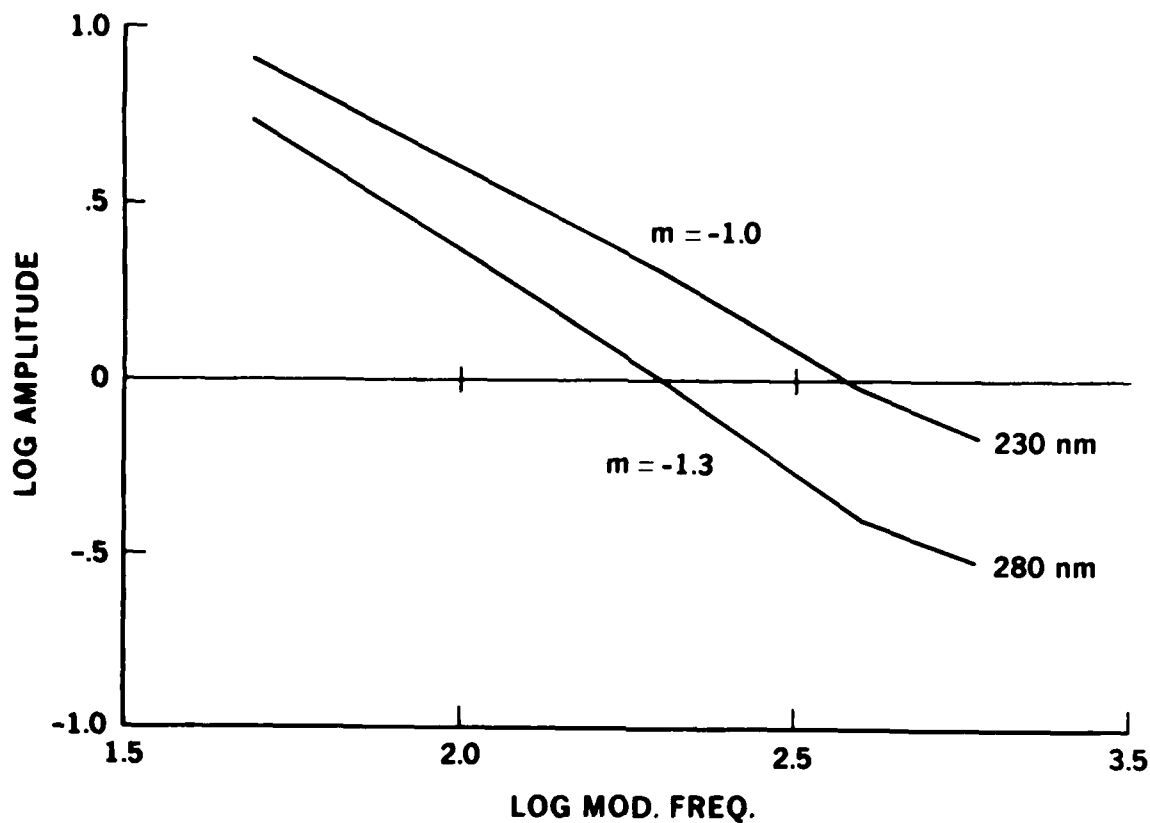


Figure 34. Plot of log of photoacoustic signal amplitude at 230 nm and 280 nm vs. log of modulation frequency, indicating saturation of signal at 280 nm.

ocular lens safety and hazard are considered. The nature of these inferences may vary from conjectures, to assumptions, to hypotheses. The first of these is meant to imply a possibility statement with but few supporting evidences, whereas the last implies a stronger statement with considerable evidence.

#### A. Ocular Lens Protection Against UV Radiation Wavelength

Safety criteria for protecting ocular lenses of employees subjected to possible UV exposure in terms of wavelength have been assessed from previous work as well as this investigation. The criteria should protect against--

- (1) Wavelengths that are known experimentally to cause UV cataracts (see Fig. 2b and references 15 and 16).
- (2) Wavelengths that produce chemically reactive excited states (see Fig. 3, reference 2, and Section III C of this report).

- (3) Wavelengths that produce free radicals as evidenced from this investigation (see Fig. 1 and Section III A of this report).

Such protection can be provided by specially manufactured protective filters or goggles. The bases for safety criteria are illustrated in a composite manner in Figure 2. Corneal absorption is added to the figure to erase the sharp spike in the action spectrum of Bachem (15), which was obtained from guinea pigs *in vivo*.

On the basis of the spectra in Figure 2, the wavelengths of maximum potential hazard to the lens lie in the range of 290-300 nm. If all potential hazards are considered inclusively, the region to be avoided includes wavelengths up to 340 nm; this restriction is not practiced by manufacturers of UV goggles at the present time. A filter that eliminates the range below 340 nm will protect the human eye from potential damage to the following: (a) aliphatic amino acids in the lens proteins, (b) nucleic acids (DNA, RNA), and (c) aromatic amino acids (Trp, Tyr, Phe, and His). The presence of 340 nm as the upper limit of the wavelength to be filtered will prevent some photo-oxidation products of Trp, such as N-formyl kynurenine, from undergoing further photochemical changes.

A discussion of the techniques used to study free-radical formation through electron spin resonance (EPR) can be found in an article by Yamanashi et al. (33). This recent paper describes the EPR-monitored wavelength dependence of free-radical formation in the human lens as well as the cornea. The spectral feature of having their maxima close to 290 nm, negligible intensity above 340 nm, and appreciable intensity toward 260 nm is common to both of these tissues; hence, the  $\lambda \leq 340$ -nm criterion is important for the safety of both the lens and cornea. The similarity of the lens and the cornea action spectra for free-radical production is attributed to the proteinaceous nature of these tissues.

#### B. Ocular Lens Protection Against Radiation Dosage

Consideration of maximum allowable irradiance may be divided into two inquiries. Assuming that a protective goggle is not worn, (a) what is the threshold for acute lens damage? (i.e., what dosage produces immediate thermal denaturation), and (b) what is the irradiance that just initiates chemical changes in the lens protein that may eventually cause cataract? We do not have answers to either of these questions; however, from previous data (26) the irradiance that causes acute thermal effects in an extracted primate lens must be at least a few hundred  $\text{mW}/\text{cm}^2$ . In particular,  $400 \text{ mW}/\text{cm}^2$  (351-363 nm) caused acute damage through thermal denaturation of the lens proteins in primate and rabbit lenses. *In vivo*, the cornea, aqueous humor, and iris attenuate the thermal effect; hence, more than  $400 \text{ mW}/\text{cm}^2$  irradiance is required to cause acute damage. For the sake of comparison, in a single, continuous exposure of a rabbit lens to IR ( $1.0 \mu\text{m}$ ), an irradiance of  $4.5 \text{ W}/\text{cm}^2$  for approximately 1 minute was required to thermally denature the lens (44). In the case of UV, the electronic energy must be converted to thermal energy. Thermal diffusivity and the optical properties (e.g., composite optical absorption) of the material determine how efficiently this conversion takes place in the cornea-aqueous-iris-lens complex. It is certainly less efficient

than the thermal denaturation process resulting from exposure to an IR laser which requires negligible conversion. In most occupational situations, the high-intensity UV sources are either UV lasers or high-pressure xenon or mercury arc lamps, and high-level intensities are an integral part of such equipment; the use of protective goggles is therefore absolutely essential. Less definitive is the consideration of maximum allowable irradiance required to produce latent lens damage.

To determine the maximum allowable irradiance for chronic or latent UV cataract, we referred to the following previous works:

(1) Epidemiologically, brunescent cataract is associated with ground-level solar radiation, so countries near the equator have a higher incidence of UV cataracts than other countries (45-47).

(2) The appreciable occurrence of brunescent cataracts in the United States has been correlated with the relative irradiance of ground-level solar radiation (48).

(3) Medical records on the surgical removal of brunescent cataracts indicate that for these cataracts to develop to their full extent, such that surgical removal would be necessary to restore vision, an age of at least 50-60 years is usually necessary.

(4) Experimentally induced UV cataracts in mice are similar in biochemical constituents to those of humans. Further, the degree of UV cataract is shown to be related to the concentration of free radicals produced.

From these observations we may conclude that--

(1) The level of UV irradiation that causes molecular-level damage, which may lead to brunescent cataract, is within the range of ground-level solar radiation, and

(2) The irradiance dependence of free-radical production in the human lens in vitro may be used to determine an approximate maximum allowable irradiance.

In Sections II B and III B we discussed the experimental procedure and the results obtained in our attempt to determine the irradiance level just sufficient to produce a detectable EPR signal due to UV-induced free radicals. We gave only a ballpark figure (more work would be necessary to do otherwise) for the maximum safe UV irradiance for chronic exposure since the experiment was performed in vitro with an extracted human lens. Additional irradiance may be required to produce free radicals in the lens in vivo.

### C. Role of the Tryptophan-Excited Triplet State in UV-Induced Cataractogenesis

Molecules can exist only in discrete energy states, and the total energy of a molecule can be represented as the sum of electronic, vibrational, and rotational energies, all of which are quantized. With each electronic state,

a number of vibrational states are associated; and with each of these, a number of rotational states. The creation of an electronically excited state requires a photon of energy,  $hc/\lambda$ , where  $\lambda$  is in the UV-visible range (i.e., 10-770 nm). A transition from the ground to an excited state is accompanied by significant changes in electronic distribution within the molecule. Electronically excited states of some molecular systems are more chemically reactive than their ground states.

The involvement of photoexcited states and free radicals in UV-induced cataract has been suggested by Kurzel et al. (1), based on the observation that the phosphorescence excitation spectrum of a human lens is identical to that of tryptophan and has a maximum similar to that in Bachem's action spectrum of UV-induced cataractogenesis in guinea pigs and rabbits (15). The EPR spectra of UV-irradiated cataractous human lenses exhibit  $\Delta M_S = \pm 2$  transitions at a magnetic field of 1455 Gauss with a microwave frequency of 9.092 GHz and a free-radical signal with  $g = 2.003$ . With respect to irradiation time, the intensity of the half-field signal ( $\Delta M_S = \pm 2$ ) decreases while the free-radical signal increases. The assignment of the half-field signal to the photoexcited triplet state of tryptophan by Weiter and Finch (3) is consistent with phosphorescence excitation data (1). The intensity of the signal with  $g \approx 2$  ( $H \approx 3240$ ,  $f = 9.092$  GHz) correlates with the age of the lens as well as the concentration of fluorescent pigments reported by Lerman and Borkman (8). The relative intensities of two such fluorescent species present in the human lens are indicators for age and for the morphological classification of cataractous lenses. The rate of decay of the  $\Delta M_S = \pm 2$  triplet-state signal of tryptophan and the buildup of the free-radical signal in several animal species were found to be nearly identical by Yamanashi and Zuclich (20b). Another  $\Delta M_S = \pm 2$  triplet-state signal, in addition to that of the triplet state of tryptophan, was found at  $H = 1575$  Gauss with a microwave frequency of 9.113 GHz in UV-irradiated rhesus monkey lens (20b).

To confirm Kurzel's suggestion that the excited triplet state of tryptophan plays an important role in UV cataractogenesis, we obtained an EPR-monitored excitation spectrum of the tryptophan triplet state via  $M_S = \pm 2$  signal. (This data was given in Fig. 3.) It offers, within the spectral region of 290-300 nm, evidence for the involvement of tryptophan and its electronically excited states in the production of free radicals.

The following list summarizes the evidence for tryptophan involvement in UV-induced cataract formation:

(1) The action spectrum for UV cataractogenesis occurs within the same spectral region as the excitation spectrum for phosphorescence in the human lens (2).

(2) The excitation spectrum for phosphorescence in the human lens is almost identical to that of protein-bound tryptophan (2).

(3) The maximum of the action spectrum for UV-induced free radical production (as noted in Fig. 1) occurs in the same wavelength region as both the maximum of the action spectrum of UV cataractogenesis and the maximum of the excitation spectrum for tryptophan (see Fig. 2).

(4) Among the molecular species in the ocular proteins that absorb in the UV region (including phenylalanine, histidine, cysteine, and nucleic acids), none have first excited singlet states in the 280- to 300-nm region. Tyrosine and tryptophan are the only two that have first excited singlet states in this region (49).

(5) Tryptophan (not tyrosine, whose phosphorescence maximum is 395 nm) has the lowest lying excited triplet state (phos. max = 450 nm); hence, it has the highest probability of being an "energy sink" among the protein constituents (49).

(6) Tryptophan (not tyrosine, whose molar extinction is only 290 at 275 nm) has the highest molar extinction (absorption) coefficient (6500 at 280 nm) among UV-absorbing molecular species in the proteins. It also has the highest quantum efficiency for fluorescence (49).

(7) A photo-oxidation product of tryptophan may be involved in cataractogenesis (46), but not in the initial formation of free radicals since it does not absorb in the 280-300-nm region. Typical examples are N-formyl kynurenine,  $\lambda_a = 320$  nm, kynurenine,  $\lambda_a = 360$  nm, and anthranilic acid,  $\lambda_a = 320$  nm.

(8) The kinetics of the decay of the tryptophan triplet state (monitored via  $\Delta M_S = \pm 2$  EPR signal intensity) are identical to the kinetics of the buildup of the free radicals (20).

In molecular electronic excitation processes, the excited triplet state is created via an intersystem crossing from the singlet state (since the ground state of most molecules is a singlet, and direct excitation to the excited triplet state is spin (or multiplicity) forbidden) and hence has a low probability. The energy diagram and molecular scheme involving the  $S_1$  and  $T_1$  states of free tryptophan are shown in Figure 35. The intersystem crossing is also spin forbidden; however, this restriction is overridden by (a) coupling of electron spin and orbital angular momenta, and (b) probability of vibrational coupling. Phosphorescence is also a spin-forbidden process and is observed only when other competing vibrational processes are suppressed experimentally (e.g., by lowering the temperature). Therefore, monitoring the EPR  $\Delta M_S = \pm 2$  transition intensity with respect to wavelength reveals how the  $T_1$  state is populated via the process  $S_0 \xrightarrow{\text{Abs}} S_n, S_n \xrightarrow{\text{Int Conv}} S_1, S_1 \xrightarrow{\text{Intsys Cross}} T_1$  and also represents an effective absorption spectrum of the system.

Since both are formed and reactive, we suggest that the  $S_1$  and  $T_1$  states of tryptophan are potentially important in UV-induced cataractogenesis. Their roles in free-radical production and their kinetics will be discussed in the sections to follow.

#### D. Possible Role of a Photo-Oxidation Product of the Tryptophan Triplet State as an Intermediate in UV-Induced Free-Radical Formation

For the kinetic theory model presented in Section III D to be correct, experimental kinetics of all species involved (e.g.,  $^3\text{Trp}$ ,  $^3\text{NFK}$ , and  $R^*$ ) must conform to one set of predicted rate constants  $k_i$  and  $k_{ij}$ . As shown in

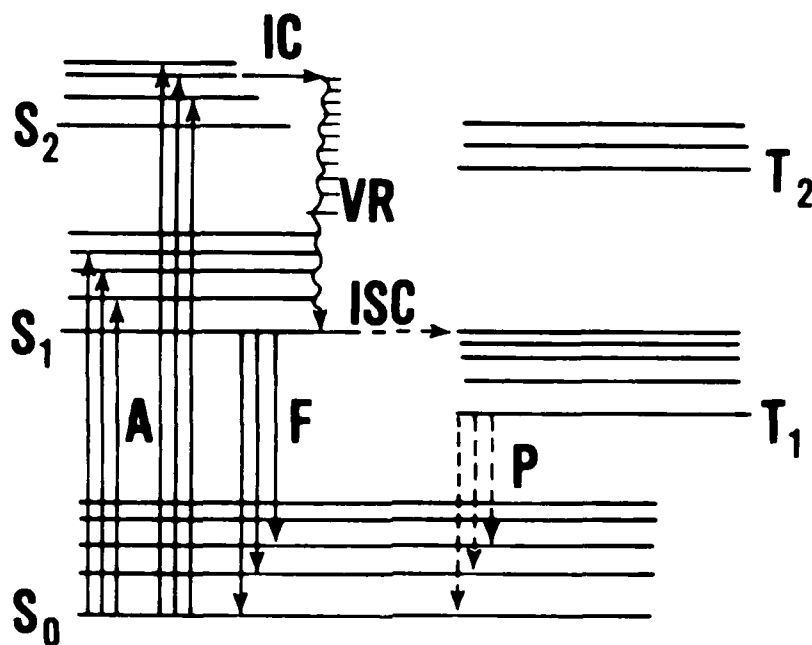


Figure 35. Jablonski-type diagram for molecular electronic processes: A = absorption, F = fluorescence, P = phosphorescence, IC = internal conversion, VR = vibrational relaxation, and ISC = intersystem crossing. (IC's and VR's for S<sub>1</sub> - S<sub>0</sub> states and T<sub>2</sub> - T<sub>1</sub> are not shown in order to avoid confusion in the diagram.)

the computed curves in Figure 4, the kinetics of <sup>3</sup>NFK and <sup>3</sup>Trp are predicted properly; however, that of the radical R<sup>•</sup> is not. This leads us to suspect that the monitored parameter d[R<sup>•</sup>]/dt is likely to be a multicomponent parameter. This assumption is supported by the results of our spin trapping experiment and also by the fitting of d[R<sup>•</sup>]/dt with a two-component exponential function. The unsuccessful fitting of R<sup>•</sup> in the model of <sup>3</sup>NFK as the intermediate between <sup>3</sup>Trp and R<sup>•</sup> does not rule out this possibility, but it suggests that R<sup>•</sup> is not a unique species produced solely by this scheme. The role of <sup>3</sup>NFK in cataractogenic crosslinking is discussed in Section IV F. Via the EPR technique, <sup>3</sup>NFK has been found in both UV-irradiated rhesus-monkey and rabbit lens (20), and both of these species are susceptible to UV cataractogenesis. Although d[R<sup>•</sup>]/dt in the lens does not conform to the predicted kinetics, it is of interest to examine if a component of d[R<sup>•</sup>]/dt does.

#### E. Two-Component Kinetics of Free-Radical Formation in the Lens and Its Implication with Regard to UV Cataractogenesis

In Section III E we showed that the experimental kinetics of UV-induced free-radical formation was computer fitted successfully with a two-component

exponential function, Eq. 19. One of the two rate constants was found to be common to the lens and the cornea, and tryptophan in the protein was suspected as the origin of the free radical associated with this rate constant. The ocular safety aspect of these observations is that the free radical that may cause cataractogenic crosslinking in the lens may also cause UV actinic keratopathy in the cornea. This conjecture is based on the following analogies between UV cataract and UV actinic keratopathy.

Lens UV cataract

UV chronic cornea actinic keratopathy

Yellowish-brown pigmentation progresses with repeated exposure.

Yellowish bandlike pigmentation progresses with repeated exposure.

Absorption (320-340 nm) and fluorescence (440-520 nm) increase progressively.

Fluorescent droplets increase progressively.

For UV-induced free-radical formation,  $\lambda_{\max} \approx 290 \text{ nm}$ .

For UV-induced free-radical formation,  $\lambda_{\max} \approx 290 \text{ nm}$ .

Contains protein-bound tryptophan.

Contains protein-bound tryptophan.

Possesses one common rate constant for  $d[R^{\cdot}]/dt$  with the cornea.

Possesses one common rate constant for  $d[R^{\cdot}]/dt$  with the lens.

Occurs mainly at locations subjected to high solar radiation.

Frequently occurs in persons living in countries near the equator.

Severe case constitutes dense opacification.

Severe case shows completely opacified band across the cornea.

The similarity of UV-induced cataract (cataracta brunescens) and UV-induced chronic actinic keratopathy implies that preventive methods which would work for one would probably work for the other.

F. Free-Radical Species Produced Under Monochromatic and Nonmonochromatic Irradiation of the Human Lens and Related Materials: Spin Trapping and Implications of Experimental Results

The DMPO spin trapping results, described in Section III F may be summarized as follows:  $-H^{\cdot}$ ,  $-OH^{\cdot}$ , and  $-C^{\cdot}$  radicals were found in the lens in both the water-soluble and urea-soluble fractions;  $-H^{\cdot}$  and  $-C^{\cdot}$  radicals were found in the urea-insoluble fraction. The presence of hydrogen atoms is consistent with the theory of cataractogenic mechanisms proposed by Kurzel et al. (2) and confirms the previous findings of Evans and Yamanashi (21).

Typical nonocular proteins, such as lysozyme and albumin, gave DMPO spin-adduct hyperfine splittings very similar to those of the ocular protein fractions. They are also similar to DMPO spin adducts of aromatic amino acids; i.e., His, Phe, Try, and Trp. Poly-DL-tryptophan yielded a similar spectrum to that of Trp and to those of the ocular proteins. Ribonuclease, on the other hand, showed no spin adduct spectrum under broad-band irradiation and only a low-intensity oxygen-centered radical adduct at  $\lambda = 300 \text{ nm}$ . The



aliphatic amino acids examined showed adduct spectra indicating that the concentration of radicals was negligible as compared to that of the proteins or aromatic amino acids. Cataractogenic 8-MOP gave a spin adduct spectrum similar to Trp, but the relative intensity of DMPO-H, DMPO-OH, and DMPO-C varied considerably. The relative intensity of the spin adduct signals varied among the aromatic amino acids as follows: tryptophan > tyrosine > phenylalanine > histidine for a given irradiation time and sample concentration, under irradiation at  $\lambda = 290$  or  $300$  nm. This means that the molar extinction coefficients of these aromatic amino acids at these wavelengths are in the same order, and the excited states (likely to be  $S_1$  states) must be involved in the production of the trapped free radicals.

The similarity of the spin adduct spectra for Trp (and any proteins or peptides containing Trp) may be explained by the Trp energy sink hypothesis, which states that since Trp has the lowest electronic state,  $^3\text{Trp}_1$ , among the amino acids, any excitation energy higher than  $^3\text{Trp}_1$ , furnished to a peptide or a protein, tends to populate this state via various modes of energy transfer.

The negligible spin adduct signal intensity of the aliphatic amino acids may be explained since the  $S_1$  level of all aliphatic amino acids is considerably higher than that of  $^3\text{Trp}_1$ ; therefore, the  $S_1$  states of these are not populated sufficiently to cause appreciable free-radical population.

The virtual absence of a spin adduct spectrum in ribonuclease (a peptide with no tryptophan) under broad-band excitation may mean that (a) Trp is the major species in the protein that produces free radicals, or (b) Trp is the species that mediates in the free radical production in the protein. The latter inference may involve photosensitization, catalysis, or other processes in which Trp is chemically unchanged but has its excitation energy transferred to reactants.

DMPO spin trapping of ocular lens protein giving the evidence of  $-\text{H}^\cdot$ ,  $-\text{OH}^\cdot$ , and  $-\dot{\text{C}}$  does not rule out the possibility of other oxygen-centered radicals such as  $-\text{OOH}^\cdot$ ,  $-\text{OO}^\cdot$ , or  $-\text{N}^\cdot$  and  $-\text{S}^\cdot$ . Spin traps capable of distinguishing between  $-\text{OOH}^\cdot$  and  $-\text{OH}^\cdot$  have only recently been introduced by Finkelstein et al. (50); traps capable of capturing  $-\text{S}^\cdot$  to form a stable radical have not been reported. Trapped  $-\text{H}^\cdot$  radicals must come from some functional group in a protein (or peptide) leaving another paramagnetic species. Energetically, the formation of  $-\text{N}^\cdot$  and  $-\text{S}^\cdot$  radicals from amines and sulfhydryl groups is possible.

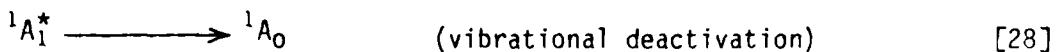
In the following sections, we propose primary and secondary photochemical processes that may lead to cataract formation in the ocular lens.

#### 1. Proposed Mechanism of UV-Induced Cataractogenesis: Primary Photochemical Processes

In the lens proteins, the aromatic amino acids Trp, Tyr, Phe, and His are capable of absorbing near-UV photons; hence the primary interaction would be



where  ${}^1A_0$  denotes any one of the above amino acids in the ground state and  ${}^1A_n^*$  denotes excited singlet states, where  $n = 1, 2, 3, \dots$ ,  $\nu = c/\lambda$ , and  $250 < \lambda < 340$  nm.



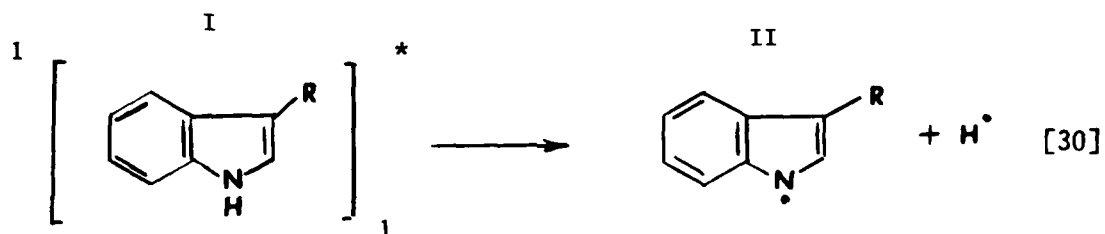
The highest singlet state is extremely short-lived, so it is quickly converted vibrationally to  ${}^1A_1^*$ , the first excited singlet state. If no other molecule is reacting,  ${}^1A_1^*$  will emit fluorescence  $h\nu_f$ , undergo an intersystem crossover to excited triplet state  ${}^3A_1^*$ , or vibrationally deactivate itself to  ${}^1A_0$ . The electronic energy levels of  ${}^3\text{Trp}^*$  are the lowest among the singlet or triplet excited states of His, Phe, and Tyr. Further,  $E({}^1\text{Trp}_1^*) > E({}^3\text{Trp}_1^*)$  by Hund's rule,\* where  $E(\ )$  denotes the energy of the state in the parenthesis. Intermolecular electronic energy transfer takes place among the aromatic amino acids' excited states following Förster's energy transfer criteria.\*\* Singlet-to-triplet intermolecular energy transfer is of the dipole-dipole type; hence the transfer distance may be 50 Å or greater, so transfer between nonadjacent aromatic amino acids is possible. Triplet-triplet intermolecular transfer is an exchange interaction; hence it is diffusion controlled, so two molecules have to be within collisional distance of each other. The latter type of energy transfer has lower probability in the peptide chains. The dominance of Trp fluorescence and phosphorescence in the lens crystallin proteins (as well as many other proteins) is a manifestation of (a) intermolecular energy transfer taking place, and (b) the electronic excitation energy ending up in the excited states of the lowest energy, namely  ${}^1\text{Trp}_1^*$  and  ${}^3\text{Trp}_1^*$ . For this reason these tryptophan-excited states are considered important in any UV-induced biological effect as the initial reactive excited-state species.

\*Hund's rule: In a given molecular (or atomic) electronic manifold, electronic states of highest multiplicity have the lowest energy level.

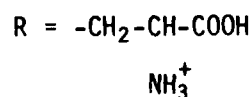
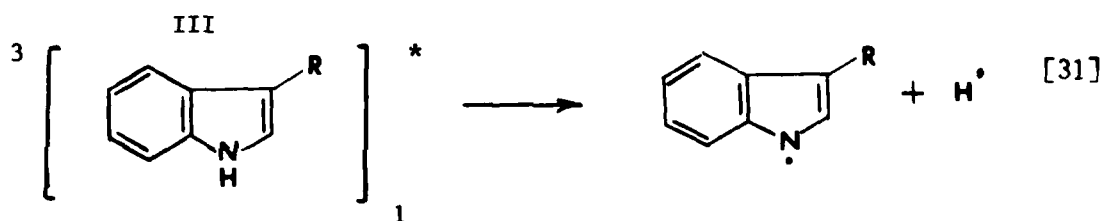
\*\*Förster's criteria: For an intermolecular energy transfer to take place, the absorption spectra of the "donor" and the emission spectra of the "acceptor" must overlap, at least partially.

## 2. Secondary Reactions and Possible Crosslinking of Peptides

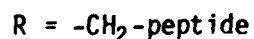
Once reactive excited states are formed, they can deactivate themselves (either radiatively or nonradiatively) or undergo various chemical reactions. Although we do not rule out the excited states of His, Phe, and Tyr, we feel that  $^1\text{Trp}_1^*$  and  $^3\text{Trp}_1^*$  are the most probable species in the lens proteins that may undergo further chemical reactions of the form seen in Eqs. 30 and 31.



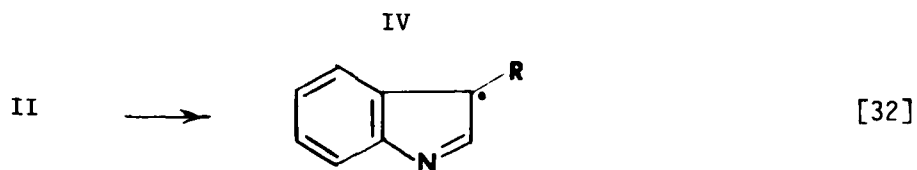
Intersystem crossing



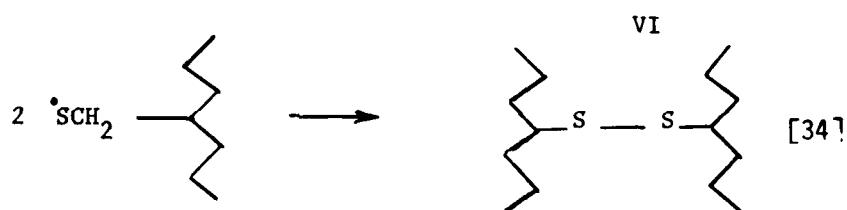
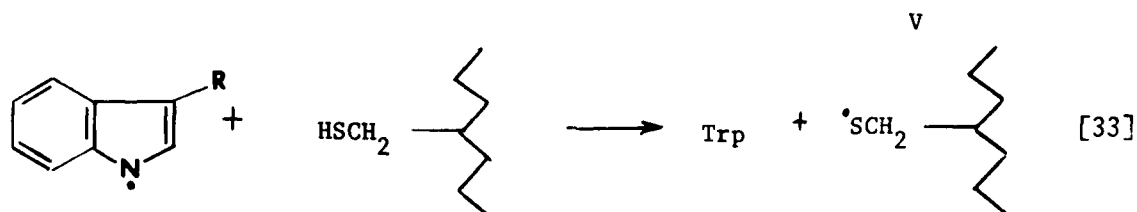
or



These reactions illustrate two of the possible processes resulting in N-H bond cleavage. Since the N-H bond is the weakest in the indole ring, with bond strength of only 75-80 kcal/mol, it can be cleaved relatively easily by the absorption of radiation in the range 300-365 nm. The process of electron abstraction from the singlet state, followed by N-H bond cleavage, has been demonstrated by Pailthorpe and Nicholls (42). The abstraction of electrons from the triplet state is also possible.

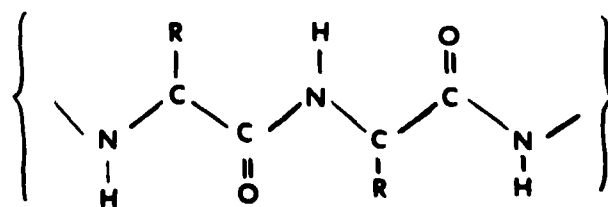


The radical species II rearranges itself to yield the sterically more stable form IV. However, either II or IV may undergo various nonphotochemical reactions in a peptide; for example,

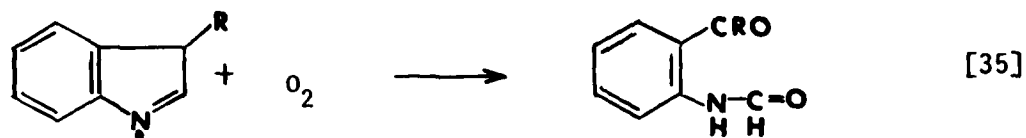


Crosslinking via two Cys radicals

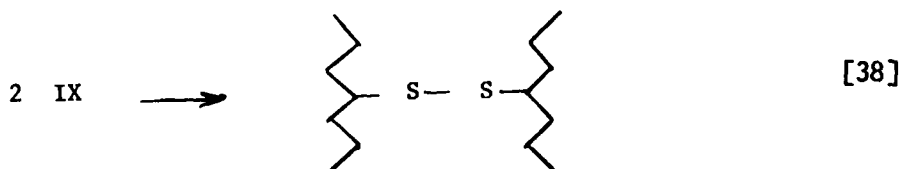
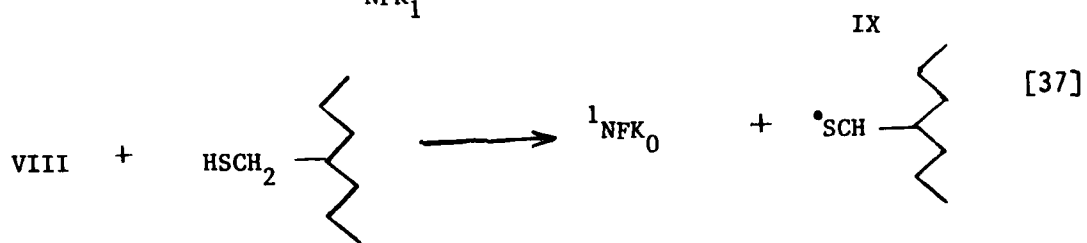
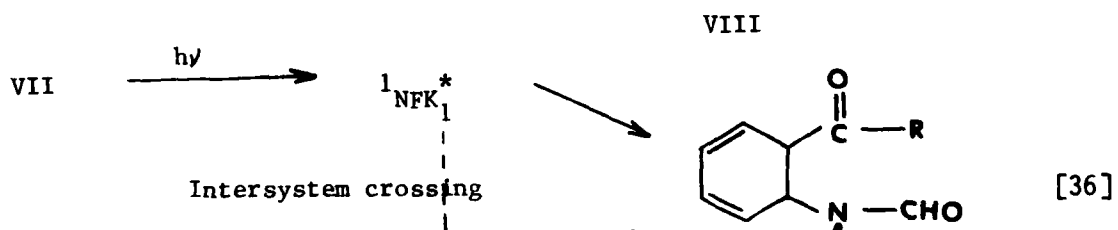
Equations 33 and 34 illustrate the reaction of radical II with cysteine residue (shown below) in which a portion of the peptide chain is represented by the symbol



The product V is a sulfur-centered radical, two of which may crosslink two adjacent peptides VI or two branches of the same peptide. The photo-oxidation of Trp may proceed via IV to produce N-formyl kynurenine (NFK) as shown in Eq. 35.

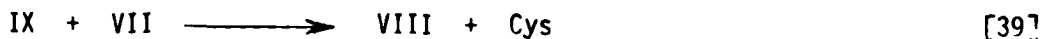


In addition, NFK(VII) may be further photo-excited to its singlet or triplet state so as to produce free radicals, as shown in Eqs. 36-38.

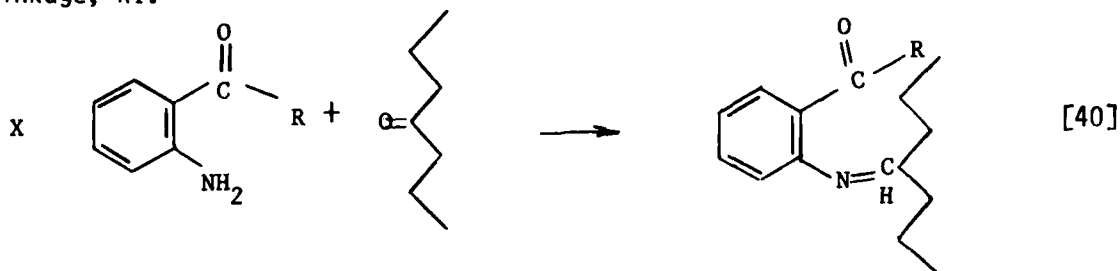


Crosslinking via two Cys radicals induced by photo-excited states and free radicals of N-formyl kynurenine

The NFK radical VIII may abstract a hydrogen atom from Cys to produce a sulfur-centered radical, two of which would be able to crosslink adjacent peptide chains. The cysteine radical IV may abstract the ex-indole hydrogen from NFK to form NFK radical VIII.

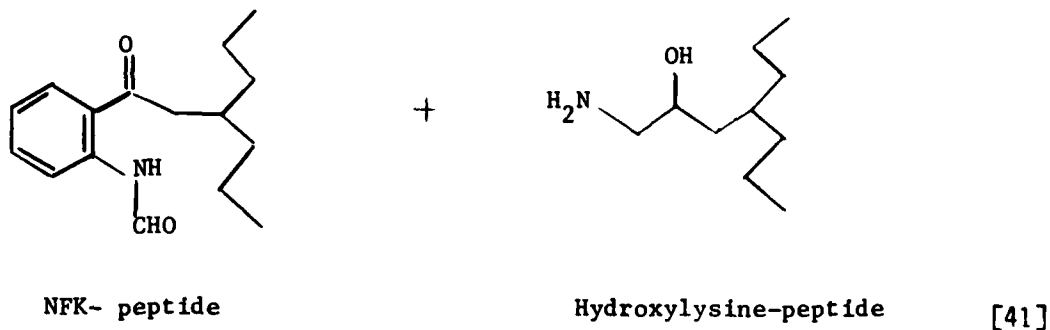


Further oxidation of NFK would result in anthranilic acid X, which may react with a carbonyl group of an adjacent peptide to form a Schiff-base type crosslinkage, XI.



Crosslinking via NFK-R and a ketonic group in a peptide  
(R may be any peptide)

Further, the formyl oxygen of NFK may undergo an analogous reaction with an amino group in a peptide chain to form crosslinking of the type in Eq. 41.

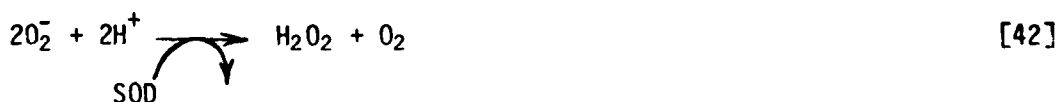


Crosslinking via NFK-Hyl

Our EPR spin trapping results agree with the suggested mechanism in terms of the UV-induced production of  $-H\cdot$  and  $-C\cdot$ . Although not discussed in this report the production of  $-OH$ ,  $-OOH$ , and  $-OO$  is possible, especially when the oxidation proceeds via singlet-excited oxygen in the presence of a sensitizer. Unfortunately, with our present spin trap DMPO, a differentiation between  $-OH$  and  $-OOH$ , while not impossible, is difficult; and the detection of  $-S\cdot$  is impossible due to its instability with either nitron or nitroso spin traps. The kinetic behavior of  $NFK^*$ , observed by Yamanashi and Zuclich (20b) and theoretically computed by us, is also consistent with the proposed mechanism in Eqs. 4-14, provided that the  $NFK$  radical is resonance-stabilized to form a carbon-centered radical. Good agreement between theory and experiment relating the kinetics of  $^3NFK^*$  and the buildup of  $g = 2.003$  EPR signal is lacking because (a) the  $g = 2.003$  radical signal is a composite of more than two signals, and (b) the S/N ratio of the  $\Delta M_S = \pm 2$  EPR signal from  $^3NFK^*$  is extremely low.

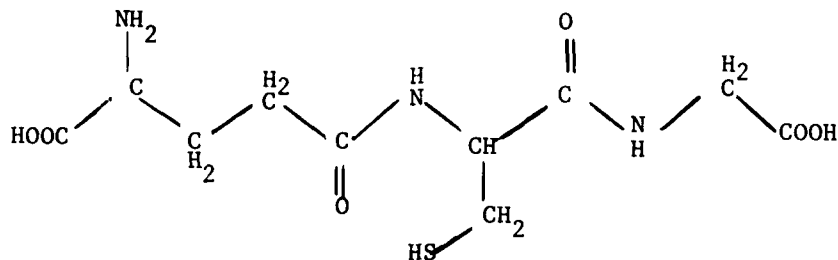
### 3. Sensitization, Inhibition, Protection, and Repair in UV-Induced Cataractogenesis

Based on the molecular-level mechanism suggested above, we now consider how the process of UV-induced crosslinking among peptides may be accelerated, slowed down, or reversed. We know that although the rate of metabolism is very slow in the lens, the lens does have several protective mechanisms against UV radiation that involve enzymes, some of which are catalase, glutathione reductase, and superoxide dismutase (SOD).

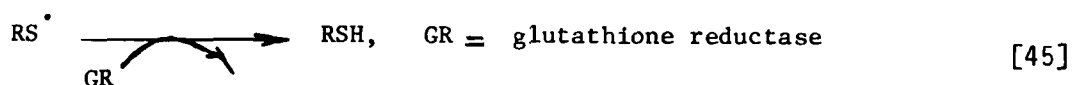
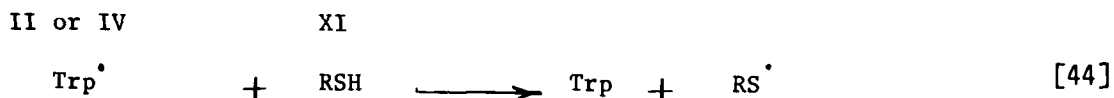


Superoxide anion  $O_2^-$  and hydrogen peroxide  $H_2O_2$  are extremely reactive and capable of producing irreversible damage to various biomolecules. They are formed during various hydroxylation and oxygenation reactions. Superoxide dismutase removes  $O_2^-$  as quickly as it is formed, while catalase removes  $H_2O_2$  analogously. The protective action of superoxide dismutase and catalase is probably accelerated by ascorbic acid, glutathione, and vitamin E, which readily accept electrons and may serve a backup function by scavenging free radicals (51).

Glutathione (RSH)



In the cataractogenic scheme involving photo-induced Trp radicals, one of the protective and repair mechanisms involving glutathione and glutathione reductase can be written:



where these reactions may be repeated as long as there is Trp<sup>•</sup> to scavenge; hence, UV cataractogenesis can be accelerated by any process that (a) enhances the rate of production of <sup>1</sup>Trp<sub>1</sub><sup>•</sup> or <sup>3</sup>Trp<sub>1</sub><sup>•</sup>, (b) enhances the production of Trp<sup>•</sup>, or (c) slows down the reaction in Eq. 45.

Examples of the above are--

- (1) Processes that increase the efficiency of the intermolecular energy transfer to the <sup>1</sup>Trp<sub>1</sub><sup>•</sup> state
- (2) Enhanced spin-orbit coupling between <sup>1</sup>Trp<sub>1</sub><sup>•</sup> and <sup>3</sup>Trp<sub>1</sub><sup>•</sup> via the external heavy atom effect
- (3) The presence of electron donor molecules, such as quinones or semi-quinones, that initiate or speed up the chain reactions producing free radicals and any processes that tend to deactivate protective enzymes.

On the other hand, UV cataractogenesis can be inhibited or slowed down by any process that (a) inhibits or interferes with the rate of production of <sup>1</sup>Trp<sub>1</sub><sup>•</sup> or <sup>3</sup>Trp<sub>1</sub><sup>•</sup>, (b) inhibits or interferes with production of Trp<sup>•</sup>, or (c) enhances the action of protective enzymes.



Some of these UV-cataract inhibitory processes are--

- (1) Processes that contribute to a decrease in the efficiency of the intermolecular energy transfer to  $^1\text{Trp}_1^*$  or  $^3\text{Trp}_1^*$
- (2) Processes that tend to decouple spin-orbit interaction in  $^1\text{Trp}_1^*$  and  $^3\text{Trp}_1^*$
- (3) Presence of electron acceptor or free-radical scavenger molecules such as ascorbic acid (vitamin C), vitamin E, and glutathione
- (4) Presence of any cofactors that enhance the action of protective enzymes.

Once crosslinks between peptides are formed not only by disulfide linkage but also by covalent linkages, it is extremely difficult to uncrosslink them, even in vitro. However, the use of ascorbic acid and vitamin E may slow down and hence prevent UV cataractogenesis.

Drugs used medicinally for nonocular purposes, such as prednisone acetate or 8-MOP, are efficient electron donors, and repeated usage of these drugs is known to enhance UV-induced cataract (18).

#### G. Fingerprinting of UV-Damaged Ocular Lens Proteins with 2-D Electrophoresis

The mass-charge profile of a typical 2-D electrophoresis, when accompanied by a standard, serves as a fingerprint for proteins. The particular advantage of being 2-D is that two closely related proteins that cannot be distinguished by the 1-D method are often resolvable in the added dimension. Species difference, denaturation, mutation, and chemical alteration are only a few of such applications. Application of the 2-D method to analysis of UV-damaged ocular lens protein is still in the development stage. The following is a summary of the results from our ocular lens irradiation analysis.

- (1) The UV exposure of  $\beta_L$  and  $\gamma$  crystallins produced higher molecular fraction not exceeding mol wt = 13,700.
- (2) The UV exposure of  $\beta_L$  and  $\gamma$  crystallins produced new peptides in the more acidic region (left side of the 2-D plate).
- (3) The UV exposure caused an aggregation among subunits of similar composition.
- (4) Some fractions of  $\beta_L$  and  $\gamma$ , which appeared during the early part of the irradiation exposure in both the control samples, may have resulted from IR modification of these protein fractions.

If necessary, the molecular weight and the charge of the protein examined may be approximated using several known standard samples; however, for identification purposes involving various irradiation conditions, a 2-D pattern with a "standard" run simultaneously is sufficient.

#### H. Fluorescence Analysis of UV-Irradiated Lens Crystallin Proteins; $\gamma$ -Crystallin as a UV Susceptibility Factor

Significant inferences obtained from our fluorescence study of the cow- and rabbit-lens crystallin proteins are--

- (1) A significant progressive decrease of Trp fluorescence, accompanied by a progressive increase of emission around 450 nm, in the  $\gamma$  crystallin of rabbit lens suggests that the photo-oxidation of Trp produces products of Trp, such as NFK, 3-OHK, and anthranilic acid.
- (2) These progressive changes in the fluorescence of Trp and other fluorogens at about 450 nm were negligible in the cow  $\gamma$ -crystallins. This may be related to the relative UV susceptibility, as observed earlier (20a), with cow lens being more resistant than rabbit lens to UV damage.
- (3) The  $\alpha$ ,  $\beta_L$ , and  $\beta_H$  crystallins showed a significant decrease in Trp fluorescence and an accompanying increase in emission at about 450 nm. This observation is consistent with the hypothesis that Trp is the altered species in the UV irradiation of the lens.
- (4) The shape of the broad fluorescence emission at about 450 nm (extending from 400-520 nm) suggests the presence of more than one fluorogen. This observation is confirmed by a recent study by Fujimori (52).

#### I. Photoacoustic Measurements (PAS)

Interpretation of the PAS results described in Section III I may be summarized as follows:

- (1) The depth profile of the PAS of the lens is possible, as seen from the differences between the PAS of the lens cortex and the nucleus.
- (2) Due to the saturation effect, the absolute intensity of the PAS signal from the larger intensity peaks is relatively more accurate than that of the lower intensity ones.
- (3) In characterizing the PAS spectra of a given section of the lens, the measured intensities  $I_{285}$ ,  $I_{250}$ , and  $I_{340}$  are better compared as ratios because of inherent saturation effects.

After the experiments described in Section III I, we observed that--

- The pigment whose PAS signal is near 340 nm develops even within one scan of the spectrometer, which takes about 10 minutes.
- The intensity of the PAS signal in the IR region due to water decreases considerably within a few PAS scans.

- The rate of production of the 340-nm pigment in the denatured albumin or ocular lens protein is greater (faster) than in the non-denatured proteins. (This implies that UV cataractogenesis is not only irreversible but also tends to accelerate as aggregations proliferate in the lens.)

These observations suggest that PAS data must be acquired in a cooled, constant-temperature PAS cell, and the intensity vs. irradiation time of signals  $I_{285}$  and  $I_{340}$  should be recorded and contrasted with the fluorescence experimental results in Section III H.

#### J. Summary of Conclusions

Tryptophan in lens crystallin proteins is implicated as the major molecular species responsible for UV-induced cataractogenesis. The role of the electronically excited states of tryptophan  $^1\text{Trp}_1^*$  and  $^3\text{Trp}_1^*$ , which may be created within the irradiance (or luminosity) range of ground-level solar radiation, is to produce the tryptophan radical  $\text{Trp}^\cdot$  via electron abstraction. This free-radical species may initiate several possible heterogeneous free-radical chain reactions in the peptide, some of which may result in several different types of covalent crosslinking between peptides. N-formyl kynurenine may also be produced from  $\text{Trp}^\cdot$ . The photo-excited states of NFK, written as  $^1\text{NFK}^*$  and  $^3\text{NFK}_1^*$ , may produce the NFK $^\cdot$  radical which may either be oxidized to form anthranilic acid or react with the reactive group in the peptide to produce more free radicals--which in turn produce more crosslinkings; however, these free-radical chain reactions do not go on indefinitely because native free-radical scavengers are present. Together with its coenzyme, glutathione reductase functions to terminate free-radical chain reactions. Spectroscopic (UV-vis absorption, fluorescence, phosphorescence, PAS, and EPR) and biochemical studies (previous and present) have given evidence to support the free-radical mechanism and tryptophan photo-excited states as the initiating reactive molecular species in UV cataractogenesis.

By measuring the wavelength dependence of free-radical production in the human lens and by obtaining action spectrum of the production of  $^3\text{Trp}_1^*$ , as well as confirming that both of these are similar to the action spectrum of UV cataractogenesis, we are confident that the hypothesis of Trp as the key species in UV cataractogenesis is well founded.

The spin trapping results and the evidence of  $-\text{H}^\cdot$  and  $-\dot{\text{C}}$  in the lens proteins support the concept of  $-\text{N}-\text{H}$  cleavage as well as subsequent chemical reactions involving free radicals. Our experimental and theoretical studies on the kinetics of free-radical formation, and the depopulation of excited states such as  $^3\text{Trp}_1^*$  and  $^1\text{NFK}_1^*$ , are also consistent with the proposed mechanism.

#### K. Suggestions for Further Investigation

Due to the nature of our spin trap (DMPO), we were unable to detect sulfur-centered radicals or to distinguish hydroxide ( $-\text{OH}$ ), hydroperoxide ( $-\text{OOH}$ ), and superoxide ( $-\text{OO}$ ) radicals. We feel that oxygen-centered radicals

are also involved, along with the photo-excited states and free radicals of tryptophan, in the crosslinking of peptides. The involvement of superoxide anion radicals in relation to lenticular protein may prove to be important in the free-radical mechanism operative in UV cataractogenesis. No work has been reported on the spin trapping of sulfur-centered radicals in biological systems at room temperature. With respect to the UV cataractogenic mechanism, we suggest that additional effort be expended to study (a) spin trapping of oxygen-centered and sulfur-centered radicals, (b) spin trapping in systems with or without protective enzymes, (c) isolation and identification of chromophores that absorb in the range of 310-360 nm and fluoresce at 400-520 nm, and (d) radioisotopic labelling of species involved in the crosslinking of peptides.

#### REFERENCES

1. Kurzel, R. B., et al. Spectral studies on normal and cataractous intact human lenses. *Exp Eye Res* 17:65 (1973).
2. Kurzel, R. B., et al. Tryptophan excited states and cataracts in the human lens. *Nature* 241:132 (1973).
3. Weiter, J. J., and E. D. Finch. Paramagnetic species in cataractous human lenses. *Nature* 254:536 (1975).
4. Lerman, S., and R. F. Borkman. Photochemistry and lens aging. *Interdispl Top Gerontol* 13:154 (1978).
5. Lerman, S., et al. Photoacoustics, fluorescence and light transmission spectra of normal, aging and cataractous lenses. *Ophthalmic Res* 10:168 (1978).
6. Pirie, A. Color and solubility of the proteins of human cataracts. *Invest Ophthalmol* 7:634 (1968).
7. Lerman, S., et al. Induction, acceleration and prevention (in vitro) of an aging parameter in the ocular lens. *Assoc Res Vis Ophthalmol Annu Meeting. Abstr*, p. 84, 1975.
8. Lerman, S., and R. Borkman. Spectroscopic evaluation and classification of the normal, aging, and cataractous lens. *Ophthalmic Res* 8:335 (1976).
9. Bando, M., et al. Coloration of human lens protein. *Exp Eye Res* 20:489 (1975).
10. Truscott, R. J. W., and R. C. Augustein. Changes in human lens proteins during nuclear cataract formation. *Exp Eye Res* 24:159 (1977).
11. Lerman, S., et al. Acceleration of an aging parameter (fluorogen) in the ocular lens. *Ann Ophthalmol* 8:558 (1976).

12. Forbes, W. F., and C. R. Hamlin. Determination of -SH and -SS- groups in proteins - II. The age dependence of -SH and -SS- contents in the soluble protein fractions of the eye lens. *Exp Gerontol* 4:151 (1969).
13. Harding, J. J., and K. J. Dilley. Structural proteins of the mammalian lens: A review with emphasis on changes in development, aging and cataract. *Exp Eye Res* 22:1 (1976).
14. a. Heyningen, R. van. Assay of fluorescent glucosides in the human lens. *Exp Eye Res* 15:121 (1973).  
b. Heyningen, R. van. Fluorescent derivatives of 3-hydroxy-L-kynurenine in the lens of man, the baboon, and the grey squirrel. *Biochem J* 123:30 (1971).
15. Bachem, A. Ophthalmic ultraviolet action spectra. *Am J Ophthalmol* 41:969 (1956).
16. Pitts, D. G., et al. Ocular effects of ultraviolet radiation from 295 to 365 nm. *Invest Ophthalmol* 16:932 (1977).
17. Lerman S., et al. Induction, acceleration and prevention (in vitro) of an aging parameter in the ocular lens. *Ophthalmic Res* 8:213 (1976).
18. Freeman, R. G. Morphologic changes resulting from photosensitization of the eye with 8-Methoxypsoralen: A comparison with conventional ultraviolet injury. *Tex Rep Biol Med* 24:588 (1966).
19. Cloud, T. M., et al. Photosensitization of the eye with methoxsalen. *Arch Ophthalmol* 64:346 (1960), 66:689 (1961).
20. a. J. A. Zuclich. Ocular effects of ultraviolet laser radiation. USAFSAM Contract No. F-41609-73-C-0017, Quarterly Report, 1976.  
b. Yamanashi, B. S., and J. A. Zuclich. Triplet states of tryptophan, N-formylkynurenine, and UV-irradiated lens proteins. *Ophthalmic Res* 10:140 (1978).
21. Evans, C. A., and B. S. Yamanashi. Spin trapping studies on normal and cataractous human lens. IXth Southeastern Magnetic Resonance Conf. Abstract B2, 1977.
22. a. Forshult, S., et al. Use of nitroso compounds as scavengers for the study of short-lived free radicals in organic reactions. *Acta Chem Scand* 23:522 (1969).  
b. Chalfont, G. F., et al. A probe for homolytic reactions in solution-II. The polymerization of styrene. *J Am Chem Soc* 90:7141 (1968).  
c. Leaver, I. H., and G. C. Ramsey. Trapping of radical intermediates in the photoreduction of benzophenone. *Tetrahedron* 25:5669 (1968).

- d. Tanabe, S., and R. Konaka. Electron spin resonance studies of oxidation with nickel peroxide. Spin trapping of free radical intermediates. *J Am Chem Soc* 91:5655 (1969).
- e. Janzen, E. G., and B. J. Blackburn. Detection and identification of short-lived free radicals by an electron spin resonance trapping technique. *J Am Chem Soc* 90:5909 (1968).
23. Perkins, M. J. The trapping of free radicals by diamagnetic scavengers. In *Essays of free radical chemistry*. The Chemical Society Spec. Pub. #24, Ch. 5, p. 97, 1970.
24. Janzen, E. G. Spin trapping. *Accounts Chem Res* 4:31 (1971).
25. Lagercrantz, C. J. Spin trapping of some short-lived radicals by the nitroxide method. *J Phys Chem* 75:3466 (1971).
26. Cheng, I., and H. J. Shine. Photobenzidine rearrangements-IV. Products from photolysis of 1,4-diethyl-1,4-diphenyl-2-tetrazene. Spin trapping of N-ethylanilino and N-methylanilino radicals. *J Org Chem* 39:336 (1971).
27. Janzen, E. G., et al. The spin trapping reaction. In W. A. Pryor (ed.). *Organic free radicals*. *Am Chem Soc Symp Ser.* #67, Ch. 26, p. 432 (1978).
28. Janzen, E. G., and J. I-P. Lieu. Radical addition reactions of 5,5-dimethyl-1-pyrroline-1-oxide. ESR spin trapping with a cyclic nitron. *J Magnetic Resonance* 9:510 (1973).
29. Wargon, J. A., and F. Williams. Detection of thiyl radicals by spin trapping in the radiolysis of liquids. *J C S Chem Comm* 23:947 (1975).
30. Janzen, E. G., et al. The simultaneous detection of gas phase atoms and free radicals produced in a microwave discharge by ESR spin trapping methods. *Bull Chem Soc Jap* 46:2061 (1973).
31. Janzen, E. G. Stereochemistry of nitroxides. *Top Stereochem* 6:177 (1971).
32. Janzen, E. G., et al. Electron spin resonance of  $\beta$ -chloroalkyl nitroxides, angular dependence of  $\beta$ -chlorine hyperfine coupling. *J Phys Chem* 74:3025 (1970).
33. Yamanashi, B. S., et al. Wavelength dependence and kinetics of UV-induced free radical formation in the human lens and cornea. *Photochem Photobiol* 30:391 (1979).
34. O'Farrel, P. H. High resolution two-dimensional electrophoresis of proteins. *J Biol Chem* 250:4007 (1975).

35. Kottis, P., and R. Lefebvre. Calculation of the electron spin resonance line shape of randomly oriented molecules in a triplet state-I. The  $\Delta m = 2$  transition with a constant linewidth. *J Chem Phys* 39:393 (1963).
36. Janzen, E. G. A critical review of spin trapping in biological systems. In W. A. Pryor (ed.). *Free radicals in biology*, Vol. 4. New York: Academic Press, 1979.
37. Kibbelaar, M., and H. Bloemendal. The topography of lens proteins based on chromatography and two-dimensional gel electrophoresis. *Exp Eye Res* 21:25 (1975).
38. a. Warburg, O., and W. Christian. Isolierung und Kristallisation des Gärungsferments Enolase. *Biochem Zeit* 310:384 (1942).  
 b. Weber, K., and M. Osborn. The reliability of molecular weight determinations by dodecyl sulfate-polyacrylamine gel electrophoresis. *J Biochem* 244:4406 (1969).
39. Lowry, O. H., et al. Protein measurement with the folin phenol reagent. *J Biol Chem* 193:265 (1951).
40. Zigler, J. S., and J. B. Sidbury. A comparative study of  $\beta$ -crystallin from six mammals. *Comp Biochem Physiol* 53B:349 (1976).
41. Pirie, A. Photo-oxidation of proteins and comparison of photo-oxidized proteins with those of the cataractous human lens. *Isr J Med Sci* 8:1567 (1972).
42. Pailthorpe, M., and C. Nicholls. Indole N-H bond fission during the photolysis of tryptophan. *Photochem Photobiol* 14:135 (1971).
43. Rosencwaig, A., and A. Gersho. Theory of the photoacoustic effect with solids. *J Appl Phys* 47:64 (1976).
44. Wolbarsht, M. L., et al. Laser exposures in the maculas of human volunteers. Annual progress report, U.S. Army Contract No. DAMD 17-74-C-4133 (1976).
45. Pacurariu, I., and C. Martin. Dynamics of eye diseases of childhood and of advanced age. *Ophthalmologia* 17:289 (1973).
46. Chatterjee, A., et al. Vision survey in Himalayan area. *Am J Ophthalmol* 66:113 (1968).
47. McDonald, A. E. Causes of blindness in Canada. *Can Med Assoc J* 92:264 (1955).
48. Hiller, R., et al. Sunlight and cataract: An epidemiologic investigation. *Am J Epidemiol* 105:450 (1977).

49. Maki, A., and J. A. Zuclich. Protein triplet states. *Top Curr Chem* 54:115 (1969).
50. Finkelstein, E., et al. Spin trapping of superoxide. *Mol Pharmacol* 16:676 (1979).
51. Lehninger, A. L. *Biochemistry*. New York: Worth Publishers, Inc., 1970.
52. Fujimori, E. New photo-convertible reactions of blue-fluorescent calf  $\alpha$ -crystallin. *Photochem Photobiol* 29:625 (1979).



END

DATE  
FILMED

6 - 8 - 1

DTIC